Mono Lake Water Levels Forecasting using Machine Learning

by

Bhavarth Shah

A thesis submitted
in partial fulfillment of the requirements
for the degree of
Master of Science
School for Environment and Sustainability
in the University of Michigan
April 2024

Thesis Committee:

Dr. Drew Gronewold, Chair
Dr. Michael Craig

Bhavarth Shah

bhavarth@umich.edu

ORCID iD: 0000-0002-2391-8610

Acknowledgments

Foremost, I would like to express my sincere gratitude to my advisor, Dr. Andrew Gronewold, for putting his faith in me and bringing me on board for this study. I am deeply thankful for his guidance, support, and patience as I navigated through this thesis. His unwavering belief in me has been a guiding light, inspiring me to excel and push the boundaries of my knowledge. I am also grateful to Dr. Michael Craig for his continuous mentorship throughout my master's studies.

I am thankful to all members of the SEAS-Hydro group for listening to my presentations and providing me with insightful feedback. I want to acknowledge Manish, Anna, Caleb, and Alex for providing valuable data for this research and for their continued support in answering my questions. I would also like to thank Vianey Rueda for reviewing the thesis draft and providing me with feedback and suggestions.

I am thankful to the staff at the University of Michigan's Great Lakes ITS Advanced Research Computing for their time and technical support, which helped me run machine learning models on the Great Lakes system. The Great Lakes platform immensely expedited our experimentation process.

Lastly, but most importantly, I would like to thank my friends, loved ones, and family for their unconditional love and support. You are the reason I find myself here and you continue to inspire me to work hard and bring good to the world.

Table of Contents

Abstract

This thesis explores the application of advanced machine learning techniques to forecast water levels in Mono Lake, California, a critical ecological and hydrological resource. Given the complex interplay of factors influencing water levels, such as precipitation, evaporation, natural runoff, and diversions, accurately predicting these levels presents a significant challenge. Various machine learning models, including Support Vector Machine (SVM), Random Forest (RF), and Long Short-Term Memory (LSTM), were developed to forecast Mono Lake water levels. These machine learning models integrate historical water levels, multiple precipitation datasets using a Bayesian model, and outputs from the Large Lake Statistical Water Balance Model (L2SWBM) – an advanced Bayesian model.

A novel contribution of this study is the development and application of the LSTM algorithm, training, and optimization process to develop an Ensemble model for forecasting water levels, which in simple terms develops a group of forecasts from multiple LSTM models to improve the prediction accuracy of Mono Lake water levels forecasts. By training on historical data from 1970 to 2009 and validating model predictions against historical data from 2009 to 2018, the study offers a comprehensive evaluation of the model's performance, followed by forecasts from 2019 to 2023. The findings reveal that the LSTM Ensemble models can accurately predict future water level fluctuations, demonstrating the potential of machine learning in supporting Mono Lake water resources management. Notably, this thesis identifies a critical balance in model complexity, where neither overly simplistic nor excessively complex models yield the most accurate predictions. Instead, a balanced approach, incorporating nuanced model training and optimization

methods emerges as crucial tools for minimizing model overfitting and capturing the nuanced patterns of Mono Lake's water levels. The insights from these training and optimization exercises provided pivotal learning to improve accuracy. Hence, machine learning models like this can be used for informing water diversion strategies, ecological conservation efforts, and policy development, ensuring Mono Lake's sustainability amidst changing environmental conditions.

By providing a detailed analysis of Mono Lake's water level dynamics and the predictive capabilities of LSTM Ensemble models, this thesis contributes valuable knowledge to the fields of hydrology, environmental management, and machine learning, offering a blueprint for leveraging machine learning in the stewardship of natural resources. The implications of this research extend beyond Mono Lake, suggesting a broader applicability of machine learning in hydrology, climate forecasting, and water resource management. As climate change and human activities increasingly impact water resources, the integration of predictive modeling like machine learning into natural resource management offers a path forward for balancing ecological preservation with human needs, ensuring the sustainable management of water bodies worldwide.

Chapter 1 Introduction

The well-being and economic livelihoods of communities are closely intertwined with water levels, particularly for those located near and dependent on bodies of water like lakes (Håkanson et al., 2000). Fluctuations in water levels have far-reaching implications on water quality, the lake's ecosystem, and the livelihoods of nearby communities that depend on the lake (Woolway et al., 2022). These processes include circulation patterns that are pivotal for water mixing and sediment resuspension (Molinos et al., 2015), which are vital in maintaining ecological balance. Consequently, changes in water levels may lead to shifts in water quality (White et al., 2008), ultimately affecting the health of aquatic ecosystems and humans, if consumed without water treatment. Accurately predicting and managing water levels is thus of paramount importance. Water level fluctuations are a complex hydrological phenomenon, influenced by a myriad of factors including meteorological conditions and the exchange of water between the lake and adjacent watersheds (Altunkaynak, 2007; Karimi et al., 2012).

1.1 Objective of the Research

The primary objective of this research is to forecast the water levels of Mono Lake. However, predicting these levels presents a considerable challenge, due to the complexities tied to historical fluctuations of the water levels in Mono Lake. These variations are influenced by a multitude of factors, including precipitation, evaporation, temperature, humidity, and water exchange between the lake and adjacent watersheds through runoff (Ficklin et al., 2013; State of the Lake).

To address the challenge of forecasting the water levels of Mono Lake, this research explores three distinct approaches (Figure 1). First, we focus on using historical water levels to create three separate machine learning models: Support Vector Machine (SVM), Random Forests, and Long-Short Term Memory (LSTM). These models identify trends in historical data and learn from these trends to predict future outcomes. Secondly, we integrated multiple precipitation datasets using a Bayesian model. This method amalgamates data from three separate sources, providing comprehensive and dependable inputs, that are used for training the machine learning models, particularly the LSTM model. Lastly, we used the Large Lake Statistical Water Balance Model (L2SWBM)(Gronewold et al., 2020) – an advanced Bayesian model, to combine multiple datasets of precipitation, evaporation, and runoff. The L2SWBM output is used as input for the Random Forest model and the LSTM model.

The LSTM model architecture is designed to handle multiple input features and predict various output features. These features are precipitation, evaporation, runoff, and diversions, which have a strong influence on water levels. By incorporating these multiple features separately, the LSTM model can effectively capture the complex interactions among different factors influencing water levels and implicitly identify the most significant drivers. We further refined this LSTM model by optimizing the model parameters, essentially creating a member of the 12 LSTM forecast, which we call an LSTM Ensemble model. This LSTM Ensemble model showcases improved accuracy in forecasting Mono Lake's water levels.

Additionally, understanding and forecasting these water level changes are not merely academic exercises, they hold significant implications for water resource management, biodiversity

conservation, and the sustainable use of environmental resources. The accuracy of these forecasts is important and relevant to Mono Lake's management and thereby to its ecosystem and the surrounding environment. This research compares the machine learning-based water levels forecast with the historical water levels of Mono Lake as recently as the last few years, from 2019 to 2023, assessing how closely these advanced machine learning models approximate the real-world water level values. The research aims to provide critical insights for involved stakeholders to develop an effective water management strategy.

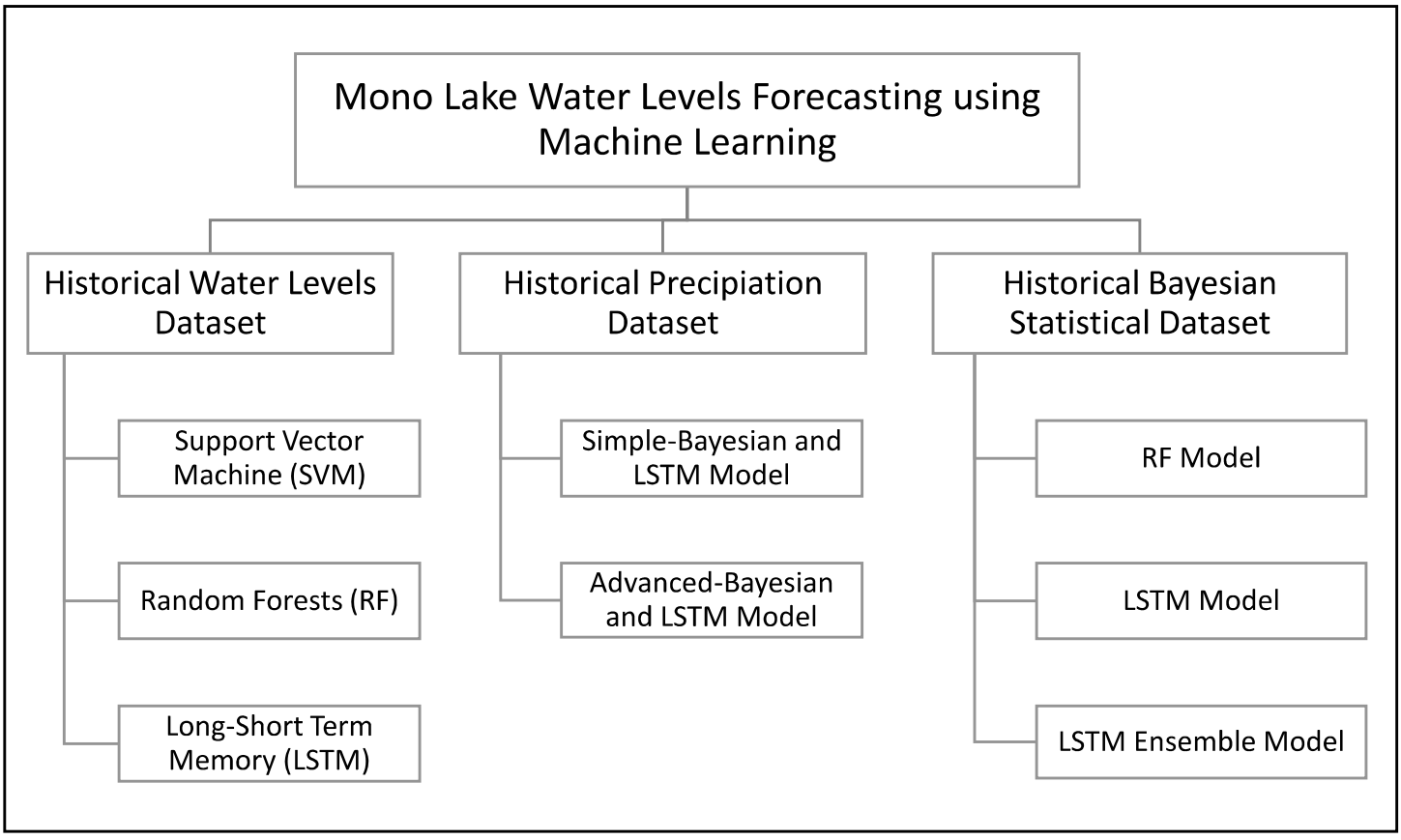

Figure 1: This figure provides a visual representation of the different methodologies employed in the Mono Lake water levels Forecasting using Machine Learning.

1.2 Study Area: Mono Lake

Mono Lake is situated at the eastern edge of the Sierra Nevada in California (Figure 2). It is located at a latitude of 38.016° N and a longitude of 119.0093° W (*Mono Lake Volcanic Field | U.S. Geological Survey*, n.d.). From a geological perspective, Mono Lake is part of the Mono Basin with no outlet to the ocean (Geographic Names Information System, USGS). Due to this unique circumstance, the dissolved salts from runoff accumulate in Mono Lake, subsequently increasing the pH values of the water, resulting in an average pH level of around 9.8 (Oxburgh et al., 1991). The primary tributaries of Mono Lake include Lee Vining Creek, Rush Creek, and Mill Creek, which flows through Lundy Canyon. (Geographic Names Information System, USGS).

Covering more than 70 square miles, Mono Lake is also home to abundant brine shrimp and alkaline flies that provide food for the millions of migratory birds that visit each year (*About Mono Lake*, n.d.; *Natural History*, n.d.). Riparian forests of cottonwood and willow along the shore of Mono Lake are created by freshwater runoff flowing into the lake (Mccreedy & Heath, 2004). In addition to its ecological significance, Mono Lake is also a place for recreational activities, offering year-round tourism for tours, canoeing, field seminars, and other activities.

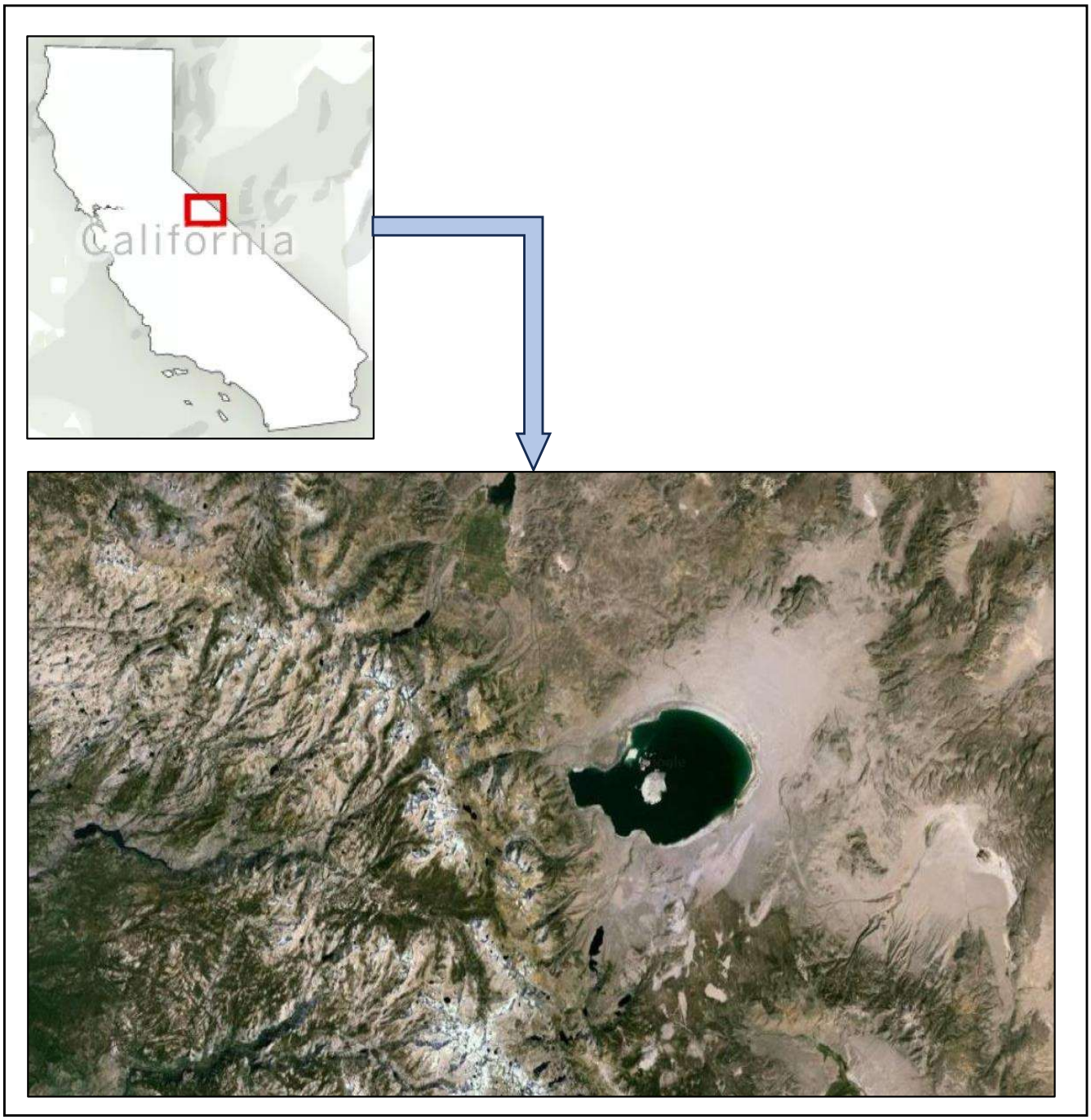

Figure 2: The study area is located on the eastern edge of the Sierra Nevada in California, which is highlighted in red box. The top view of Mono Lake is also represented in the figure above. Source: (L.A.'s New Water War: Keeping Its Supply from Mono Lake - Los Angeles Times, n.d.; Mono Lake - Google Maps; OpenStreetMap).

Furthermore, Mono Lake plays a crucial role as a water source for the population of Los Angeles, California, supplying fresh clean water to around 200,000 residents of the city (Collins & Liu, 2023). Fresh water from Owens River that would otherwise flow into Mono Lake is diverted to Los Angeles through the Los Angeles Aqueduct (The Mono Basin Project), henceforth referred as diversions. Following the start of diversions in 1941, Mono Lake's water levels plummeted from 6,417 feet to 6,372 feet over a 40-year period (Stine Scott, 1993). Hence, diversions caused the lake to lose half its volume and double its salinity (Stine Scott, 1993). The ecological consequences were severe, including threats to the population of the California Gull and threats to the lake's ecosystem (*State of the Lake*, n.d.-b).

In response to these environmental conditions, the year 1994 marked a pivotal decision with the California State Water Resources Control Board's unanimous approval of Decision 1631 (SWRCB Mono Lake Decision 1631, 1994). This decision required that Mono Lake be allowed to increase the water levels to 6,392 feet above sea level (SWRCB Mono Lake Decision 1631, 1994). Decision 1631 introduced a tiered structure of diversions whereby the Los Angeles Department of Water and Power (LADWP) would be limited on the amount of water they can divert according to the levels of Mono Lake. According to Decision 1631, when Mono Lake's level is between 6,380 and 6,391 feet, LADWP is permitted to divert up to 16,000 acre-feet of water annually. However, if the water lake level falls to between 6,377 and 6,380 feet, LADWP will decrease its diversions to a maximum of 4,500 acre-feet per year and if Mono Lake falls below 6,377 feet, the LADWP is restricted from diverting any water (SWRCB Mono Lake Decision 1631, 1994).

The selection of Mono Lake as the study area is not only due to its unique and complex hydrological system but also due to its significant relevance to both the Mono Lake Committee (MLC) and the Los Angeles Department of Water and Power (LADWP). The accurate prediction of the future Mono Lake water levels is important for developing data-informed water resource management strategies that benefit all stakeholders involved.

1.3 Historical Studies on Water Levels Forecasting

In previous decades, a diverse range of tools and models have been developed to forecast water levels, taking into account various influencing factors and significantly aiding in water resource management (Aksoy et al., 2013; Khatibi et al., 2014). For example, Gronewold et al. showed the efficacy of using the Advanced Hydrologic Prediction System (AHPS) in capturing the seasonal and inter-annual patterns of Lake Erie's water levels (Gronewold et al., 2011). Another study by VanDeWeghe et al. employed a statistical approach for projecting plausible climate-related regional water supply scenarios into localized net basin supply sequences (VanDeWeghe et al., 2022). This method preserved spatial and temporal correlations between hydrologic components, enabling explicit representation and manipulation of component marginal and conditional probability distributions (VanDeWeghe et al., 2022). The challenge of addressing climate or unprecedented seasonal changes using statistical models, particularly in the Great Lakes system, has also been a focal point of several studies (Gronewold & Stow, 2014). In addition, advanced statistical algorithms have been increasingly experimented with to tackle climate change scenarios. For instance, Myakisheva et al. developed a forecasting model using ARIMA (Auto-Regression Integrated Moving Average), incorporating both historical and other climate variations, specifically to study climate change impacts on lake water levels (Myakisheva et al., 2021). Other

statistical techniques like Gene Expression Programming and Adaptive Neuro-Fuzzy Inference Systems have been applied to predict daily lake levels for Lake Urmia in Northwestern Iran, enhancing model forecasting performance over various intervals. Another recent study introduced periodicity (month number of the year) into a statistical model for Lake Michigan, thereby significantly improving forecasting accuracy (Demir, 2021). However, these models often require considerable time and computational resources (P. S. Yu et al., 2006). Physics-based hydrodynamic models, while offering enhanced accuracy and reliability, also demand a comprehensive input data set, including lake bathymetry, inflow and outflow conditions, and a full suite of meteorological variables. This requirement can make their application challenging, especially in regions with limited data availability (Huang et al., 2010; Zhu et al., 2020).

1.4 Introduction to Machine Learning in Hydrology

Recently, the application of machine learning models in hydrology has seen substantial growth (Deng et al., 2022; Obringer & Nateghi, 2018; Wang & Wang, 2020; Wee et al., 2021). Traditional machine learning models such as artificial neural networks (ANNs) (Altunkaynak, 2007; Buyukyildiz et al., 2014; Yarar et al., 2009), recurrent neural networks (RNN) (Güldal & Tongal, 2010; Kisi et al., 2012; Yarar et al., 2009), and extreme learning machines (ELM) (Bonakdari et al., 2019; Kisi et al., 2012) have been extensively developed and implemented in hydrology. These models represent a significant shift from traditional statistical approaches, offering new capabilities in predictive accuracy and efficiency.

Moreover, machine learning models have demonstrated excellent results in predicting various climatic parameters, such as precipitation, evaporation, natural runoff, and others (Hussein et al.,

2021; Slater et al., 2023). A recent study successfully developed a rainfall forecasting model using only conventional machine learning architectures, yielding more reliable results compared to complex statistical models (Barrera-Animas et al., 2022). Furthermore, the concept of ensemble learning, which involves combining results from multiple machine learning models, has also proven effective in enhancing machine learning model forecasting accuracy. Most recently a study by Sengoz et al. integrated results from eight different Numerical Weather Prediction (NWP) models to create an ensemble machine learning model for North American precipitation forecasting, which significantly surpassed the performance of baseline models (Sengoz et al., 2023).

Machine learning models have also shown good performance in evaporation forecasting. A study utilizing artificial neural networks (ANNs) for monthly evaporation forecasting reported highly reliable results with an R^2 value of 0.905 (Tezel & Buyukyildiz, 2016). Another research explored multiple machine learning approaches, including extreme learning machine (ELM), gradient boosting machine (GBM), quantile random forest (QRF), and Gaussian process regression (GPR) for evaporation forecasting (Abed et al., 2022; Al Sudani & Salem, 2022). The gradient boosting method, in particular, exhibited superior results in monthly pan evaporation forecasting (Al Sudani & Salem, 2022). Another research compared Random Forest (RF) with two deep learning techniques, namely convolutional neural networks (CNNs) and deep neural networks (DNNs), and showed improvement in estimating monthly pan evaporation rates (Abed et al., 2022).

Machine learning models have shown commendable accuracy in natural runoff forecasting. A recent study applied complex algorithms of backpropagation (BP) neural network, generalized

regression neural network (GRNN), extreme learning machine (ELM), and wavelet neural network (WNN) for short-term 7-day forecasting of runoff (Xiao et al., 2021). The study showed improvement in accuracy in early warning capabilities of floods and droughts using machine learning (Xiao et al., 2021). Another study developed a deep learning multi-dimensional ensemble approach by combining three different deep learning neural networks thereby enhancing the runoff prediction performance (Liu et al., 2022). In the context of Mono Lake water levels forecasting, an early model was developed in 1985 by Peter Vorster. This model considered a mass balance approach, which consisted of inflows and outflows for determining changes in Mono Lake water levels (Peter Vorster, 1985). Despite the advancement of deep learning (DL) techniques like Multilayer Perceptrons (MLPs), Convolutional Neural Networks (CNN), Long Short-Term Memory networks (LSTMs), Restricted Boltzmann Machines (RBMs), and others, there has been limited application of Machine Learning and particularly ensemble machine learning in water levels time series Forecasting. The current research combines Vorster's mass balance concept with a machine learning approach to predict inflows and outflows, and thereby forecast water levels. This study aims to overcome the limitations of existing models and fill the gap in integrating mass balance with machine learning for increasing accuracy in Mono Lake water levels forecasting.

Chapter 2 discusses the study's methodology, encompassing data collection, the algorithms of machine learning models, and the concepts of deep neural networks. Chapter 3 represents the results from each of the machine learning model, analyzing their results in detail. The study concludes with Chapter 4, offering a summary and brief for future research.

Chapter 2 Methodology

2.1 The Water Balance Equation (WBE) of Mono Lake

The Water Balance Equation (WBE) for Mono Lake is fundamentally a mass balance equation, which is pivotal in understanding the lake's hydrological dynamics (Fry et al., 2020). This equation is used to calculate the lake's volume, here forth referred to as lake storage or simply storage. The WBE for Mono Lake is expressed as follows:

$$\boldsymbol{\Delta S = P - E + R - D} \quad \textbf{(1)}$$

$Where,$

$\Delta S = Change\ in\ storage\ (kAc - Ft)$

$P = Precipitation\ (kAc - Ft)$

$E = Evaporation\ (kAc - Ft$

$R = Natural\ Runoff\ (kAc - Ft)$

$D = Diversions\ (kAc - Ft)$

Precipitation is an inflow parameter that encompasses both rain and snow in Mono Lake and is added to the WBE. Natural runoff is another inflow parameter that mainly consists of streamflow resulting from snowfall on the Sierra Nevada that melts and flows into the lake during warmer months(*State of the Lake*, n.d.-b). Evaporation is an outflow parameter that is subtracted in the WBE. Diversions include stream diversions by the Los Angeles Department of Water and Power (LADWP) through the LA Aqueduct. Lastly, the 'Change in storage' represents the change in the lake's volume over a one-month time step. In this study, all WBE units are measured in thousand-acre feet (kAc-Ft). Additionally, the change in storage in kAc-Ft is calculated using stage-volume

curve calculations, which convert historical monthly lake water levels into volumes. This method allows for precise calculation of change in storage, where the specific formula for the stage-volume curve and the methodology for data collection are discussed in the next section.

2.2 Data Collection

This section outlines the data collection methods used in this research, focusing on data preparation for water levels, precipitation, the Large Lake Statistical Water Balance Model (L2SWBM), and the stage-volume curve method to calculate the monthly change in storage.

The first approach following our methodology used a water levels dataset which consists of the historical water levels of Mono Lake measured in feet (Ft). The water levels dataset has a monthly frequency spanning from 1/4/1941 to 12/1/2018. This dataset was sourced from the Mono Lake Committee website (Mono Lake Levels 1979-Present (Monthly)). The second approach used precipitation data, specifically from ERA6 (Hersbach et al.; Lavers et al., 2022), CRUTS_adj (NOAA Physical Sciences Laboratory, n.d.), and MERRA3 (MERRA, NASA). The precipitation datasets span from 1/1/1980 to 12/1/2021. These precipitation global datasets have been extrapolated for our study area for the Mono Lake basin by hydrology experts (Gossard et al., 2023). We utilized a Bayesian model to combine these three datasets. The precipitation output from these Bayesian model is subsequently employed in machine learning models to analyze precipitation patterns.

Furthermore, for our third approach, the outputs of precipitation, evaporation, and runoff datasets are harmonized using the state-of-the-art Bayesian model, referred to as Large Lake Statistical

Water Balance Model (L2SWBM) for closing Mono Lake water balance (Gossard et al., 2023). For this research, we have selected the median values, produced by the L2SWBM. The median values were selected due to the central tendency of the group as it is not exceptionally skewed by high or low values. The timeframe covered for this dataset spans from 1/1/1970 to 12/1/2018.

Regarding the stage-curve calculations, we used the Smoothed Pelagos Corporation Bathymetry Data (Table A-1. Bathymetry of Mono Lake, n.d.) of Mono Lake as a reference point to correlate known water levels with their respective volumes. The detailed values of the Smoothed Bathymetry Data of Mono Lake are available in Appendix I. Specifically, using the Bathymetry data to convert known water levels into corresponding change in storage for each month, spanning from 1/1/1970 to 12/1/2018. The data for Mono Lake water levels was collected from the Mono Lake Committee website (Mono Lake Levels 1979-Present (Monthly)). In this calculation, we used stage-volume interpolation to calculate the volume of water in Mono Lake corresponding to the known water level and subsequently calculated the change in storage for each month. The following formula was used for the calculations conversion of water levels to lake volume:

$$\boldsymbol{Volume_{WL} = Higher\ Volume + \left[\frac{(Water\ Level - Lower\ Stage) * (Higher\ Volume - Lower\ Volume)}{(Higher\ Stage - Lower\ Stage)}\right]} \quad \textbf{(2)}$$

Where,

$Volume_{WL} = Mono\ Lake\ volume\ corresponding\ to\ water\ level$

$Higher\ Volume =$

$Higher\ limit\ of\ volume\ correspoding\ to\ the\ water\ level\ from\ the\ Bathymetry\ table$

$Lower\ Volume =$

$$Lower\ limit\ of\ volume\ correspoding\ to\ water\ level\ from\ the\ Bathymetry\ table$$

$$Higher\ Stage =$$

$$Higher\ limit\ of\ water\ stage\ correspoding\ to\ water\ level\ from\ the\ Bathymetry\ table$$

$$Lower\ Stage =$$

$$Lower\ limit\ of\ water\ stage\ correspoding\ to\ the\ water\ level\ from\ the\ Bathymetry\ table$$

Using this calculation, we first determined the volume of Mono Lake in thousand-acre feet (kAc-Ft) for each monthly water level and we then calculated the change in volume (or storage) by computing the difference between the final volume and the initial volume.

Finally, with the calculated values of change in storage and from the L2SWBM values of precipitation, evaporation, and natural runoff, the only remaining component in the Water Balance Equation (WBE) is the diversions. Here we used the water balance equation to calculate the diversions per month which is also in the same unit (kAc-Ft) for the period from 1/1/1970 to 12/1/2018.

2.3 Machine Learning Algorithms and Deep Neural Networks

This section details the information on implemented machine learning algorithms and deep neural networks. Our focus is on leveraging machine learning algorithms to predict future water levels as well as the components of the WBE for Mono Lake to ultimately forecast water levels. This process encompasses several key steps, including data cleaning, pre-processing, model selection, and implementation of machine learning models, and the evaluation of their performance.

2.3.1 Machine Learning Methods

Machine Learning (ML) methods can be broadly classified into three primary categories: supervised learning, unsupervised learning, and reinforcement learning (Mosaffa et al., 2022). In supervised learning, machine learning algorithms are trained using labeled datasets. These datasets provide known input and output data, which the algorithms use to learn and then predict those outputs. The accuracy of these predictions is evaluated by comparing the algorithm's outputs with historical output data (Google Cloud, n.d.). Unlike supervised learning, unsupervised learning algorithms are trained on datasets without predefined output labels. These algorithms identify structures, patterns, or trends within the data autonomously, without human intervention or guidance on what specific outcomes to predict. Reinforcement learning involves algorithms that learn to make decisions by performing selective actions in any given environment. In other words, the learning process is guided by a system of rewards and penalties, where the algorithm aims to maximize rewards and minimize penalties through self-learning and optimal decision-making (IBM, n.d.). For the purposes of this study, we are only focused on Supervised Machine Learning. This approach is particularly well-suited for our case of predicting future water levels of Mono Lake, as we have a historical dataset with known inputs (such as precipitation, evaporation, runoff, and diversions) and known outputs (such as water levels), allowing the algorithms to learn from this data and make accurate predictions.

2.3.2 Development of Machine Learning Models

The development of supervised machine learning models involves a structured process encompassing the following key steps: (1) data pre-processing, (2) feature selection, (3) training, (4) validation, (5) hyperparameter tuning, and (6) forecasting (Badillo et al., 2020). Each of these

steps plays an important role in the implementation of the machine learning model, which varies based on the model's algorithm design and training process. Detailed discussions on each of the machine learning model's algorithms and implementation will follow in the next sections.

In the data-preprocessing step, the dataset is cleaned, transformed, and prepared for subsequent modeling steps (Szymańska, 2018). Key tasks here include handling missing values, removing any duplicates, and most importantly, normalizing the dataset. Normalization aims to bring the range of input dataset across a comparable scale, for example between 0 and 1, thereby ensuring a high-quality, structured dataset for effective modeling. The next step feature selection involves identifying the most relevant and significant features (or variables) in the dataset that impact the target outcome (Tsagris et al., 2018). In our study, the pivotal features are the components of the water balance equation: Precipitation, Evaporation, Natural Runoff, and Diversions. Each of these features significantly influences the change in storage, which, in turn, affects the Mono Lake water levels. The next step of the training process involves using a dataset to teach the machine learning model to make predictions by recognizing patterns within a dataset (Raschka, 2018). In our case of supervised machine learning modeling, the model is trained on a set of input features and their corresponding output. The goal is to find the optimal parameters or weights for the model that minimize the difference between the predicted and historical observed values during the training process. This is achieved through iterative optimization algorithms like gradient descent and others. The next step after training is validation in which we evaluate the model performance on a separate dataset that was not used during the training (Raschka, 2018). This step helps to evaluate the model's ability to generalize over unseen data and prevents model overfitting or underfitting. As the name suggests hyperparameters tuning is the determination of optimum parameters (e.g.,

number of neurons, layers, lookback period, regularization, and others) for a machine learning model (Raschka, 2018). The final step is forecasting, where the fully developed and fine-tuned machine learning model is used to make future predictions (Makridakis et al., 2018). The following section details information on the Bayesian model which we used to combine the precipitation datasets (ERA6, CRUTS_adj, MERRA3) for machine learning model input.

2.3.3 Bayesian Model for Precipitation Datasets

Bayesian modeling is a statistical approach that uses Bayes' theorem to combine multiple data sources to produce more reliable, consistent, and representative estimates of multiple datasets than those derived from any single source or dataset (van de Schoot et al., 2021). This method utilizes the Bayesian framework, integrating prior knowledge with new data to iteratively update beliefs about a parameter (Castanedo, 2013). In our method, Bayesian modeling is applied to estimate precipitation values from three distinct precipitation datasets (ERA6, CRUTS_adj, MERRA3), each characterized by its own uncertainty and bias. Bayesian reasoning updates prior beliefs about a parameter with new data, leading to a posterior distribution. This process is defined by Bayes' theorem:

$$P(\theta \mid X) = \frac{P(X|\theta) * P(\theta)}{P(X)} \quad \textbf{(3)}$$

$Where,$

$P(\theta \mid X) = \ Posterior\ probability\ of\ the\ parameters\ \theta, given\ the\ data\ X$

$P(X \mid \theta) = Likelihood\ of\ observing\ the\ data\ X, given\ the\ parameters\ \theta$

$P(\theta) = Prior\ probability\ of\ parameters$

$P(X) = Evidence\ (likelihood)\ of\ the\ data$

In the Bayesian framework for our model, we define priors representing initial beliefs about the parameters before observing the data. For precipitation values, we assume a normal and half-normal distribution for the true values with a mean (μ) and standard deviation (σ) set as zero and ten, respectively. This assumption is based on the absence of any strong initial beliefs about the precipitation values, hence a high standard deviation indicating a wide range of variability until the data guides us to a more precise range through Bayesian inference. The model's priors for precipitation values are described as follows:

$$Precipitation \sim N(\mu_x, \sigma_x^2) \quad \textbf{(4)}$$

$For\ i = 1,2,3, \dots n$

$Where,$

$N = \ Normal\ distribution$

$\mu_x = mean\ of\ the\ precipitation$

$\sigma_x = Standard\ deviation\ of\ the\ precipitation$

Here the priors for μ_x and σ_x can be described as:

$$\mu_x \sim N(0,10^2) \quad \textbf{(5)}$$

$$\sigma_x \sim HalfNormal(10) \quad \textbf{(6)}$$

Additionally, we assume that each dataset is presumed to have an associated measurement error, modeled as a half-normal distribution. This decision is to reflect any inherent uncertainty in each dataset's measurements. The likelihood function links the observed data from each dataset to the estimated precipitation values through Bayesian interference while accounting for measurement errors. The likelihoods for each dataset are modeled as normal distributions centered around the

precipitation values, with standard deviations representing the measurement errors, thus capturing the variability and potential inaccuracies in each precipitation dataset.

Building upon the established model framework, the application of Markov Chain Monte Carlo (MCMC) methods marks a crucial phase in our Bayesian model. MCMC sampling stands as a cornerstone for Bayesian inference, particularly valuable in models where deriving analytical solutions for the posterior distribution is complex (van Ravenzwaaij et al., 2018). In our study, MCMC sampling is used to approximate the posterior distributions of precipitation values and the measurement error variances for each dataset. MCMC is used for sampling from the posterior distribution, facilitating the estimation of parameters of interest.

To ensure efficient sampling and convergence, MCMC sampling is created across two distinct scenarios. These two scenarios created two models that vary based on the number of samples drawn from the posterior distribution and the number of tuning steps employed during the MCMC sampling process: **(1)** Simple Bayesian model: This model undergoes 50 tuning steps to adjust the sampling algorithm, subsequently drawing 100 samples to approximate the posterior distribution and **(2)** Advanced Bayesian model: This model entails 1000 tuning steps for algorithm adjustment, followed by the generation of 2000 samples to approximate the posterior distribution.

Following the MCMC sampling process, we compute the credible intervals for precipitation values. These intervals denote the range within which the true values are probable to reside with a specified certainty, thus quantifying the uncertainty in our estimates. Specifically, we calculate the 95% credible interval using the 2.5^{th} and 97.5^{th} percentiles of the posterior distribution samples.

This range indicates where the true parameter values are expected to lie with a 95% probability, according to the posterior distribution. The same credible intervals are calculated for each of the above two distinct scenarios.

The subsequent phase, following the use of the Bayesian model, involves leveraging these output values to train machine learning models. Specifically, the Bayesian Model's output values were used as input for the Long Short-Term Memory (LSTM) model. The algorithm and architecture of the LSTM model are elaborated in the following section.

2.3.4 Support Vector Machine (SVM)

The Support Vector Machine (SVM) is a powerful and versatile supervised machine learning algorithm, suitable for both classification and regression tasks (Gunn, 1998). In the context of regression, which is our focus, SVM aims to identify a hyperplane in an N-dimensional space (where N represents the number of features) that distinctly categorizes the data points within the input dataset. The primary objective of the algorithm is to establish a plane with the maximum margin, meaning the greatest possible distance (difference) between the data points of different classes (Gunn, 1998). The SVM algorithm performs with the help of a kernel, which effectively maps input dataset into high-dimensional feature spaces that allows the algorithm to fit the maximum-margin hyperplane in a transformed feature space. Kernels can be linear, polynomial, radial basis function (RBF), or sigmoid, but we implemented a linear kernel (Gunn, 1998). For a linear SVM, the primary aim is to discover the optimal hyperplane that segregates linearly within the feature space. The optimization problem is formulated as follows:

$$w \cdot x + b = 0 \quad \textbf{(7)}$$

$Where,$

$w\ is\ the\ weight\ vector$

$x\ is\ the\ feature\ vector$

$b\ is\ the\ bias\ term$

The objective function in SVM aims to minimize loss and is represented as follows:

$$min_{w,b}\frac{1}{2}\left|\left|w\right|\right|^2 \quad \textbf{(8)}$$

$This\ is\ subject\ to\ the\ constraint\ for\ each\ \ i^{th} data\ point\ of\ y_i(w\cdot x_i+b)\geq 1,$

$where\ y_i\ are\ the\ class\ labels.$

The regularization parameter (C) in the linear kernel SVM is set to 1, balancing the trade-off between reducing training data error and minimizing the weight vector. The objective function with regularization is therefore:

$$min_{w,b}\left(\frac{1}{2}\left|\left|w\right|\right|^2+C\sum_{i=1}^{n}\zeta_i\right) \quad \textbf{(9)}$$

$Subject\ to\ y_i(w\cdot x_i+b)\geq 1-\zeta_i$

$Where,$

$\zeta i\ are\ slack\ variables\ that\ allows\ for\ misclassification\ of\ the\ margin$

$C\ controls\ the\ tradeoff\ between\ maximizing\ the\ margin\ \&\ minimizing\ classification\ errors$

In our study, SVM is applied to the historical water levels of Mono Lake. The selected features (X) are 'year' and 'month' derived from the date, with water levels as the target variable (y). The

model undergoes training across 80% of dataset which we refer to as training dataset and remaining 20% of dataset which we refer to as validation dataset. The model performance is evaluated on the validation set, which is unseen and unknown to the model and not used in the training process. Before forecasting future water levels, we retrained the SVM model on the entire dataset including training dataset and validation dataset to yield maximum attainable accuracy in forecasting future water levels. Specifically, the retrained model is utilized to forecast water levels for the next 60 months (5 years), from 2019 to 2023 after retraining over the entire dataset from 1941 to 2018. This forecast involves generating a new DataFrame for future dates, including 'year' and 'month', and applying the SVM model to predict water levels for these specific future dates, which is from 1/1/2019 to 12/1/2023.

2.3.5 Random Forest (RF)

The Random Forest algorithm is a sophisticated machine learning method widely utilized for both classification and regression tasks. The algorithm functions by constructing a multitude of decision trees during the training period and gives the mean prediction of the individual trees for the regression tasks (Breiman, 2001). Our study has employed Random Forests across three distinct variations. Firstly, the Mono Lake water levels forecasting, where we directly apply Random Forests to the historical water levels dataset of Mono Lake. Secondly, the Random Forests are implemented to predict the components of the water balance equation, including precipitation, evaporation, natural runoff, and diversions. By predicting these components, we can determine the values of change in storage using water balance equation, which in turn, enables us to calculate Mono Lake's water levels. Finally, we explore the use of hyperparameters tuning within the Random Forest model, this time to forecast the components of the water balance equation. The

objective of fine-tuning the model is to mitigate any overfitting and enhance the model's capability in forecasting with higher accuracy (Probst & Boulesteix, 2018).

As mentioned, Random Forest is comprised of decision trees (Breiman, 2001). The construction of each tree is driven by splitting the input data based on features, which are precipitation, evaporation, runoff, and diversions. The criterion of the model is to minimize the Mean Squared Error (MSE) for regression. The MSE is computed in random forests as follows:

$$MSE = \frac{1}{N}\sum_{i=1}^{N}(f_i - y_i)^2 \quad \textbf{(10)}$$

$Where,$

$N = \ Number\ of\ data\ points$

$f_i = Value\ returned\ by\ the\ model\ at\ the\ data\ point\ i^{th}$

$y_i = Actual\ value\ at\ the\ data\ point\ i^{th}$

Random Forest was used due to its ability to handle complex, non-linear relationships among features, which makes it an important tool for analyzing and predicting the dynamics of water balance equation components of Mono Lake. After the construction of individual decision trees, the model aggregates their mean predictions to generate a final output, effectively harnessing their randomness and collective intelligence.

Now for the first case, the Random Forest model is applied to the historical water levels dataset of Mono Lake. In this dataset, the Water Levels are designated as the target variable (y), which the

model is targeting to predict. Here also, the historical dataset is divided into 80% training and 20% validation. This approach ensures that after the training process we can evaluate model performance on an unseen validation dataset. The model configuration in training employs the Random Forest Regressor, setting the number of trees to 100. The random state of the model is fixed to ensure reproducibility, given the inherent randomness of the Random Forests model. In other words, if the model is run again the model output will remain constant. The model's performance is assessed on the validation set using Root Mean Square Error (RMSE) and Mean Absolute Error (MAE), following the training process. Upon completion of model evaluation, the Random Forest model is retrained on the entire dataset to enhance its learning capability. Subsequently, the model forecasts water levels for the next 60 months (from 1/1/2019 to 12/1/2023).

For the second case, the Random Forest model is applied to the water balance components of Mono Lake, which includes Precipitation, Evaporation, Natural Runoff, and Diversions as generated by the L2SWBM model. The date column is formatted into a datetime structure to facilitate time-series analysis. The features are 'Precipitation (kAc-Ft)', 'Evaporation (kAc-Ft)', 'Natural Runoff (kAc-Ft)', and 'Diversions (kAc-Ft)', each serving both as an independent variable and as a target in a self-predictive model structure. The dataset is divided into 80% for training and 20% for validation. Specifically, the training dataset spans from 1/1/1970 to 2/1/2009, and the validation dataset starts from 3/1/2009 to 12/1/2018. This approach also utilizes the Random Forest Regressor class with 100 individual decision trees, each contributing to its own predictions of the respective feature. The model does not impose a limit on the depth of each tree, allowing them to expand indefinitely until all data points in a leaf belong to the same class. This flexibility enables the model

to capture complex patterns within the data, albeit with a potential risk of overfitting. A fixed random state is used to ensure reproducibility of predictions, ensuring consistent results across multiple runs with the same model configuration.

After training, the model's performance is evaluated on the validation set using metrics such as Root Mean Square Error (RMSE) and Mean Absolute Error (MAE). In addition to the model evaluation, the validation phase also involves calculating the Residuals for all components, which represents the absolute differences between the model predicted and historical dataset. These residuals are visually represented through plots, providing insight into the model's accuracy and areas for improvement. For future predictions, the Random Forest model is retrained on the entire dataset for each feature, using the last known value as a proxy for predicting future output. This approach is selected based on the assumption that future patterns will mirror recent observations, which is common in time-series forecasting where future external inputs are unavailable (Tyralis & Papacharalampous, 2017). The random forests model forecasts the next 60 months (from 1/1/2019 to 12/1/2023) for Precipitation, Evaporation, Natural Runoff, and Diversions. The change in storage are then computed using the Water Balance Equation (Equation 1) with results illustrated through visual plots.

In the third scenario, the Random Forest algorithm is once again applied to the water balance components of Mono Lake, but with a critical distinction, where the model undergoes fine-tuning to mitigate overfitting and enhance model performance. While the procedural steps mirror those of the previous case, the model architecture undergoes modifications to bolster its predictive capacity. The Random Forest Regressor now includes 1000 individual decision trees, which is

increased to help the model discern any complex patterns within the dataset. Furthermore, to avert overfitting, various constraints have been implemented. Minimum samples for split within a tree are set at 5, this parameter ensures that a minimum quantity of samples is necessary before further splitting a node, thereby avoiding overly granular splits that could include noise. The max features are limited to the square root of the total number of features, this setting restricts the number of features evaluated for the optimal split at each node, which allows additional randomness into the model that promotes variation across the trees. After the training phase, the model performance is assessed using RMSE and MAE. Subsequently, as the previous model the fine-tuned random forests model forecasts the next 60 months (from 1/1/2019 to 12/1/2023) for Precipitation, Evaporation, Natural Runoff, and Diversions. The change in storage are then computed using the WBE with results showcased through visual plots.

2.3.6 Long Short-Term Memory (LSTM)

Long Short-Term Memory (LSTM) models are a sophisticated subset of deep learning neural networks, belonging to the class of Recurrent Neural Network (RNN) (Greff et al., 2015). LSTM models are specifically engineered to learn patterns and retain information across lengthy data sequences, making them particularly useful for time-series analysis (Hochreiter & Urgen Schmidhuber, 1991). The core of an LSTM unit is composed of four integral components: a unit (cell), an input gate, an output gate, and a forget gate, as illustrated in Figure 3. This arrangement allows the LSTM to meticulously regulate the flow of data (information), ensuring that the network can retain relevant data over arbitrary intervals and discard less relevant or unnecessary information (Y. Yu et al., 2019).

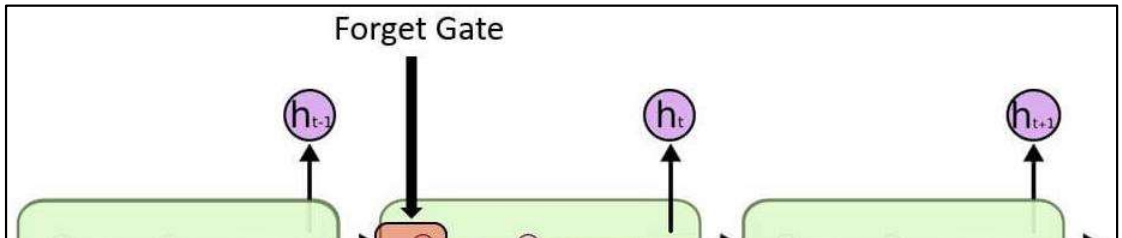

Figure 3: Illustration of a conventional LSTM unit, featuring a cell, an input gate, an output gate, and a forget gate. Source: (Gini et al., 2024).

Within the LSTM unit (cell or node), the input gate determines the relevance of incoming data for modifying the cell's memory. The sigmoid function filters the values, passing only significant ones (either 0 or 1), while the tanh function assigns a level of importance to these values, ranging from -1 to 1. The forget gate identifies which previously stored information in the cell state should be discarded. Utilizing a sigmoid function, the forget gate evaluates each number against the previous state and the current input generating a value between 0 (discard) and 1 (retain). Lastly, the output gate decides the final output based on the cell's input and its updated memory. The sigmoid function again acts as a filter, and the tanh function assigns a weighted importance to the filtered values, which are then scaled by the output of the sigmoid function. The mathematical equations for each of the gate can be written as follows:

Input gate:

$$i_t = \sigma(W_i \cdot [h_{t-1}, x_t] + b_i) \quad \textbf{(11)}$$

$$C_t = \tanh(W_C \cdot [h_{t-1}, x_t] + b_C) \quad \textbf{(12)}$$

where,

$i_t = Sigmoid\ Function$

$x_t = Current\ input$

$C_t = Tanh\ Function$

$\sigma = Sigmoid$

Wi and $W_C =$ Weight matrices for the input gate and significance values respectively

$b_i\ and\ b_c = Bias\ terms$

$h_{t-1} = Previous\ time\ step\ hidden\ stage$

Forget gate:

$$f_t = \sigma(W_f \cdot [h_{t-1}, x_t] + b_f) \quad \textbf{(13)}$$

where,

$f_t = Forget\ gate\ Function$

$W_f = Weight\ matrix\ for\ the\ forget\ gate$

$b_f = Bias\ term$

Output gate:

$$O_t = \sigma(W_o \cdot [h_{t-1}, x_t] + b_o) \quad \textbf{(14)}$$

$$C_t = f_t * C_{t-1} + i_t * C_t) \quad \textbf{(15)}$$

$$h_t = o_t * \tanh(C_t) \quad \textbf{(16)}$$

where,

$O_t = Output\ gate\ Function$

$* = \ Elementswise\ multiplication$

$W_o = Weight\ matrix\ for\ the\ output\ gate$

$b_o = Bias\ term$

$C_{t-1} =$ Previous cell state

The Long Short-Term Memory (LSTM) cycle is structured into four steps to optimize the LSTM model ability to learn and remember information across long sequences. This cycle's intricacy allows the LSTM to excel in forecasting time-series data. In first step, the input gate and tanh layer identifies and updates new information to modify the cell state. The input gate evaluates the incoming data, while the tanh function scales the values, determining their significance in the cell's state update (weightage). In the second step the forget gate identifies which information from the previous timestep should be retained or discarded. It's crucial for the model to forget irrelevant data to maintain its learning. In the third step by combing the information from the forget and input gates, and the LSTM updates its cell state (weightage). This step integrates new information and discards the old, ensuring the cell state (weightage) reflects the most current trend. The final stage utilizes the output gate and a squashing function, tanh, to filter the cell state's information, determining what will be outputted based on the current cell state and the input data (Analytics Vidhya, n.d.; Choi & Lee, 2018; Song et al., 2020). It is important to realize that these steps are

depicted for a single cell of LSTM model. Within an LSTM network there are numerous such cells, which form a layer and each cell optimizing its weights to enhance overall prediction accuracy (Figure 4).

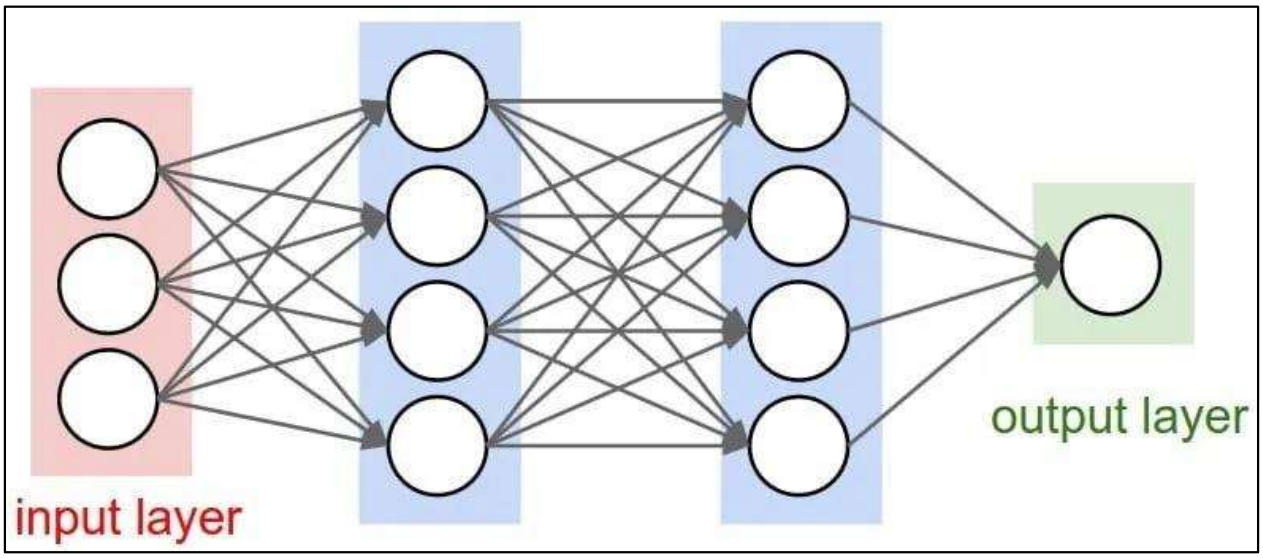

Figure 4: Demonstrates an LSTM model, showcasing an input shape of three features, two model layers each comprising four units (neurons) and the output shape is one feature respectively. This representation shows the LSTM network's layered structure, where the output from one-layer is transitioned into the input for the subsequent layer. This is especially the case in LSTM models having multiple layers. Source: (*Microsoft Cognitive Toolkit*, 2017)

Beyond the architectural framework, LSTM models also incorporate several pivotal parameters, including the learning rate, Mean Squared Error (MSE) as a loss function, epochs, batch size, and others (Bouktif et al., 2020). In our model, we have used Adam Optimizer as a learning rate. Adam optimizer is an optimization algorithm known for its effectiveness in handling sparse gradients. Adam optimizer combines the advantages of two other popular optimizers: AdaGrad and

RMSProp and calculates the adaptive learning rates using these optimizers. In addition to storing an exponentially decaying average of past squared gradients (v), the Adam optimizer also keeps an exponentially decaying average of past gradients (m). Next is MSE, which serves as the loss function, measuring the average of the squares of the errors or deviations, which is the difference between the estimator and what is estimated. In the context of neural networks, it quantifies the difference between the predicted values and the historical values. The formula for MSE is: $\mathrm{MSE} = \frac{1}{n}\sum_{i=1}^{n}\left(Y_i - \hat{Y}_i\right)^2$, where Y_i is historical value and $\hat{Y}_i$ is the predicted value. These parameters play a vital role in measuring model performance during the training and fine-tuning periods of the LSTM model.

An epoch in the neural network training encapsulates a complete cycle through the entire training dataset. The count of epochs determines the repetition frequency of this process, directly influencing the model's learning efficacy (Nakisa et al., 2018). Insufficient epochs may result in underfitting, whereas too many epochs can cause overfitting. Dropout regularization is another important technique to prevent overfitting in neural networks, which involves randomly 'dropping units' or ignoring a subset of units (neurons) during the training process. When a neuron is dropped, it's removed from the network, along with all its incoming and outgoing information, thereby improving model generalization.

Beyond these foundational aspects, LSTM models also incorporate a myriad of other hyperparameters that can be implemented during the data preparation, model architecture, training process, cross-validation, sequence length, ensemble modeling, and others (Borovkova & Tsiamas, 2019; Li & Wang, 2021; Siami-Namini et al., 2019; Song et al., 2020; Y. Yu et al., 2019).

However, discussing all that is beyond the scope of this study. For our study, we have focused on ensemble modeling, which combines results from multiple models to improve forecasting accuracy. Different member models are created by tuning above discussed hyperparameters, specifically in this case changing model architecture, sequence length (lookback period), and regularization. A cumulative of 13 models including the base LSTM model is created. The specifics of each hyperparameters tuning are mentioned in the later part of this section. The authors believe that this ensemble machine learning approach will improve the forecasting accuracy of the LSTM model.

In our study, LSTM models have been deployed across four distinct cases to forecast Mono Lake water balance components and water levels: (1) LSTM model on water balance components from L2SWBM dataset, (2) Ensemble LSTM model on water balance components from L2SWBM dataset, (3) LSTM model on precipitation dataset from Simple Bayesian Model and Advanced Bayesian Model, and (4) LSTM model on Mono Lake historical water levels.

In the first case, the LSTM model is applied to the water balance components of Mono Lake. The dataset includes Precipitation, Evaporation, and Natural Runoff, which are outputs from the L2SWBM model. The Diversions are separately calculated as discussed earlier. These datasets serve as inputs for the LSTM model. The key features in the LSTM model are Precipitation (kAc-Ft), Evaporation (kAc-Ft), Natural Runoff (kAc-Ft), and Diversions (kAc-Ft). In the historical dataset, the first 80% of data is used as training and the last 20% as validation. Hence, the training dataset spans from 1/1/1970 to 2/1/2009, and the validation dataset from 3/1/2009 to 12/1/2018. Normalization of the features is then performed using the MinMaxScaler to fit training and

validation dataset between 0 and 1. Normalization is typically performed to improve the LSTM performance, which is highly sensitive to the scale of input data. Another crucial step in data preparation for LSTM model involves creating time-stepped sequences as model input. We created a function that structures the input data so that the LSTM can learn from a specified look-back period (e.g., 48 months) to predict the next time step. Moreover, the random seed is fixed to ensure result reproducibility of the model results. The LSTM model architecture includes 4 input cells for each of the components (precipitation, evaporation, runoff, diversions), 100 units in the layer, and a dense output layer with four units for each of the four components. We used the 'adam' optimizer and 'mean squared error' as the loss function, and the model undergoes training over 50 epochs.

Once the training process is completed, the model predictions made over the validation period, where the model output is inversely scaled to revert the normalization for all the four components and then using WBE we calculate the change in storage, ΔS (kAc-Ft). Model performance on the validation set is assessed using RMSE and MAE. Additionally, residual values, representing the absolute difference between predicted and historical dataset for each component, are also calculated and visually represented. After evaluating the model, future predictions are made for each feature at a monthly interval from 1/1/2019 to 12/1/2023. Here utilizing a 48-month lookback period, the model iteratively updates its input data by dropping the oldest value in the sequence and appending the most recent prediction at the end. In other words, the first value (1^{st} of the 48-month lookback period) is dropped and the last predicted value (49^{th} of a 48-month lookback period) is appended to the model input data, and this iterative process continues throughout the forecasting period. With the corresponding forecast values for all four components, the 'Change in Storage' is calculated using WBE. The results of all components including 'Change in Storage'

are plotted over the entire period from 1970 to 2023 for visual representation. Finally, the change is storage, ΔS (kAc-Ft), is converted to water levels using stage-curve calculation.

In the second case, the LSTM Ensemble model is constructed to forecast all water balance components of WBE. To improve the performance and robustness of the LSTM model results, the hyperparameters are changed in a specific manner, as outlined in Table 1 below. While the process largely mirrors the above method in terms of data preparation, training, validation, forecasting, and visualization steps, the model architecture and training process differ significantly as represented in Table 1.

Model ID	**Layer & Units (Neurons)**	**No. of Epochs**	**Lookback Period (months)**	**Dropout**
Base	*1 Layer and 100 Units*	*50*	*48*	*0%*
Model 1	1 Layer and 100 Units	50	36	0%
Model 2	1 Layer and 100 Units	50	36	20%
Model 3	1 Layer and 100 Units	100	48	0%
Model 4	1 Layer and 100 Units	100	48	20%
Model 5	1 Layer and 100 Units	150	48	20%
Model 6	1 Layer and 100 Units	200	60	20%
Model 7	2 Layers and 400 Units	50	36	0%
Model 8	2 Layers and 400 Units	50	36	20%
Model 9	2 Layers and 400 Units	100	48	0%
Model 10	2 Layers and 400 Units	100	48	20%
Model 11	2 Layers and 400 Units	150	48	20%
Model 12	2 Layers and 400 Units	200	60	20%

Table 1: LSTM Ensemble model. The table demonstrates various configurations of the LSTM model(s), which we call members of LSTM Ensemble model. Each member is highlighting differences in hyperparameters such as the number of layers and units, epochs, lookback period,

and dropout. It is important to note that model complexity increases from the top to the bottom of the table.

In the third case, the LSTM model targets the forecasting of a single component, which is precipitation (inches). This approach differs from the previous ones by focusing on predicting one feature at a time rather than multiple components simultaneously. The dataset for this case is output from the Bayesian model discussed earlier, containing time-series precipitation data for Mono Lake. The model here follows the same standard process as above in the data pre-processing and training. However, a key adjustment in this setup is the change in the lookback period, which is 15 months, and model architecture which includes 50 units in the LSTM layer. This modification was made to strike a balance between reducing model complexity and minimizing the risk of overfitting, especially when focusing on predicting a single feature (precipitation). The model uses the 'mean squared error' loss function and the 'adam' optimizer, aligning with similar practices for LSTM regression. With the model being trained over 100 epochs and a batch size of 1, it undergoes more extensive learning over the training dataset. After training, the model performance is assessed over the validation dataset using similar metrics of RMSE and MAE. For future predictions, a similar forecasting approach as earlier of iteratively predicting and updating the input data sequence is applied. The forecasting period is of 60 months (from 1/1/2019 to 12/1/2023).

In the fourth case, the LSTM model forecasts water levels of Mono Lake directly. The dataset, spanning from 4/1/1941 to 12/1/2018, contains historical water level data only, which serves as both input and target for the model. This method focusses solely on water levels, in contrast to any

of the previous approach of predicting single or multiple water balance components. The dataset is normalized using the MinMaxScaler. The dataset is divided into training (80%) and validation (20%) sets while maintaining the chronological order. The training set covers data from 4/1/1941 to 5/1/2003, while the validation set spans from 6/1/2003 to 12/1/2018. The look-back period of 15 months prepares the input data for LSTM model. The model consists of complex structure with four LSTM layers, each with 100 units, which is designed to capture the complex data patterns. To prevent overfitting, each LSTM layer is followed by a 20% dropout. The model is compiled with the 'adam' optimizer and 'mean squared error' loss function, the model trains over 90 epochs and we evaluate the model performance using RMSE and MAE. Future water level predictions for the next 60 months (1/1/2019 to 12/12/2023) are made using the similar iteratively predicting and updating the input data sequence. The model predictions are visually compared with the historical Mono Lake water levels for further evaluation.

2.4 Model Evaluation:

To effectively evaluate the performance of various models in the context of our regression tasks, like forecasting water balance components or water levels, we used several statistical metrics. This section delves into the performance evaluation applied to assess the accuracy of our models (Ferdinandy et al., 2020). It is important to note that this model evaluation is carried out over the validation dataset for all the models. The main metrics include the Root Mean Squared Error (RMSE), Mean Absolute Error (MAE), and residuals, each offering insights into the model's accuracy and reliability.

Root Mean Squared Error (RMSE) is one of the standard ways to measure the error of a model in predicting quantitative data. It represents the square root of the average squared differences between predicted and historical datasets to a robust measure of accuracy that penalizes larger errors more than smaller ones. Mean Absolute Error (MAE) measures the average magnitude of errors in the model predictions without considering their direction. It calculates the average of the absolute differences between predicted and historical observations, treating all individual differences equally. Residuals in regression models are the differences between historical and predicted values. Ideally, residuals should scatter randomly near zero, without any discernible pattern. The equation for these metrics is as follows:

$$RMSE = \sqrt{\frac{1}{n}\sum_{i=1}^{n}\left(\mathrm{Y_i} - \hat{\mathrm{Y}}_\mathrm{i}\right)^2} \quad \textbf{(16)}$$

$$MAE = \frac{1}{n}\sum_{i=1}^{n}\left|\mathrm{Y_i} - \hat{\mathrm{Y}}_\mathrm{i}\right| \quad \textbf{(17)}$$

$$Residuals_i = \mathrm{Y_i} - \hat{\mathrm{Y}}_\mathrm{i} \quad \textbf{(18)}$$

where,

$n = Number\ of\ observations$

$\mathrm{Y_i} = Actual\ Value$

$\hat{\mathrm{Y}}_\mathrm{i} = \mathrm{Predicted\ Value}$

Beyond quantitative assessments of RMSE, MAE, and residuals, visualizations of historical and model predicted values are created to further understand the model performance. These visualizations encompass training, validation, and forecasting plots, showcasing the models' performance with respect to the historical observations. Residual plots created for Random Forests

and LSTM models, including the LSTM Ensemble model are particularly useful in our evaluation. By plotting residuals against the timescale, these plots act as diagnostic tools, highlighting areas where the model predictions align or diverge significantly from the historical data. Such visual diagnostics are invaluable for identifying model strengths and pinpointing areas requiring further refinement. By using these visualization tools across different models, we aimed to gain a comprehensive view of different model's capabilities, facilitating an informed comparison of their respective strengths and weaknesses, and iteratively improving our approach to Mono Lake water levels forecasting.

Chapter 3 Results and Discussions

3.1 Analysis of Machine Learning Forecasting Results

As mentioned earlier, this research employs three main approaches differentiated by the datasets used for the machine learning model. The first approach involves using historical water level dataset, where we specifically create three models: (1) Support Vector Machine (SVM), (2) Random Forest (RF), and (3) Long Short-Term Memory Model (LSTM). The second approach utilizes historical precipitation datasets (ERA6, CRUTS_adj, and MERRA3) combined using a Bayesian framework. The outputs from the Bayesian model were then used to create LSTM models to forecast precipitation. In the third approach we used the outputs from the advanced Bayesian model, the L2SWBM, which includes precipitation, evaporation, and natural runoffs, and we calculated the change in storage and diversions using stage-curve method and the water balance equation respectively. In this category, we specifically create three models: (1) Random Forests, (2) LSTM, and (3) LSTM Ensemble models. The outputs from the above model, which include four water balance components (precipitation, evaporation, natural runoffs, and diversions), were used to calculate the change in storage through the water balance equation. Finally, the monthly change in storage was converted to water levels using the stage-curve method. The following subsections elaborates the results from each of the three approaches.

(1) Using Historic Mono Lake Water levels:

i. *Support Vector Machine (SVM) model:*

The performance of the SVM model across the validation dataset range (4/1/2003 to 12/1/2018) is shown in Table 2, which presents the Root Mean Square Error (RMSE) and Mean Absolute Error (MAE) between the SVM model's predicted and historical water levels.

Parameters (Feet)	**RMSE**	**MAE**
Water Levels	23.06796	22.8611

Table 2: Shows the SVM model's performance using RMSE and MAE metrics in predicting water levels within the validation dataset range (4/1/2003 to 12/1/2018).

Based on the values above it can be mentioned that the model performance was poor despite the extensive training on 80% of the original dataset. Here the training data set range was 4/1/1941 to 4/1/2003. The possible reason behind the model performance can be attributed to the fact that there is massive variation in the dataset as after the period of 1948 the water levels declined drastically, due to an increase in diversions. This implies that the SVM model is not able to capture the trend over the training period and hence resulted in poor performance. Figure 5 below gives the visual representation of model performance over the validation period by showcasing the historical values represented in blue and the model results represented in red respectively. The residual values are the difference between model predictions and observed historical data over the validation time period (Figure 5b). The figure also shows the model forecasting data (Figure 5c), which is in green color and is a continuation of model prediction since the validation data.

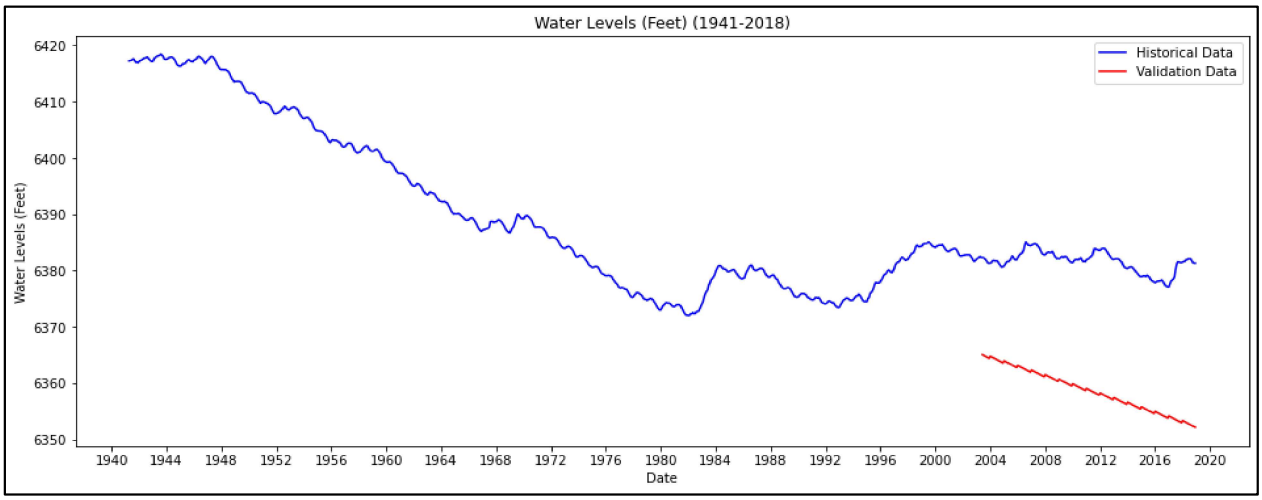
Water Levels (Feet) (1941-2018)
Historical Data
Validation Data
Water Levels (Feet)
Date

(a)

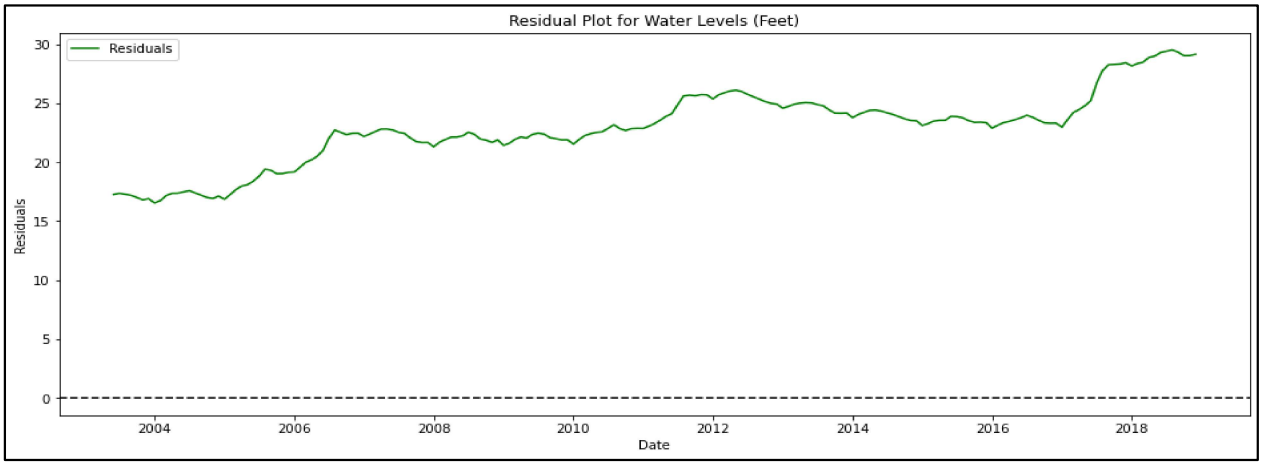
Residual Plot for Water Levels (Feet)
Residuals
Residuals
Date

(b)

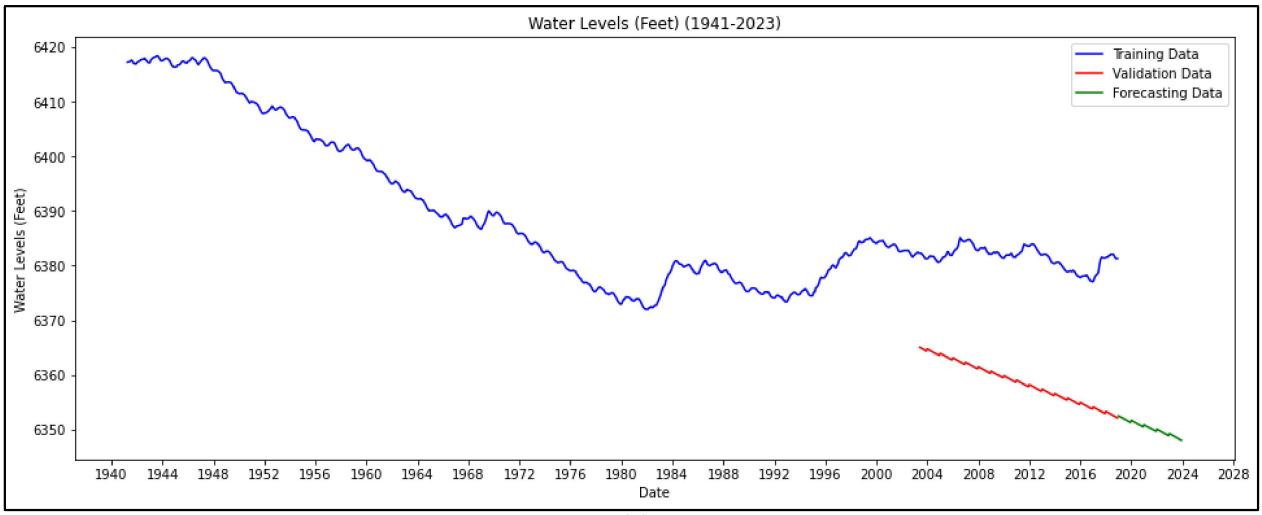
Water Levels (Feet) (1941-2023)
Training Data
Validation Data
Forecasting Data
Water Levels (Feet)
Date

(c)

Figure 5: (a) Shows the visualization of model predicted data and the historical data. (b) Represents the difference between the model predicted and the historical data, and (c) Represents the forecasting which is the continuation of the validation data by the SVM model.

ii. Random Forest (RF) model:

Table 3 below shows the Random Forest (RF) model's performance through RMSE and MAE metrics, comparing RF model water level predictions to historical data within the validation dataset spanning from 4/1/2003 to 12/1/2018.

Parameters (Feet)	**RMSE**	**MAE**
Water Levels	2.004326	1.469882

Table 3: The table shows RF model performance using RMSE and MAE metrics within the validation dataset range (5/1/2003 to 12/1/2018).

Notably, the RF model demonstrates slightly higher accuracy over the SVM model, however, the model's predictions are flat (constant). This phenomenon can be clearly seen in the Figure 6, where despite extensive training on 80% of the dataset (from 4/1/1941 to 4/1/2003), the RF model predictions are consistently flat (straight line) over the validation period (Figure 6a). This can be attributed to the nature of Random Forest model algorithm, which fall short in regression forecasting. This clearly suggests that the model, despite training, failed to learn about any trend or variation, defaulting to average constant results. In figure 6a, historical data are in blue and model predictions are in red and the residual (Figure 6b). The forecasting data are indicated in the green (Figure 6c), which is a continuation of the model prediction from the validation data.

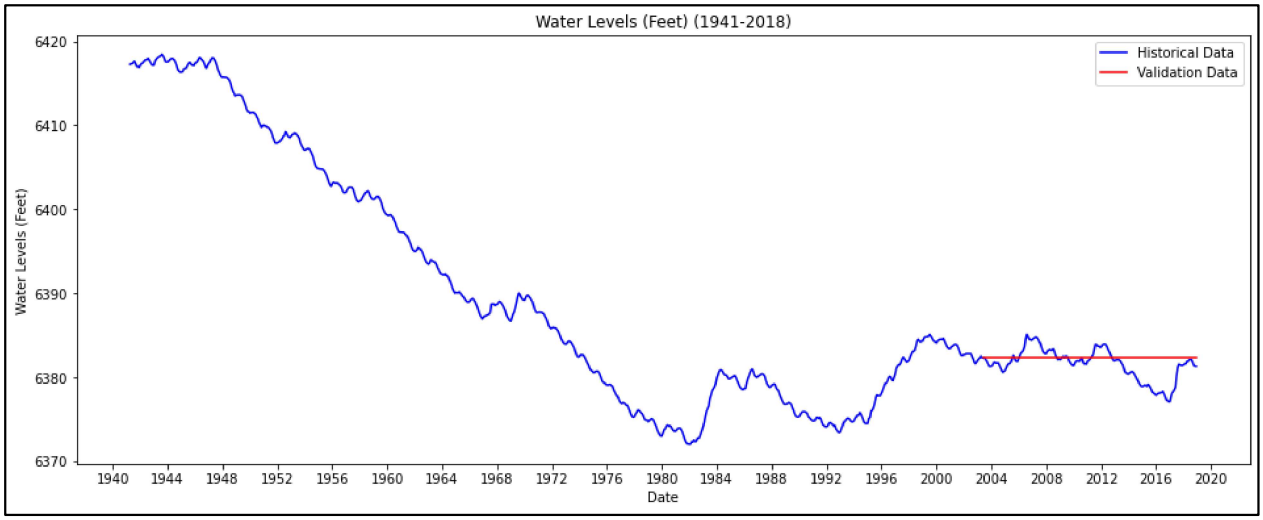
Water Levels (Feet) (1941-2018)
Historical Data
Validation Data
Water Levels (Feet)
Date

(a)

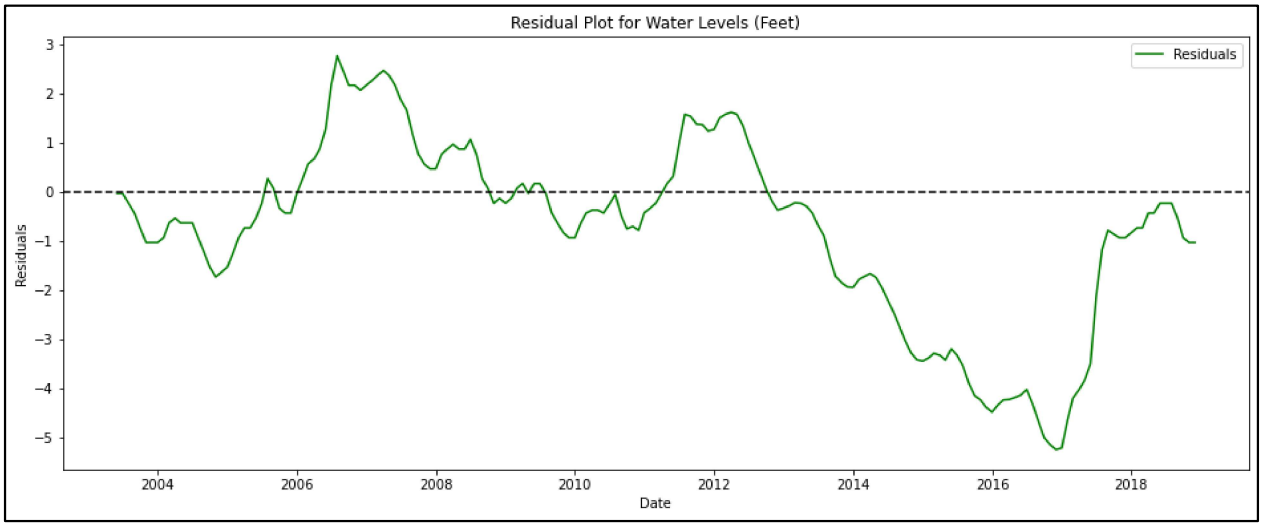
Residual Plot for Water Levels (Feet)
Residuals
Residuals
Date

(b)

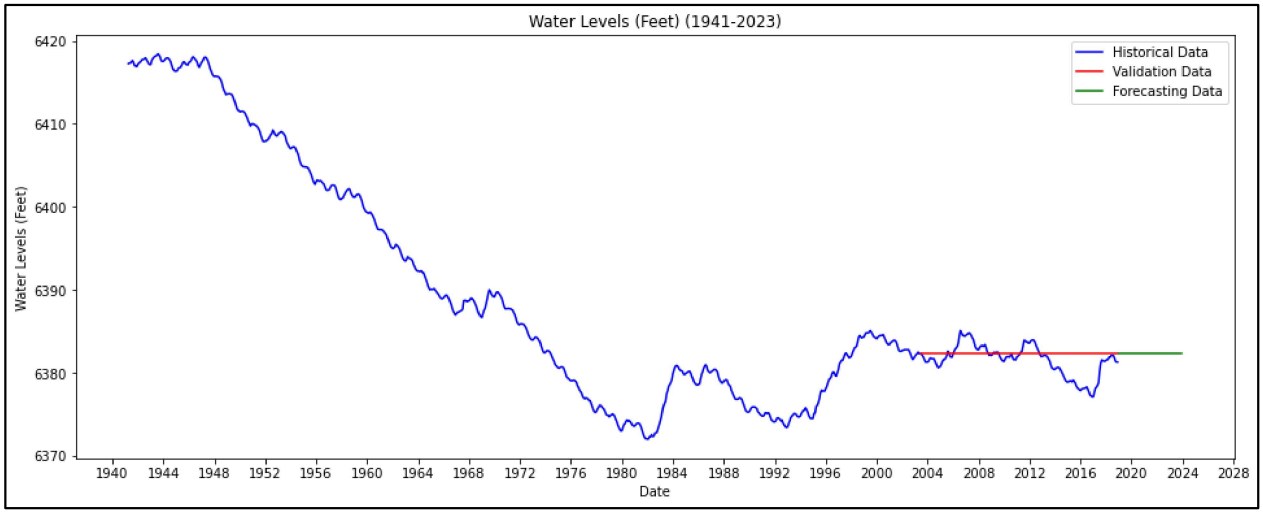
Water Levels (Feet) (1941-2023)
Historical Data
Validation Data
Forecasting Data
Water Levels (Feet)
Date

(c)

Figure 6: (a) Represents the visualization of model predicted data and the historical data. (b) Represents the difference between the model predicted and the historical data, and (c) Represents the validation as well as the true forecasting data by the RF model.

iii. Long Short-Term Memory (LSTM) Model

Table 4 below shows the results of RMSE and MAE between the LSTM model predicted and the historical data of water levels across the validation dataset. The range of validation is from 4/1/2003 to 12/1/2018. As compared to the SVM and the RF model, the LSTM model shows better performance over the validation dataset.

Parameters (Feet)	**RMSE**	**MAE**
Water Levels	1.610396	1.196895

Table 4: The table shows LSTM model performance by comparing predicted and historical data within the validation dataset range (5/1/2003 to 12/1/2018) using RMSE and MAE metrics.

Based on the model results it can be interpreted that the model performance improved slightly but there is a delay in the model prediction compared to the historical data. This pattern is discernable in the Figure 7. The model is able to learn the trend and variations in the water levels due to inherent nature of the LSTM model, which works by identifying the pattern within the datasets. However, the sharp decline in the dataset following, 1948, and the subsequent fluctuations without a clear trend challenge the model's capability in learning and subsequently forecasting. The figure 7a provides a visual comparison of model performance during the validation period, showing

historical data in blue, model predictions over validation dataset in red, and the forecasting results in green.

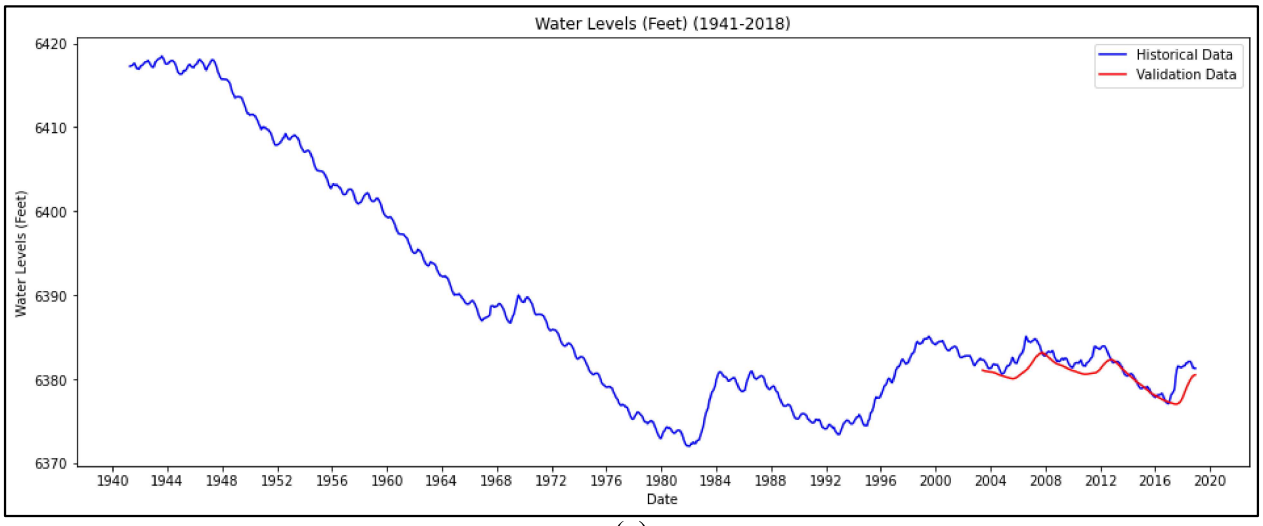

(a)

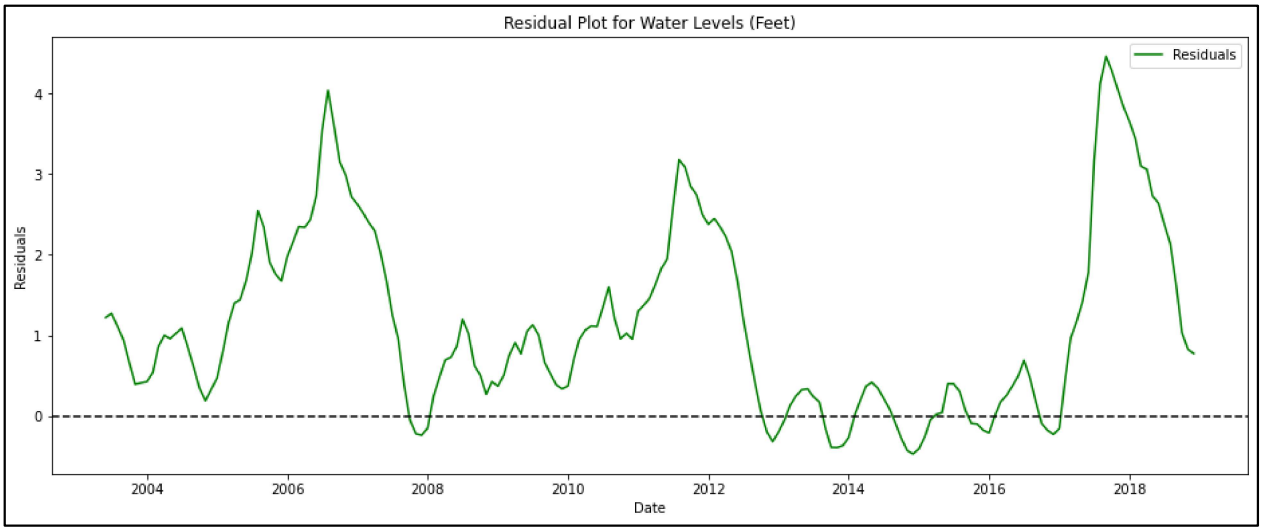

(b)

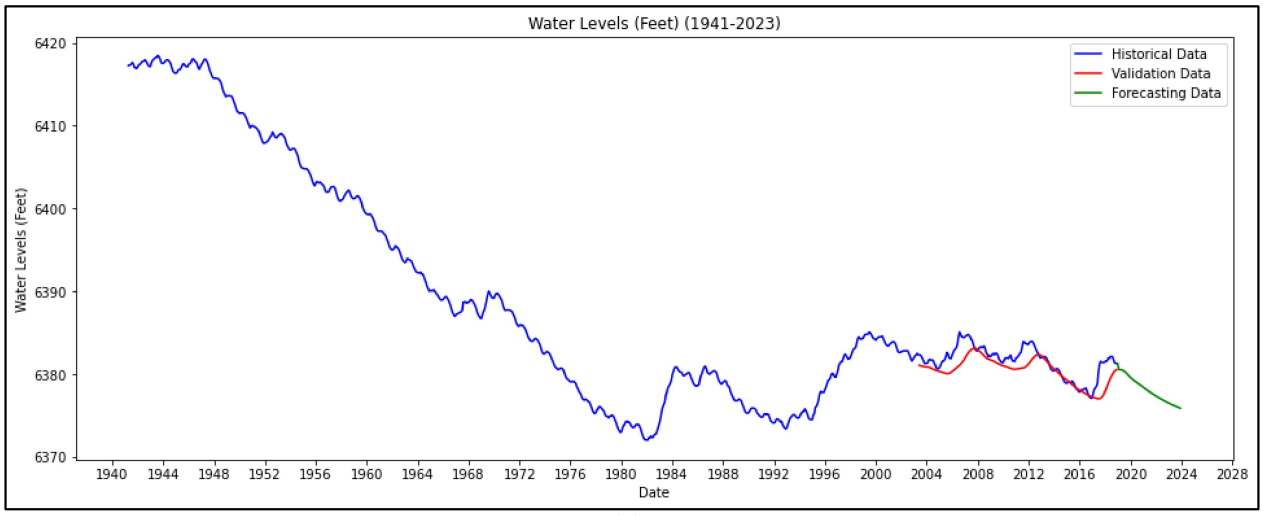

(c)

Figure 7: (a) Represents the visualization of model predicted data and the historical water level data. (b) Represents the difference between the model predicted and the historical data, and (c) Represents the validation as well as the forecasting data by the LSTM model.

(2) Using Historic Precipitation Dataset:

In this section, we will discuss the results of the LSTM model, which uses results from the Bayesian models as an LSTM input. The simple Bayesian model integrates precipitation data from three diverse datasets: ERA6, CRUTS_adj, and MERRA3. The outputs from this Bayesian model are subsequently used in the LSTM model. The dataset's training period starts from 1/1/1980 to 7/1/2013, which is initial 80% of the dataset, while the validation period spans from 8/1/2013 to 12/1/2021, which is the last 20% of the dataset. Additionally, the advanced Bayesian model follows the steps using the above three precipitation datasets.

Table 5 shows results of RMSE and MAE between LSTM model predicted and historical precipitation data, which are from the simple Bayesian model. These metrics are calculated across

the validation dataset. Based on the RMSE and MAE values it can be observed that the LSTM model's performance on the Bayesian-based historical precipitation dataset surpasses the LSTM model's performance on historical water levels dataset.

Parameters (Inches)	RMSE	MAE
Precipitation	1.779439	1.200164

Table 5: The table shows the RMSE and MAE metrics comparing LSTM model predictions with historical (simple Bayesian model) precipitation values within the validation dataset range from 8/1/2013 to 12/1/2021.

Figure 8 below provides a visual comparison between the LSTM model's predictions and the historical precipitation values, which are from the simple Bayesian model. From this figure, we observe that the LSTM model successfully captures the seasonal patterns within the precipitation data, aligning closely with the historical observations. The historical data are depicted in blue, while the model's predictions are shown in red (Figure 8a). Although the model adeptly identifies the seasonality of the dataset, it struggles to predict the occasional spikes that occur in the precipitation dataset. The residual plot, displayed in green, highlights the differences between the model predicted and historical data, showing a close alignment with the historical results as the residuals are narrowly distributed around the zero line (Figure 8b). This indicates a strong model performance in terms of fitting the historical data. Forecasting data is plotted in green (Figure 8c), which shows the LSTM model forecasting from 1/1/2022 to 12/1/2027.

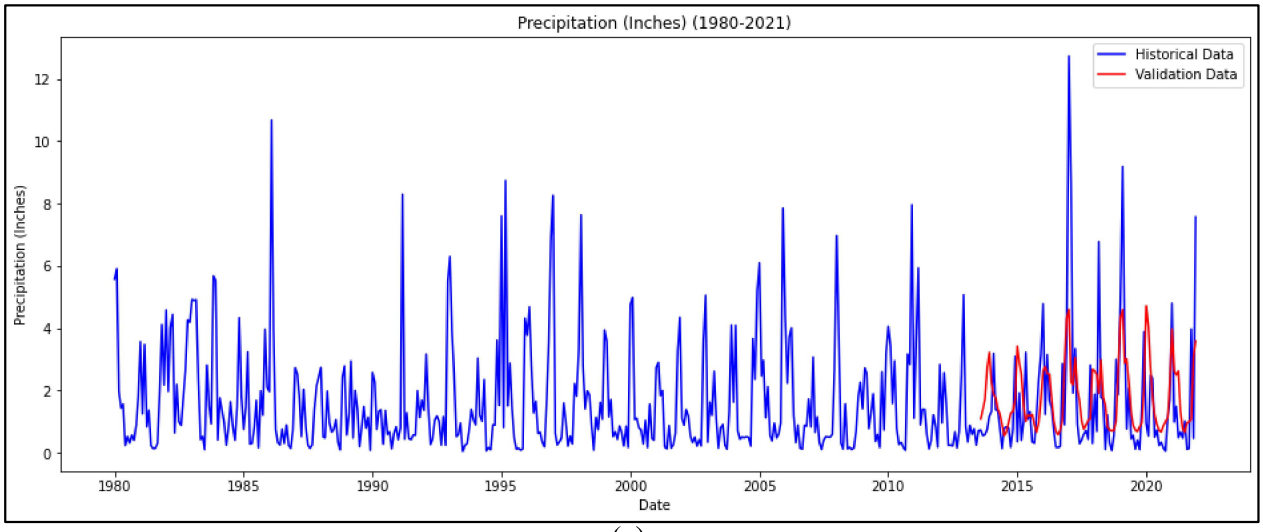
Precipitation (Inches) (1980-2021)
Historical Data
Validation Data
Precipitation (Inches)
Date

(a)

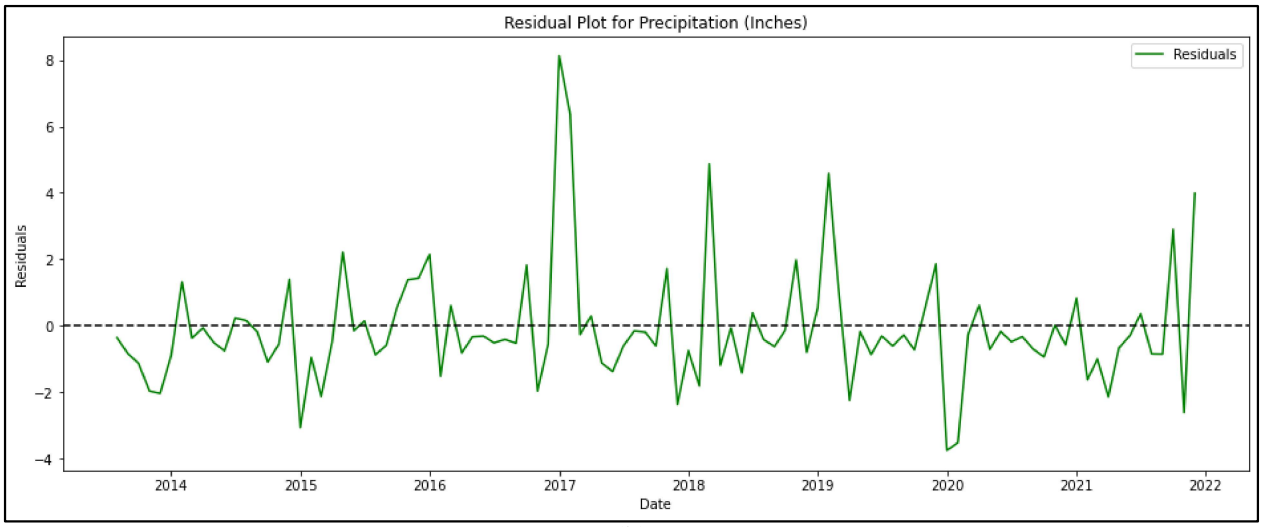
Residual Plot for Precipitation (Inches)
Residuals
Residuals
Date

(b)

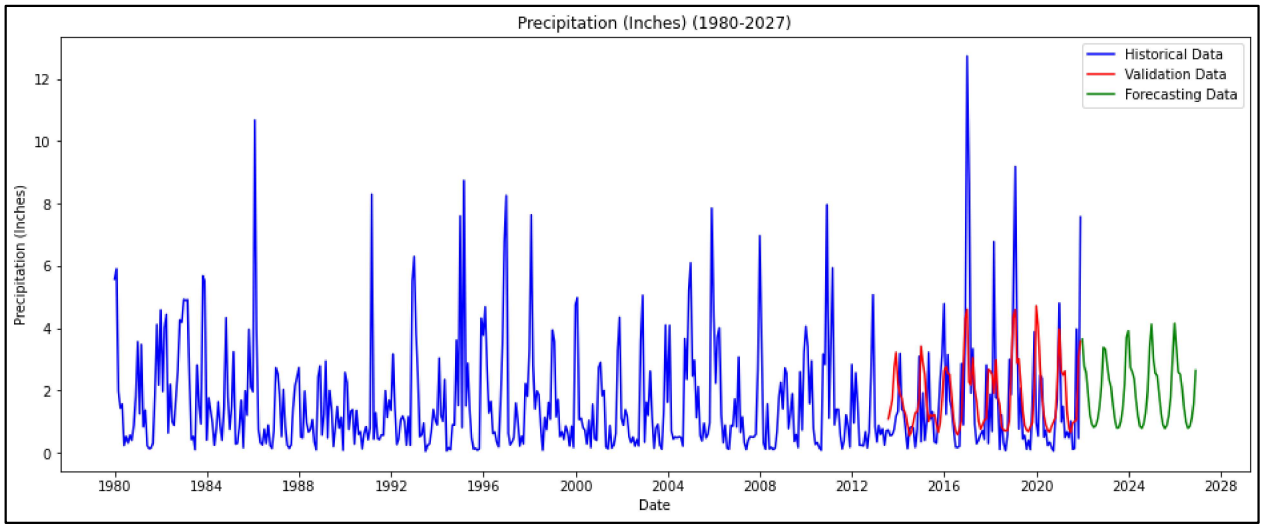
Precipitation (Inches) (1980-2027)
Historical Data
Validation Data
Forecasting Data
Precipitation (Inches)
Date

(c)

Figure 8: (a) Shows the visualization of model predicted data and the historical precipitation data from the Simple Bayesian model, (b) Represents the difference between the model predicted and the historical precipitation data, and (c) Represents the historical, validation, and forecasted dataset across the timescale from 1980 to 2027.

The LSTM model skillfully forecasts the seasonal highs and lows within the precipitation dataset, suggesting an effective understanding of the underlying seasonal patterns in precipitation. This capability to predict future trends underscores the LSTM model's potential to discern complex climatic patterns.

Table 6 presents a comparison between LSTM model predicted and historical precipitation values, which are from the advanced Bayesian model using of RMSE and MAE. These metrics are calculated across the validation dataset.

Parameters (Inches)	**RMSE**	**MAE**
Precipitation	1.812644	1.109772

Table 6: The table shows the RMSE and MAE metrics comparing the LSTM model's predictions to historical (Advanced Bayesian) values within the validation dataset range (8/1/2013 to 12/1/2021).

Figure 9 shows the LSTM model's prediction against the historical precipitation values, which are from the advanced Bayesian model. It can observed that the LSTM model successfully captures the seasonal patterns within the precipitation data. The historical data are depicted in blue, while

the model's predictions are shown in red, and they are labeled as historical data and validation data (Figure 9a). Similar to the simple Bayesian model, the LSTM model struggles to predict spikes in precipitation. The residual plot shows a good correlation of model prediction results with the historical precipitation dataset (Figure 9b). This is evidenced by the residuals clustering near the zero line. The LSTM model forecasting starts from 1/1/2022 to 12/1/2027 which is the green color (Figure 9c). The model adeptly forecasts the seasonal peaks and troughs within the precipitation data in the forecasting period. Notably, the model also forecasts an increase in the precipitation in the future. This suggests the model's capability to discern not only seasonal but also climate change patterns that are not immediately apparent.

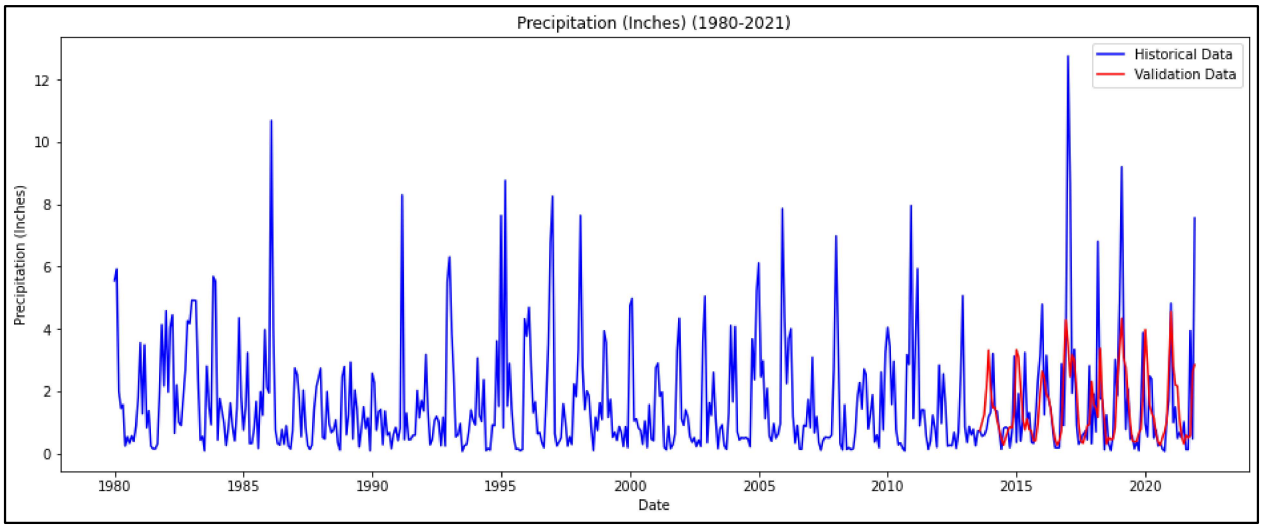

(a)

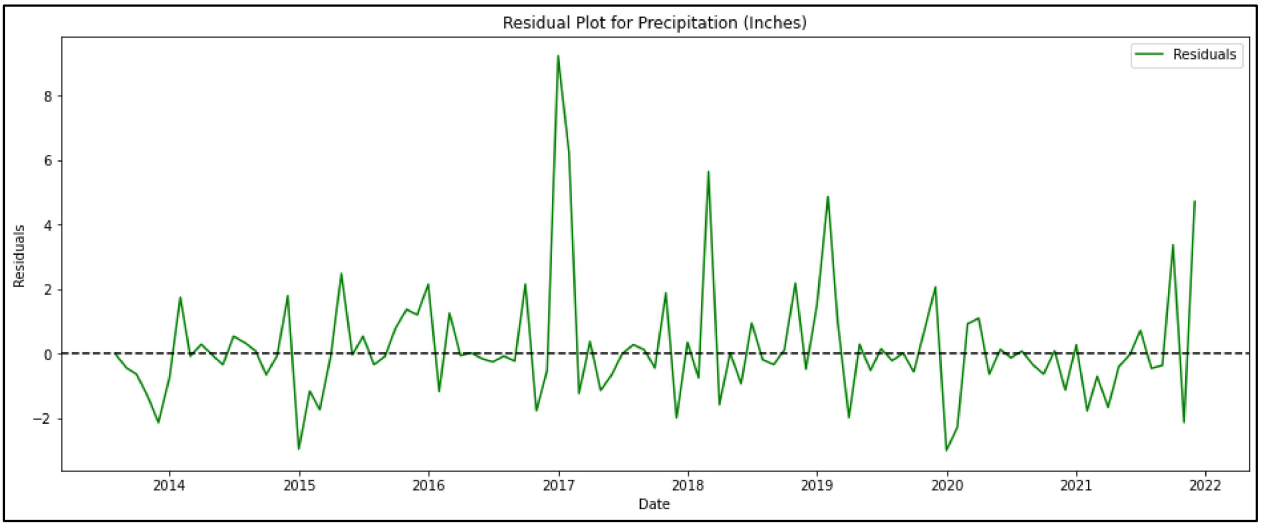

(b)

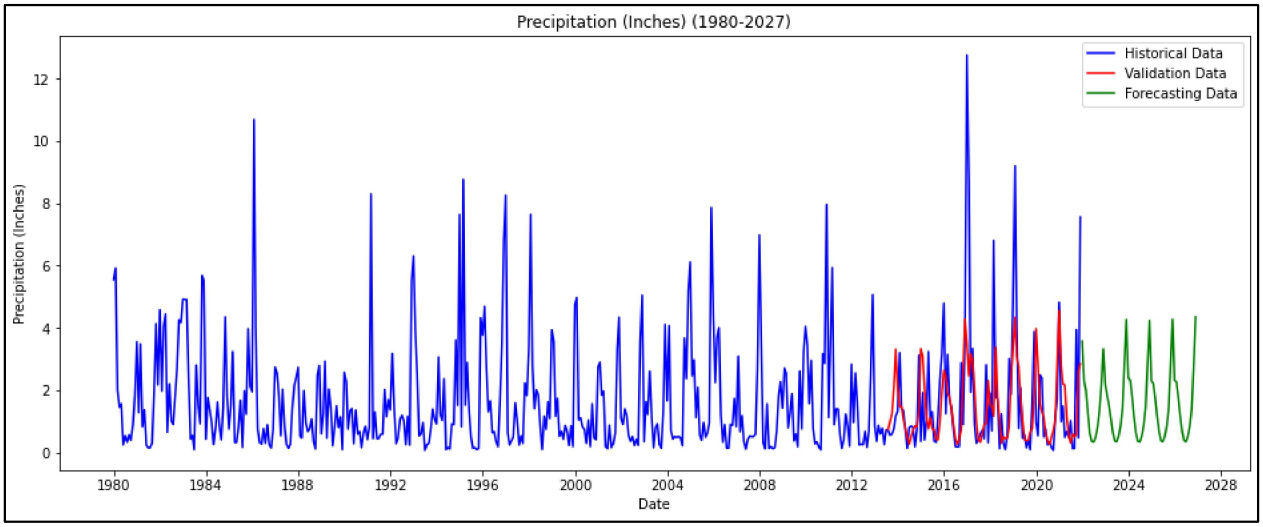

(c)

Figure 9: (a) Represents the visualization of model predicted data and the historical precipitation data from the Advanced Bayesian model, (b) Shows the difference between the model predicted and the historical precipitation data, and (c) Represents the historical, validation, and forecasted dataset across the timescale from 1980 to 2027.

One main observation is the LSTM model's increased capability to capture the seasonal trends and patterns from the dataset, when the Bayesian precipitation dataset is used as LSTM input. The authors believe that the effectiveness of LSTM model has been influenced due to the better quality of the input dataset, including less noise and trend clarification, as seen in the Bayesian model generated outputs.

(3) Using Bayesian Statistical Dataset:

As we observed in the previous section, when machine learning models leverage Bayesian data as inputs they perform better in capturing seasonal trends and patterns within the datasets. To validate this observation, this section will discuss the forecasting results of machine learning models using the Bayesian statistical dataset input, specifically using the Large Lake Statistical Water Balance Model (L2SWBM). We use the output data of water balance components from the L2SWBM. Additionally, the diversions and change in storage are computed using WBE (Equation 1). The dataset spans from 1/1/1980 to 12/1/2018 with data expressed in thousand-acre feet (kAc-Ft). For all models, the training data encompasses the period from 1/1/1980 to 2/1/2009, which is 80% of the initial dataset, while the validation set starts from 3/1/2009 to 12/1/2018, which is 20% of the final dataset. Forecasting is also consistent across all the models, which is from 1/1/2019 to 12/1/2023. The forecasting is applied to determine future precipitation, evaporation, natural runoff, and diversions, which then allows us to calculate change in storage using WBE. Using this Bayesian dataset we developed three model types: a Random Forest (RF) model, a Long Short-Term Memory (LSTM) model, and an LSTM Ensemble model.

i. Random Forest (RF) model using L2SWBM data:

As mentioned in the methodology we created two variations of the Random Forest (RF) model: A simple RF model and a fine-tuned RF model.

a) Simple Random Forest

The results of RMSE and MAE between the Simple Random Forest (RF) model predicted and the historical data of each water balance components, including change in storage, across the validation period are shown in Table 7.

Parameters (kAc-Ft)	**RMSE**	**MAE**
Precipitation	0.039	0.011
Evaporation	0.04	0.022
Natural Runoff	1.728	0.251
Diversions	0.95	0.186
Change in storage	1.108486	0.284633

Table 7: The table shows the RMSE and MAE metrics comparing the predictions of the simple RF model to historical data across the validation dataset period.

Based on the predicted data, it's evident that the model's performance closely mirrors the historical data for each of the water balance components. This observation is clearly supported by the Figure 10. In these figures, historical data is depicted in blue, while model predictions are shown in red, and the residual values representing the difference are in plot, all of which across the validation period. The close alignment in figures between the model results in red with the historical data in blue suggests exceptional model performance (Figure 10a, c, e, g, i). However, this level of accuracy raises concerns about potential overfitting, especially considering the lack of hyperparameter tuning within the Random Forest (RF) model in this case. Essentially, the model's

parameters are so closely aligned with the historical data that they appear to be exactly or closely similar. This is particularly evident in the residual plots, where the differences are nearly negligible across all parameters during the validation period. Notably, the model demonstrates the least overfitting with evaporation dataset as compared to the other components. Addressing this overfitting issue is important, which would involve fine-tuning the RF model.

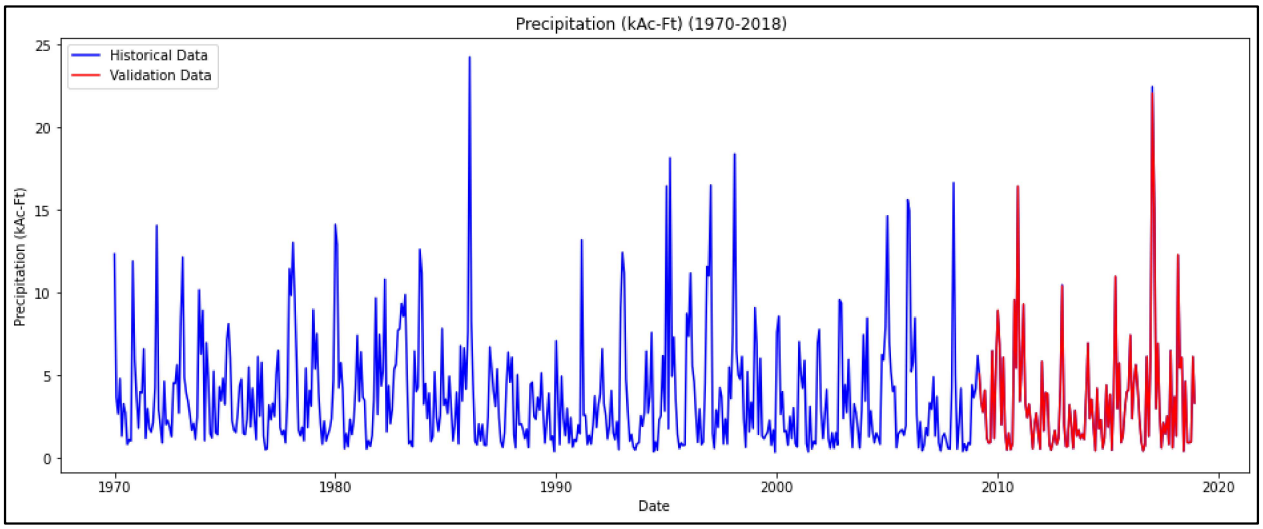

(a)

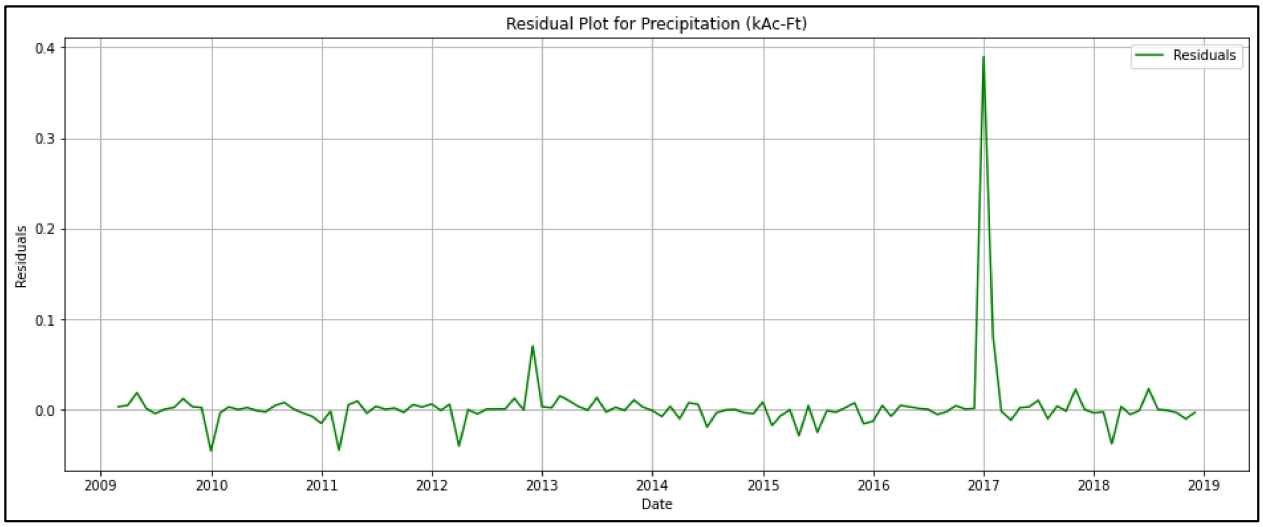

(b)

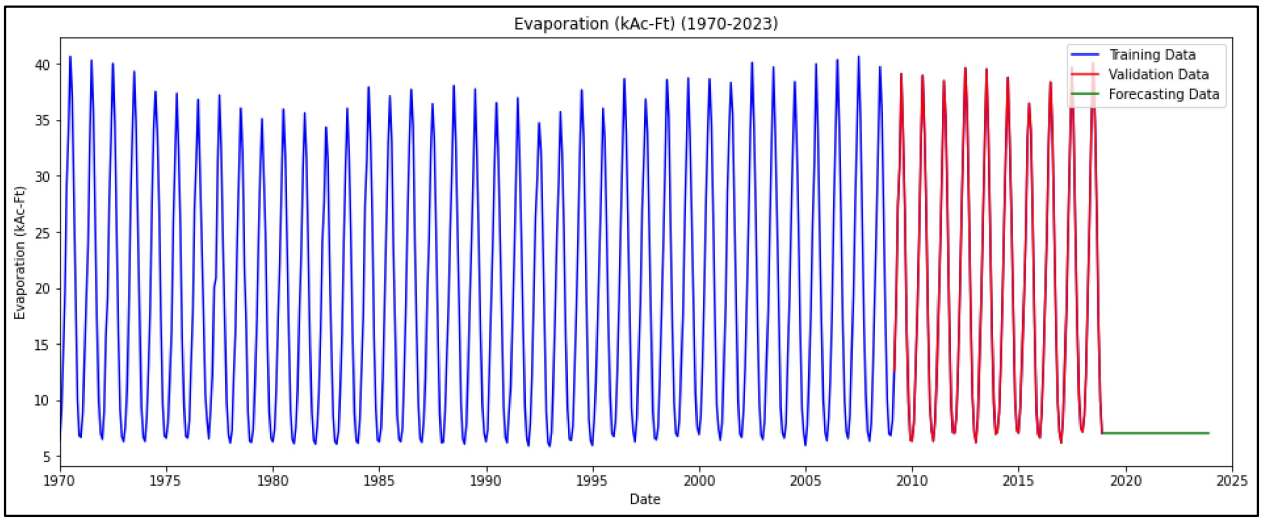
Evaporation (kAc-Ft) (1970-2023)
Training Data
Validation Data
Forecasting Data
Evaporation (kAc-Ft)
Date

(c)

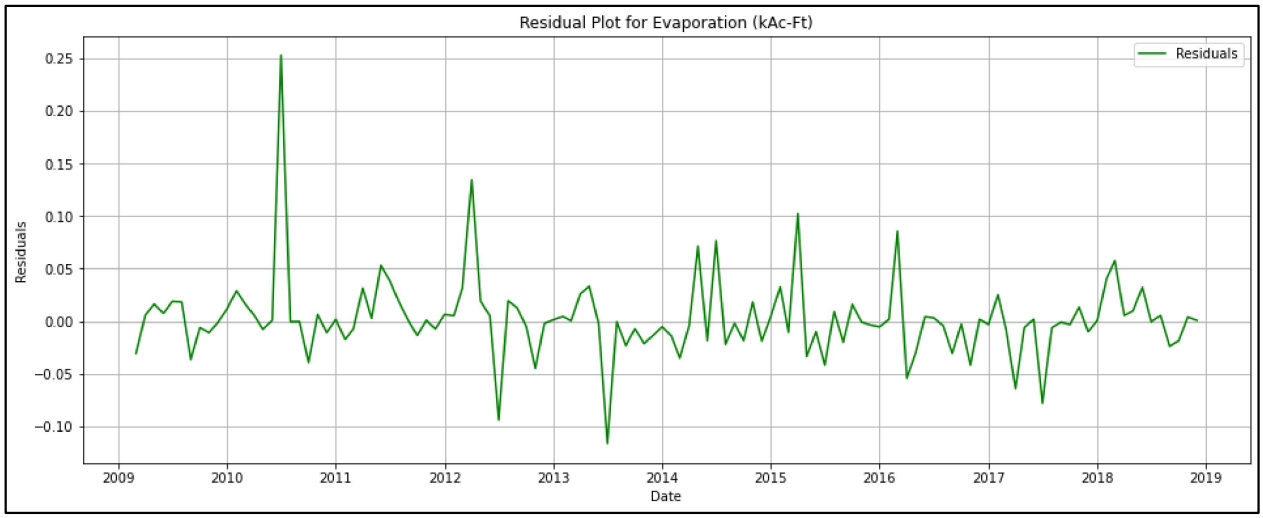
Residual Plot for Evaporation (kAc-Ft)
Residuals
Residuals
Date

(d)

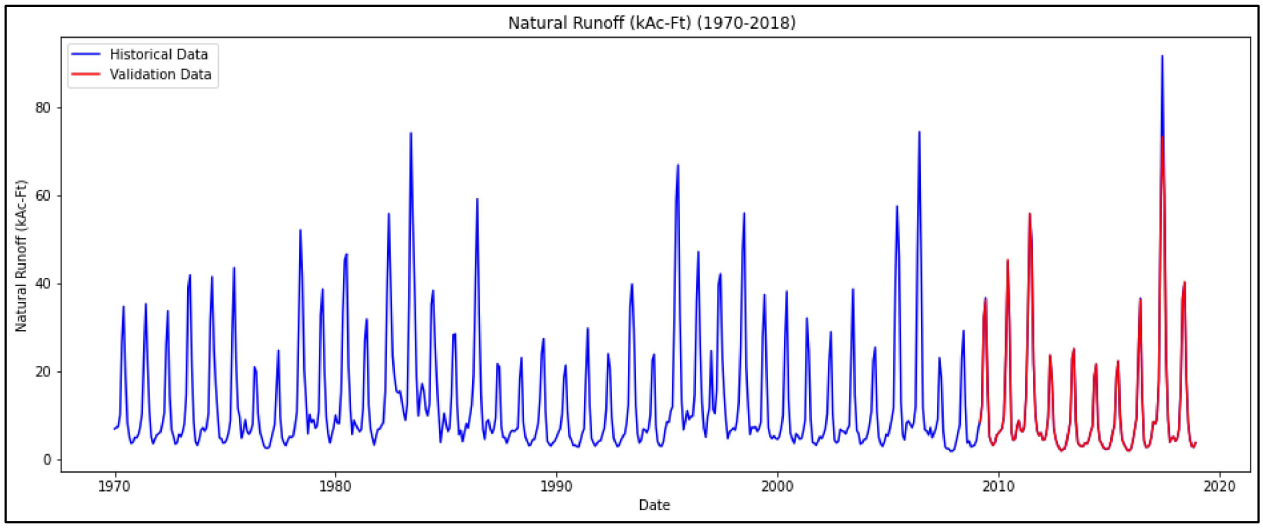
Natural Runoff (kAc-Ft) (1970-2018)
Historical Data
Validation Data
Natural Runoff (kAc-Ft)
Date

(e)

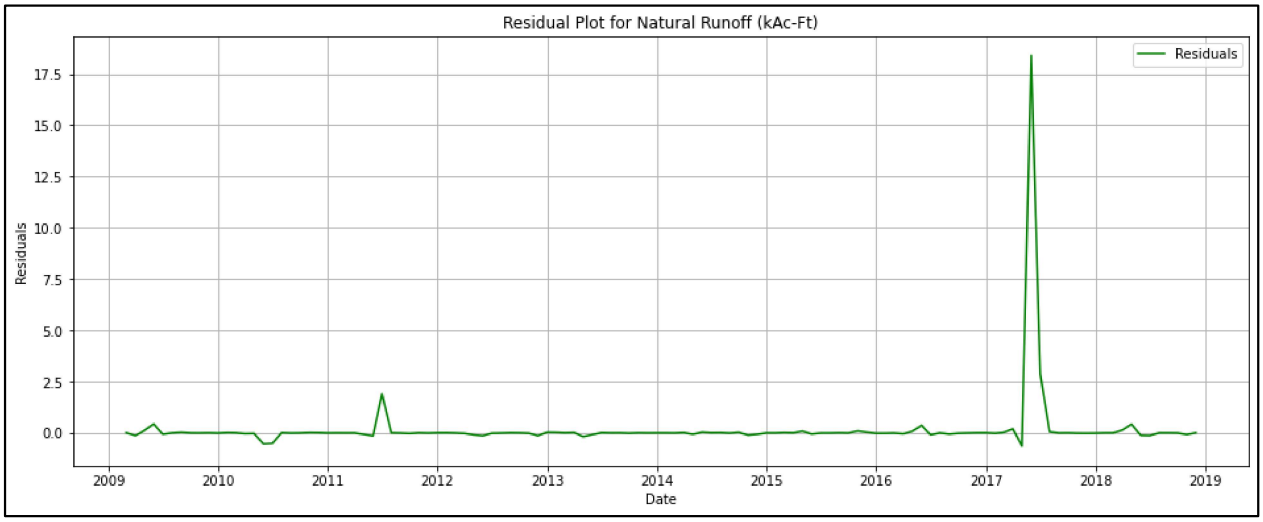
Residual Plot for Natural Runoff (kAc-Ft)
Residuals
Residuals
17.5
15.0
12.5
10.0
7.5
5.0
2.5
0.0
2009
2010
2011
2012
2013
2014
2015
2016
2017
2018
2019
Date

(f)

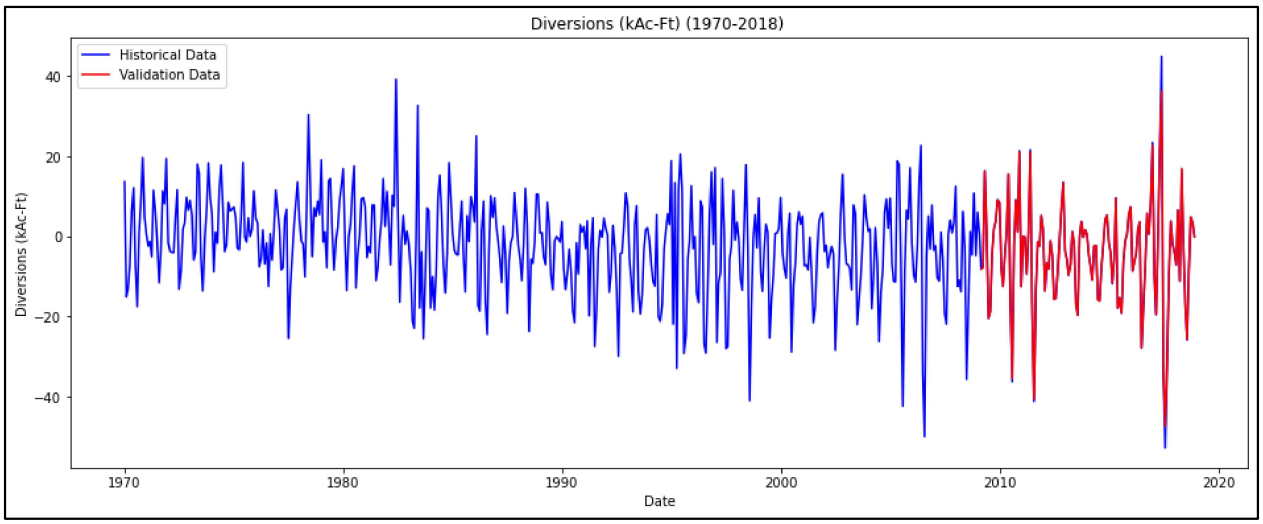
Diversions (kAc-Ft) (1970-2018)
Historical Data
Validation Data
Diversions (kAc-Ft)
40
20
0
−20
−40
1970
1980
1990
2000
2010
2020
Date

(g)

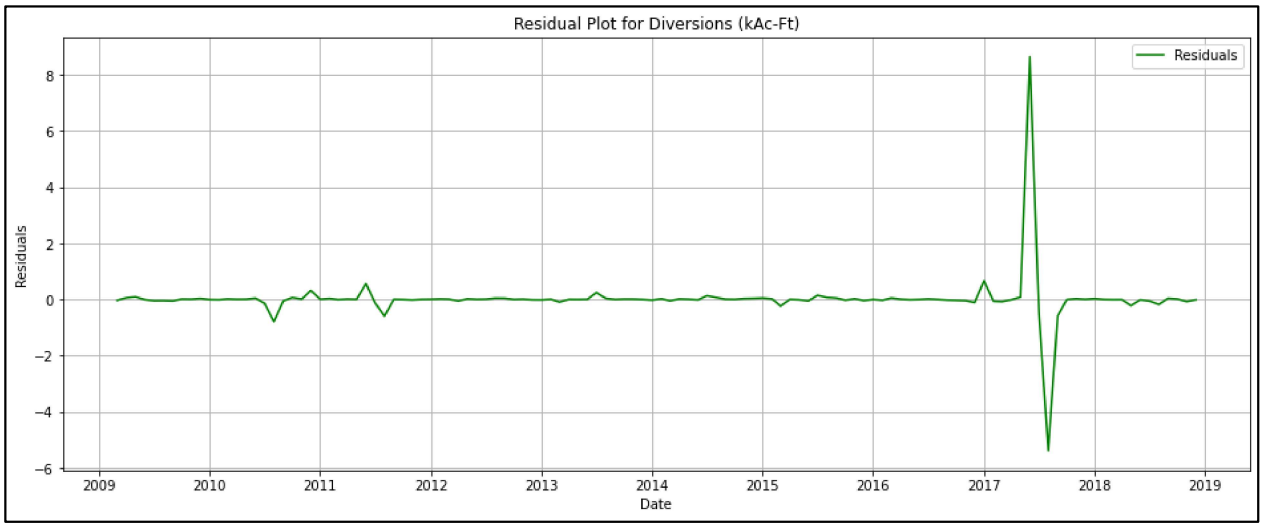
Residual Plot for Diversions (kAc-Ft)
Residuals
Residuals
8
6
4
2
0
−2
−4
−6
2009
2010
2011
2012
2013
2014
2015
2016
2017
2018
2019
Date

(h)

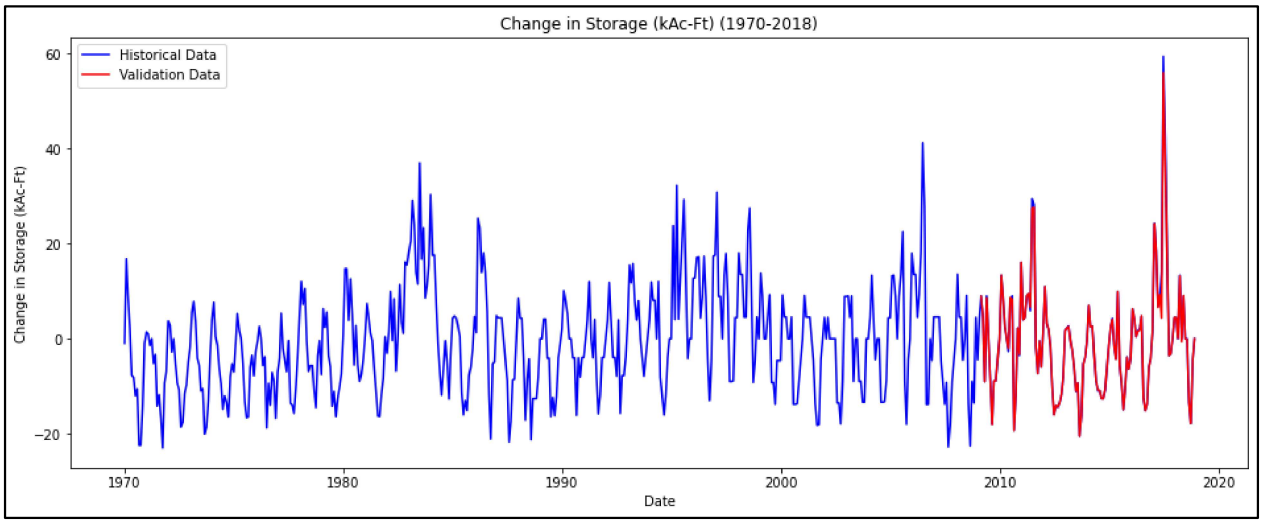

(i)

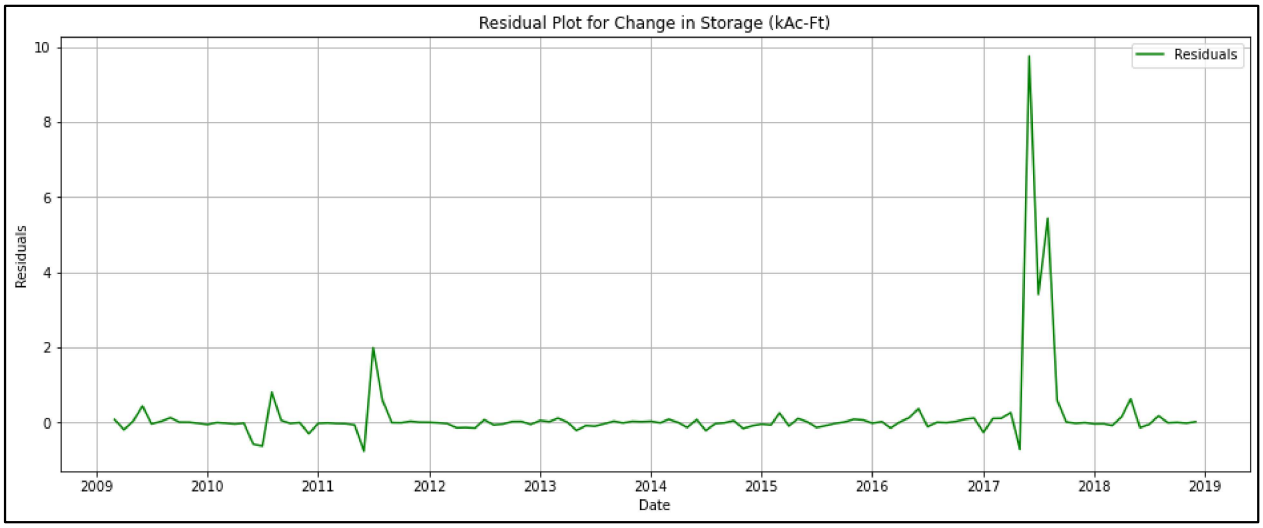

(j)

Figure 10: The subfigures (a, c, e, g, i) represents the visualization of the model's predicted and the historical data for each water balance component, including change in storage, in blue and red lines respectively across the validation dataset period. The subfigures (b, d, f, h, j) shows the residual plots for each water balance component, including change in storage, also across the validation dataset period.

Figure 11 shows the RF model results in the forecasting period, which starts from 1/1/2019 to 12/1/2023, along with representation of the historical and the validation dataset in those figures. The model's forecasting data are in green. Figure 11 underscores the RF model's limitations in regressive forecasting as discussed earlier in the RF model's results using historical water levels. Despite extensive model training, the model merely replicates the last known value from the training set throughout the forecasting period, suggesting a significant challenge in its learning capability for regressive forecasting.

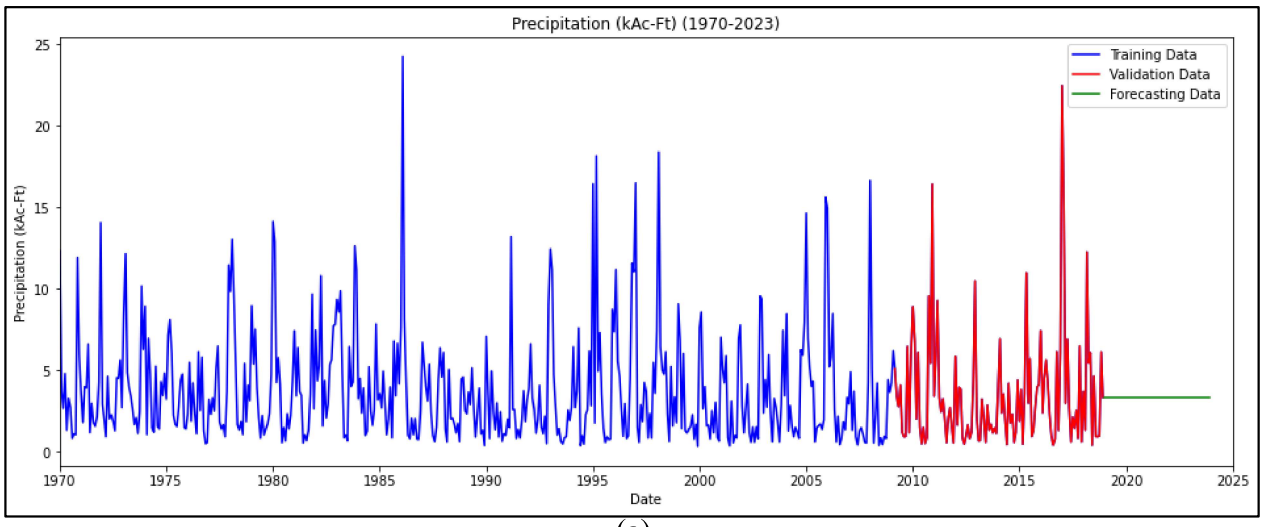

(a)

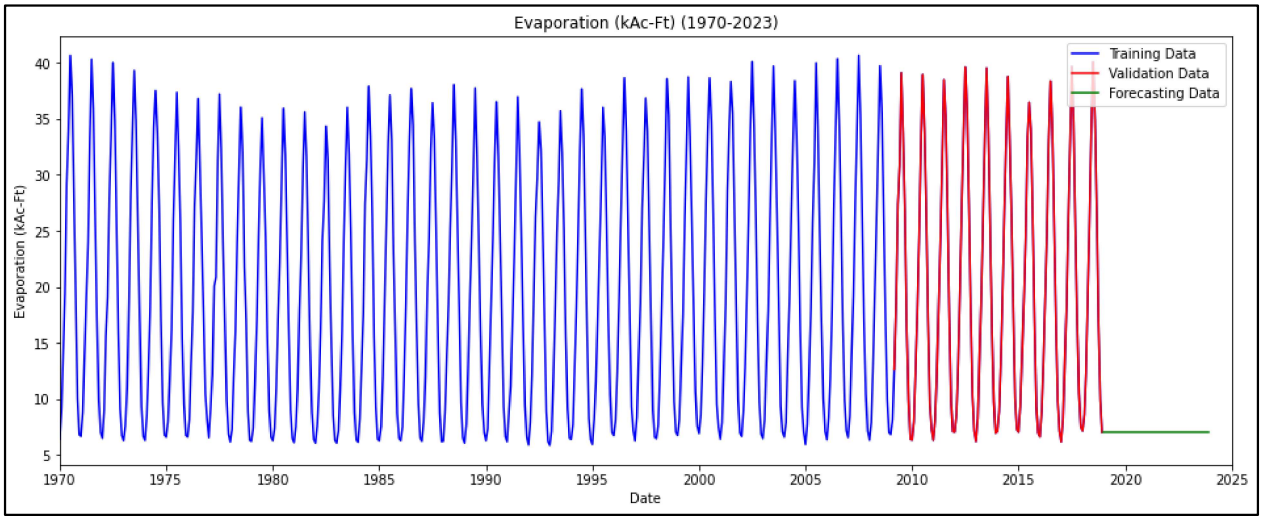

(b)

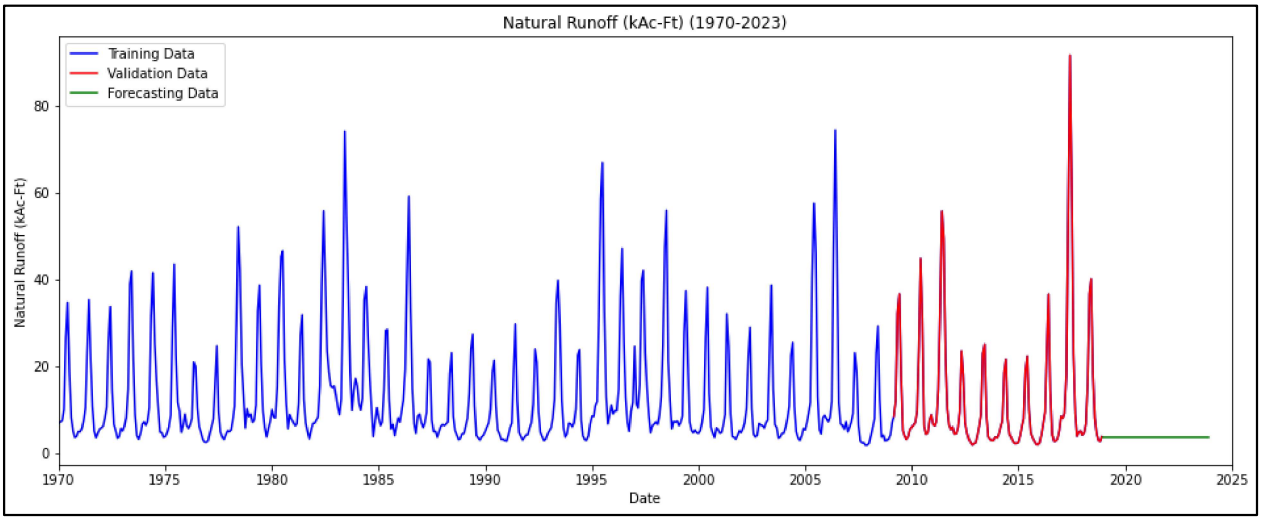
Natural Runoff (kAc-Ft) (1970-2023)
Training Data
Validation Data
Forecasting Data
Natural Runoff (kAc-Ft)
Date

(c)

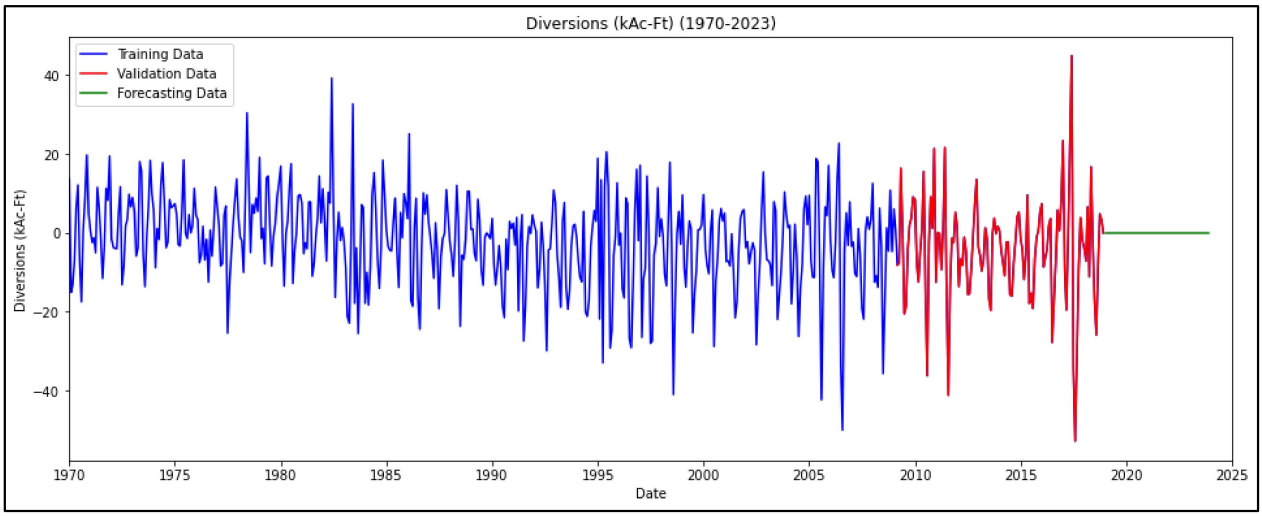
Diversions (kAc-Ft) (1970-2023)
Training Data
Validation Data
Forecasting Data
Diversions (kAc-Ft)
Date

(d)

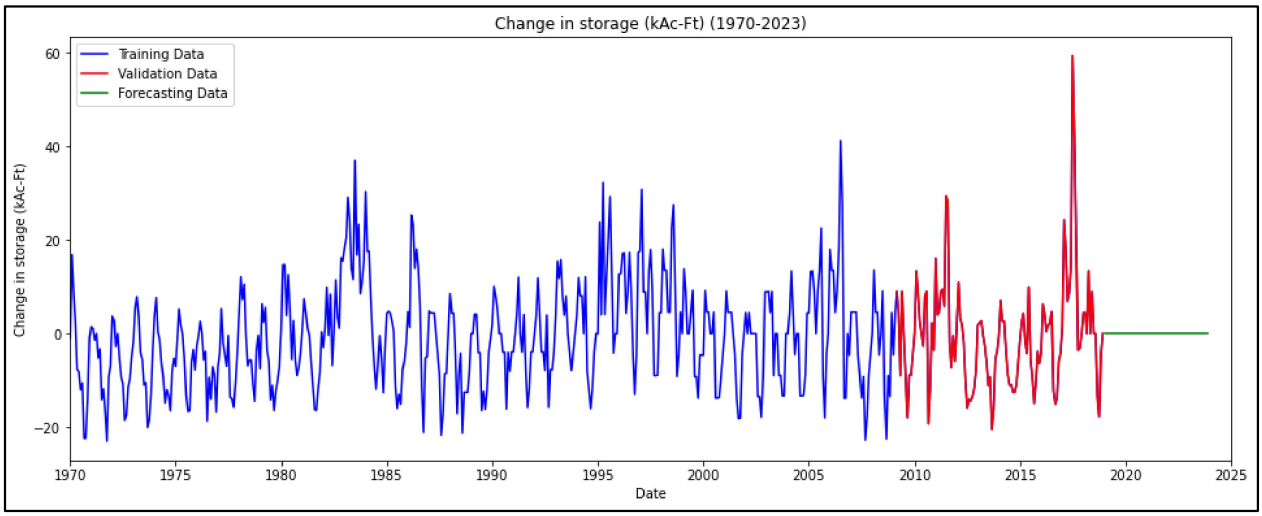
Change in storage (kAc-Ft) (1970-2023)
Training Data
Validation Data
Forecasting Data
Change in storage (kAc-Ft)
Date

(e)

Figure 11: The subfigures (a, b, c, d, e) represents the forecasting results of the RF model across the time scale of 2019 to 2023. The constant forecasting data across all components underscore a fundamental flaw in our RF model's algorithm to regressive forecasting.

b) Tuned Random Forest

The Tuned Random Forest (RF) model's performance is also analyzed using RMSE and MAE by comparing the model predicted results with the historical data for precipitation, evaporation, natural runoff, diversions, and calculated change in storage. The RMSE and MAE values are shows in Table 8.

Parameters (kAc-Ft)	**RMSE**	**MAE**
Precipitation	0.283	0.041
Evaporation	0.055	0.037
Natural Runoff	2.126	0.316
Diversions	1.627	0.29
Change in storage	1.44782	0.366284

Table 8: This table illustrates the performance of the tuned RF model across the validation dataset for each climate parameter.

A close examination reveals a slight decrease in model performance compared to the previous simple RF model, which had closely matched the historical data of each component due to overfitting. This change in performance is due to slightly reduced overfitting, which is evident in the Figure 12. Here the historical data are depicted in blue and model predictions in red across the validation period. The residual data also suggests that while the model continues to track closely to the historical data (Figure 12b, d, f, h, j), the degree of overfitting has slighty diminished due to

the fine-tuning of hyperparameters. The fine-tuned RF model shows the least overfitting for evaporation and change in storage.

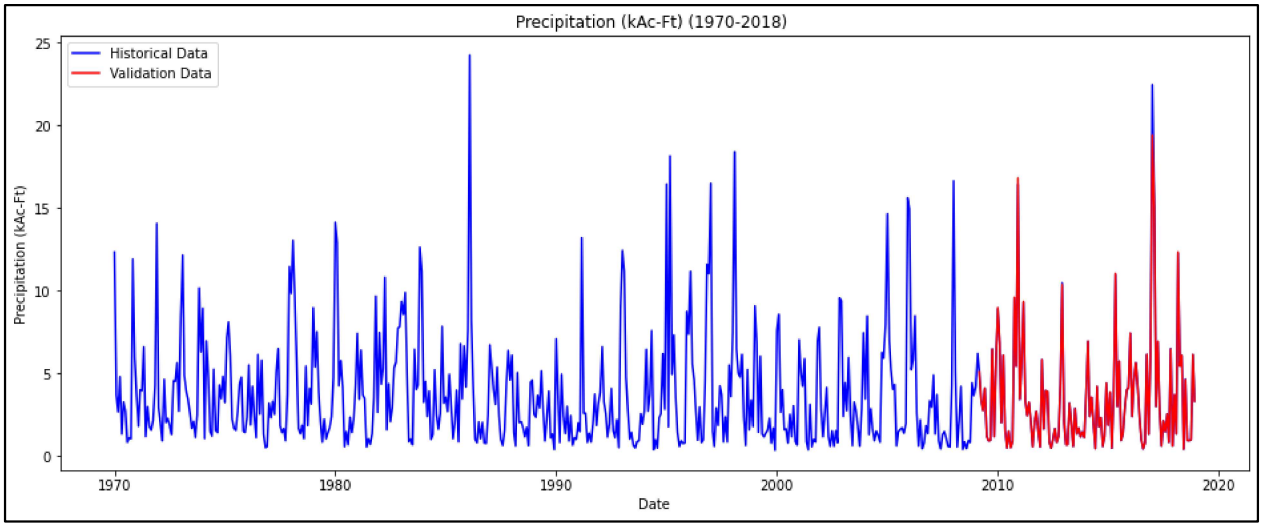

(a)

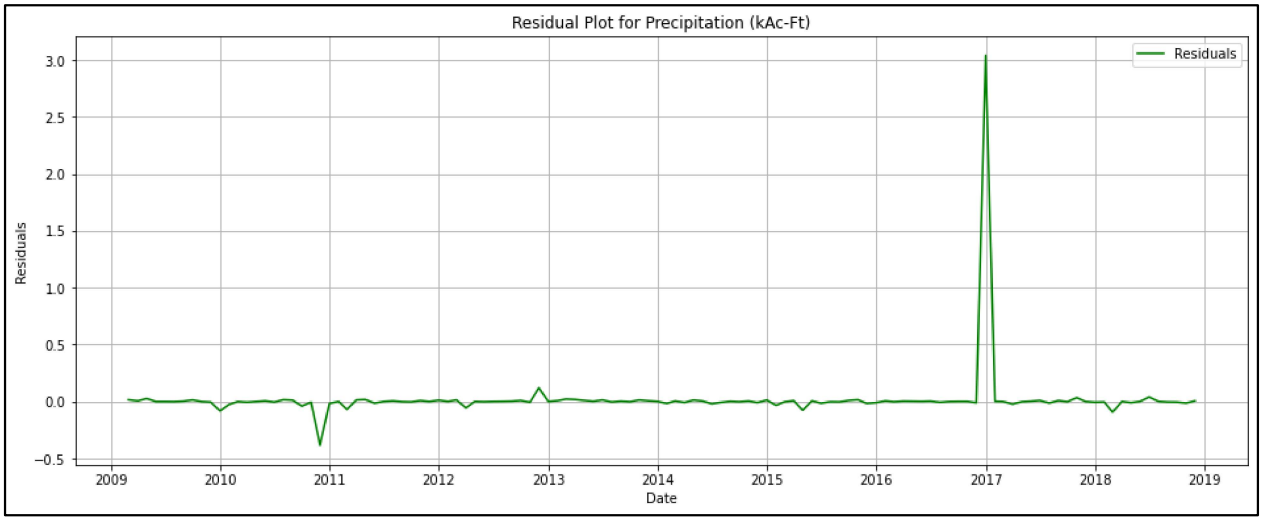

(b)

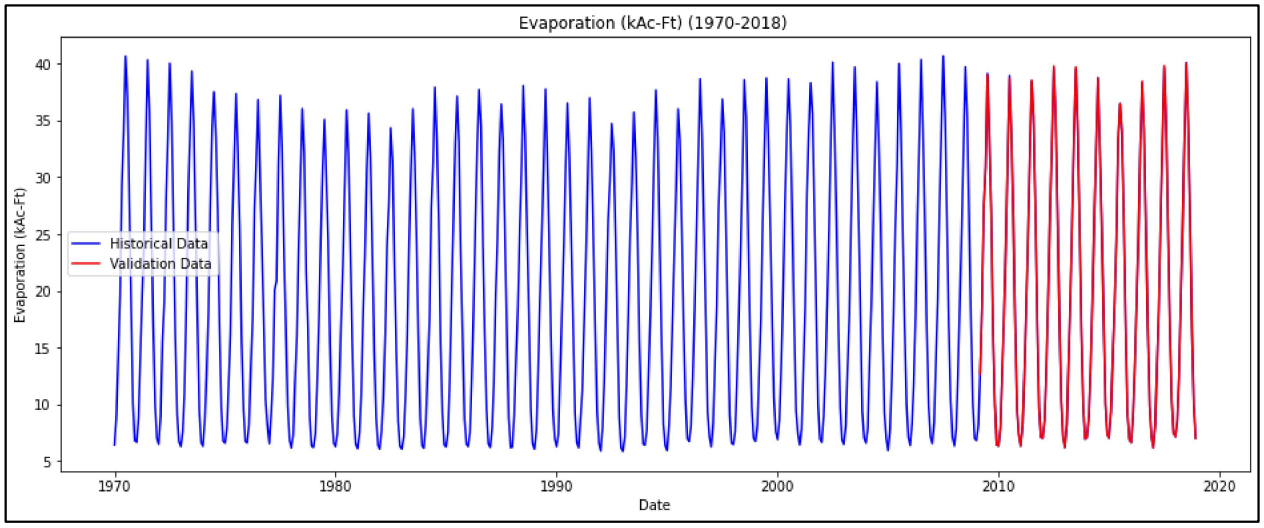
Evaporation (kAc-Ft) (1970-2018)
Historical Data
Validation Data
Evaporation (kAc-Ft)
Date
40
35
30
25
20
15
10
5
1970
1980
1990
2000
2010
2020

(c)

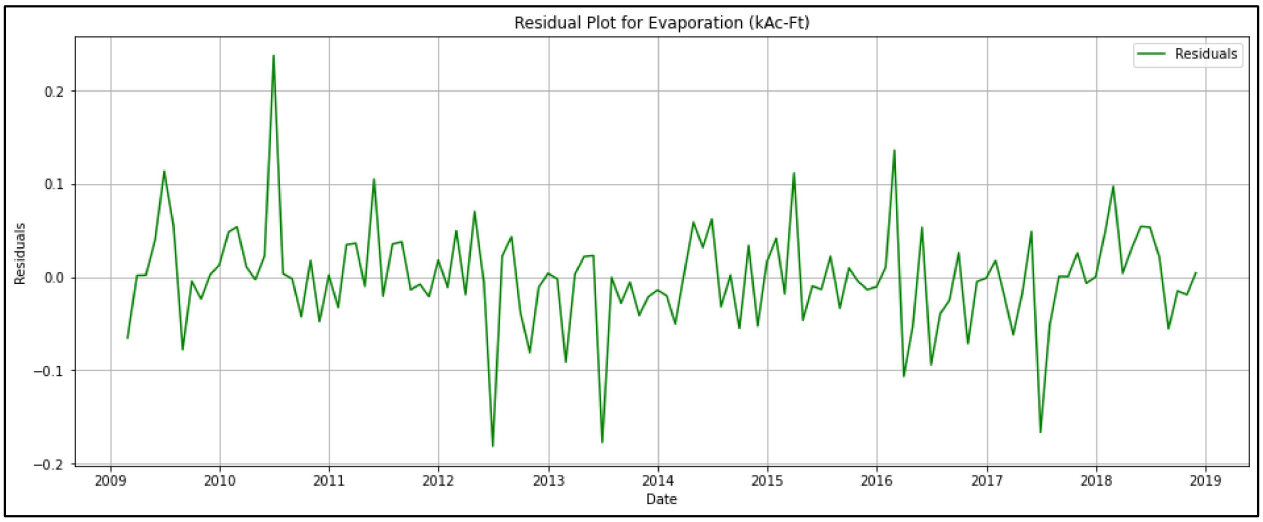
Residual Plot for Evaporation (kAc-Ft)
Residuals
Residuals
Date
0.2
0.1
0.0
−0.1
−0.2
2009
2010
2011
2012
2013
2014
2015
2016
2017
2018
2019

(d)

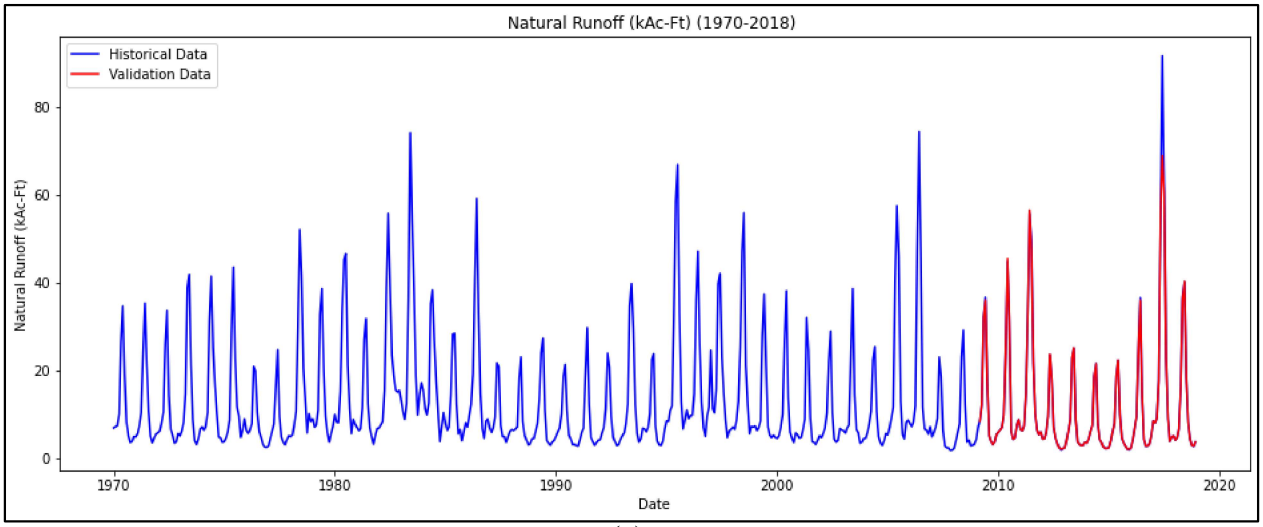
Natural Runoff (kAc-Ft) (1970-2018)
Historical Data
Validation Data
Natural Runoff (kAc-Ft)
Date
80
60
40
20
0
1970
1980
1990
2000
2010
2020

(e)

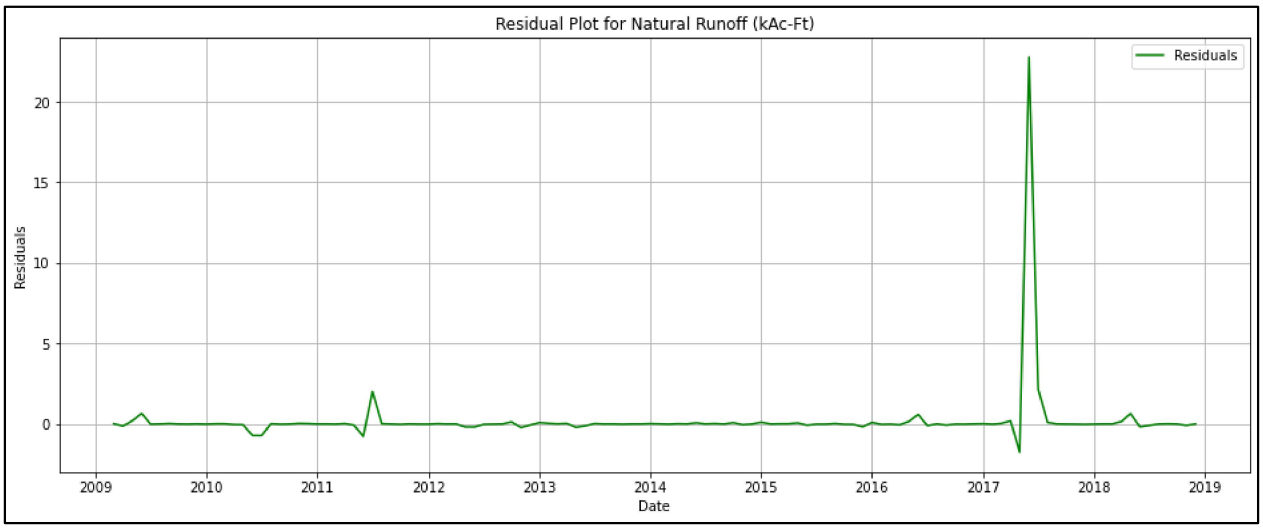
Residual Plot for Natural Runoff (kAc-Ft)
Residuals
Residuals
20
15
10
5
0
2009
2010
2011
2012
2013
2014
2015
2016
2017
2018
2019
Date

(f)

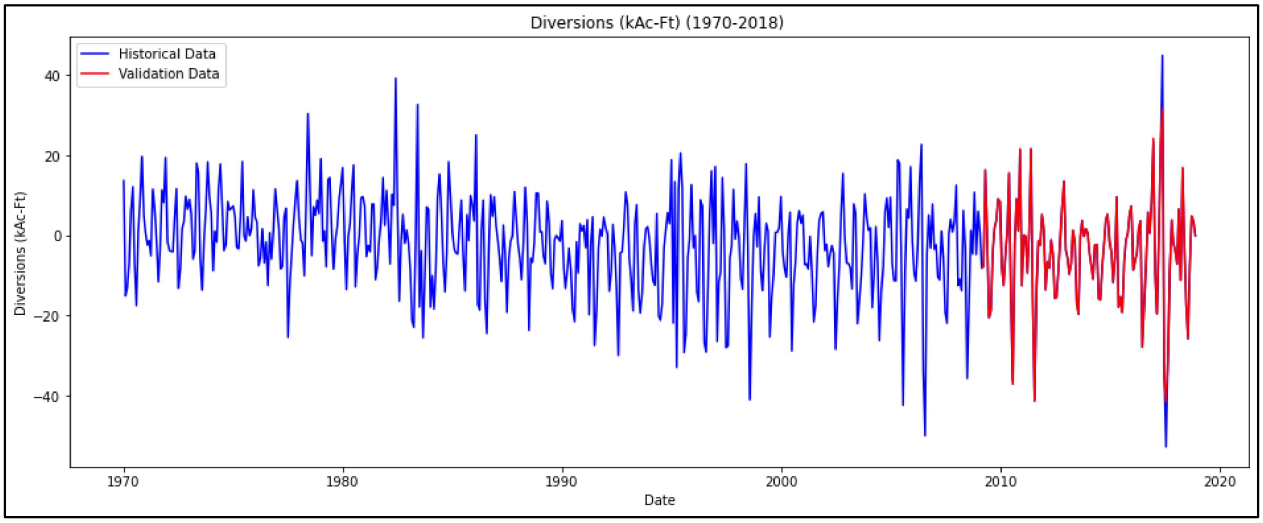
Diversions (kAc-Ft) (1970-2018)
Historical Data
Validation Data
Diversions (kAc-Ft)
40
20
0
−20
−40
1970
1980
1990
2000
2010
2020
Date

(g)

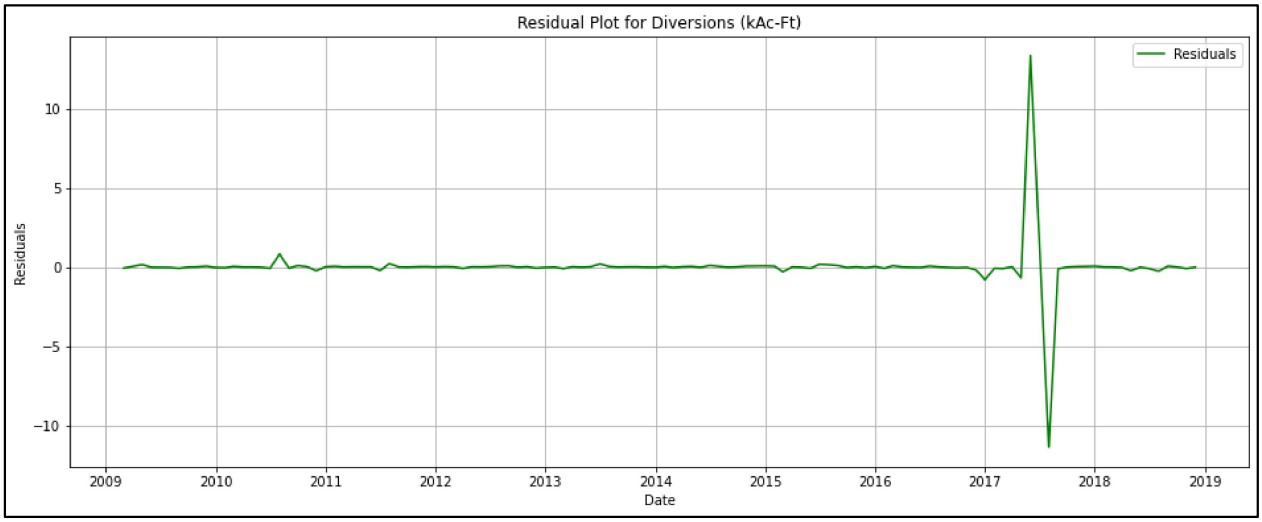
Residual Plot for Diversions (kAc-Ft)
Residuals
Residuals
10
5
0
−5
−10
2009
2010
2011
2012
2013
2014
2015
2016
2017
2018
2019
Date

(h)

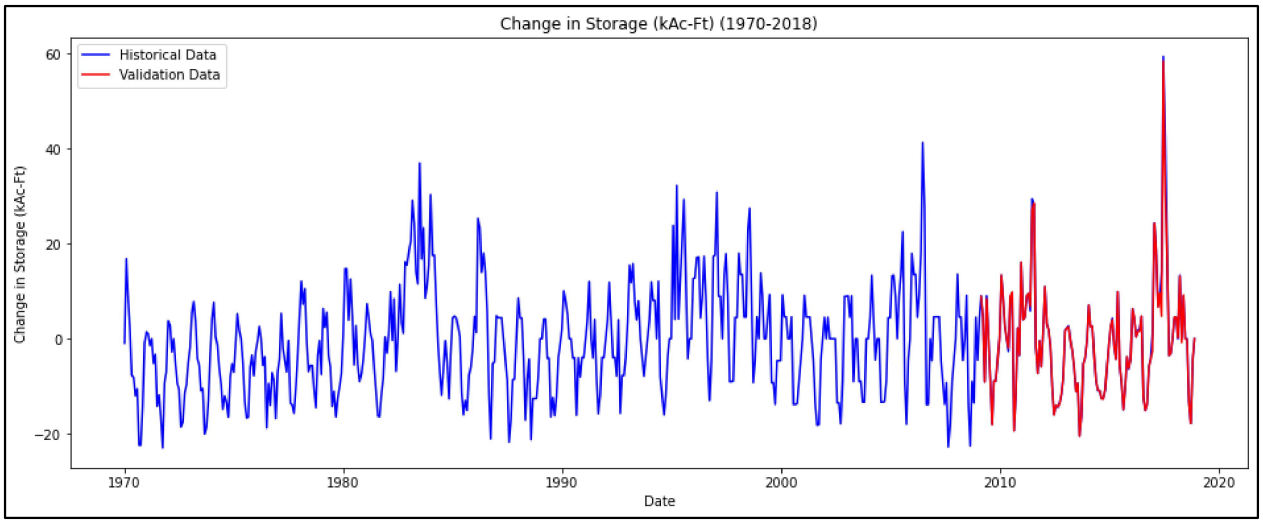

(i)

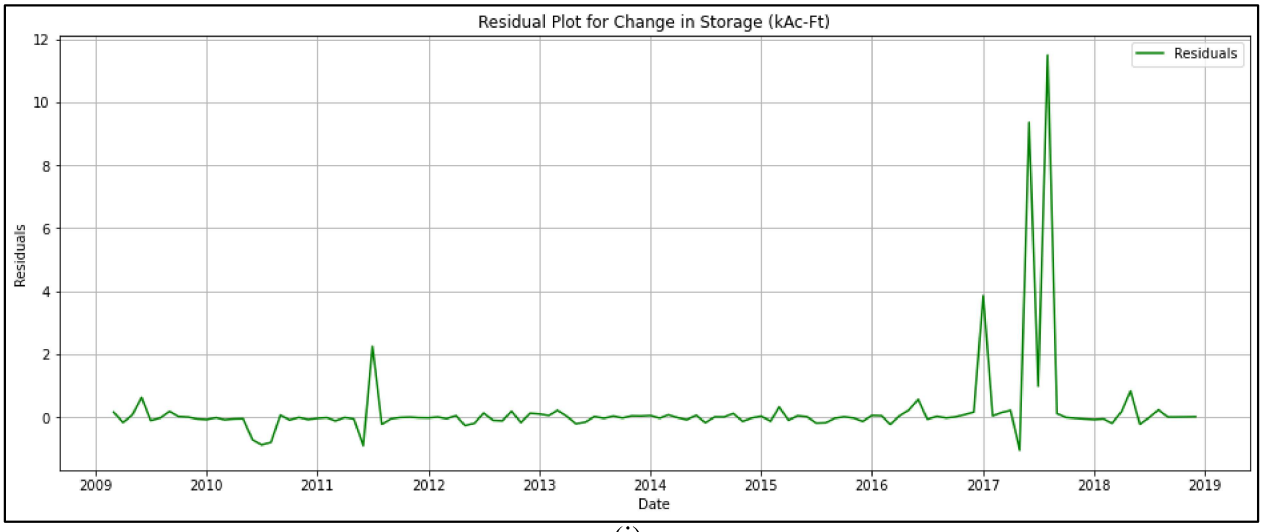

(j)

Figure 12: The subfigures (a, c, e, g, i) represents the visualization of the model's predicted and the historical data for each water balance component, including change in storage, in blue and red lines respectively across the validation dataset period. The subfigures (b, d, f, h, j) shows the residual plots for each water balance component, including change in storage, also across the validation dataset period.

Despite fine-tuning to reduce overfitting and improve the RF model's capability in regressive forecasting, the Figure 13 shows a continued challenge in the RF model's forecasting. The model forecasting results is depicted in green across the figures below, which shows that the model tends to replicate the last known value from the training dataset throughout the forecasting period. This behavior indicates a limitation in our model's ability to perform forecasts, suggesting that while the RF model excels in capturing the interdependencies among components, its use in forecasting future results is a challenge.

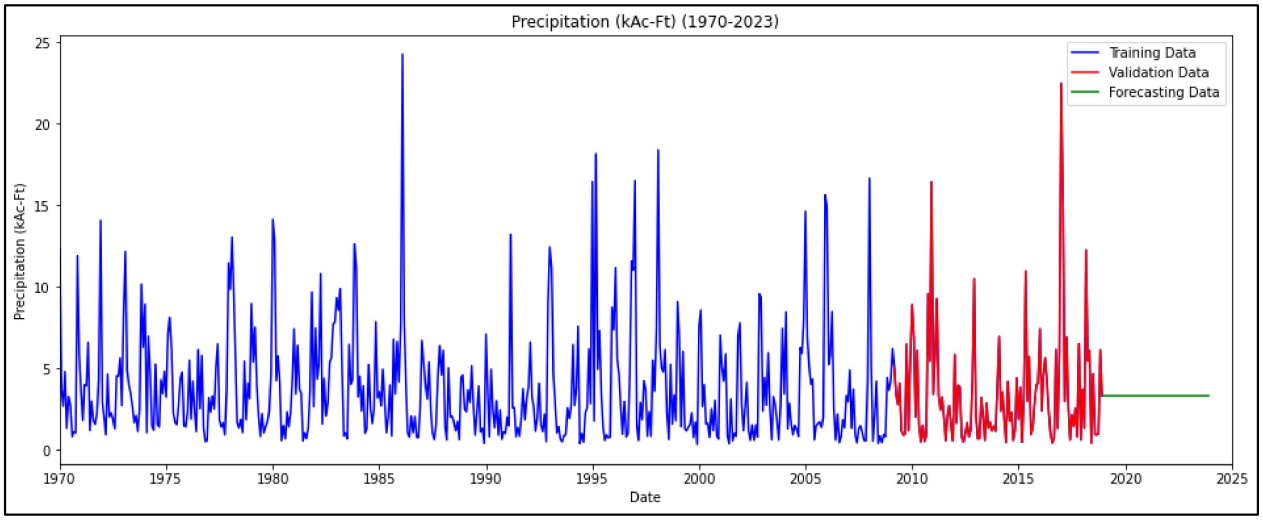

(a)

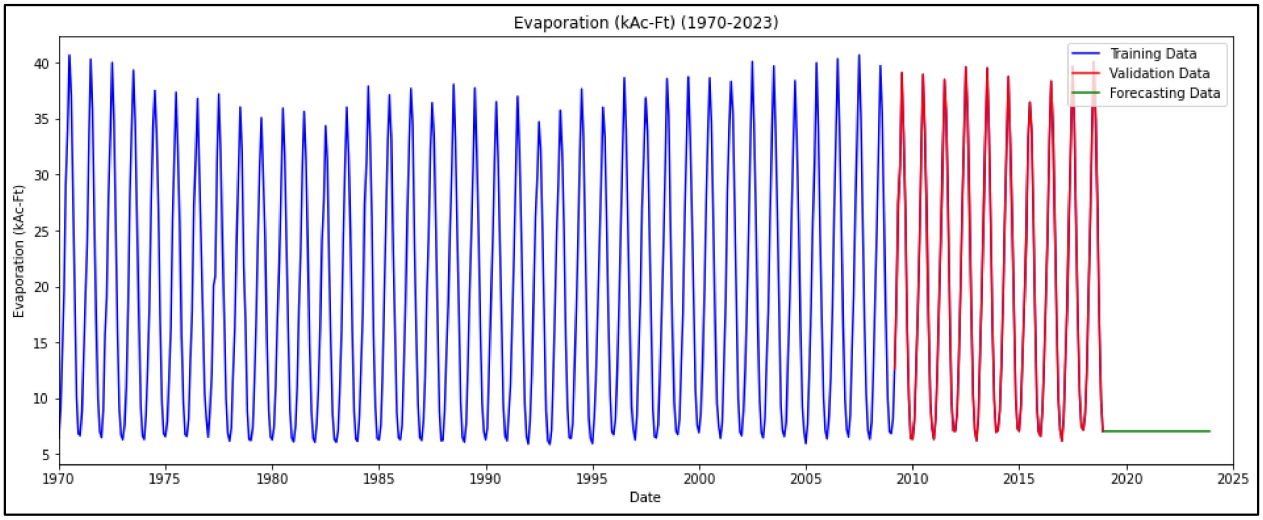

(b)

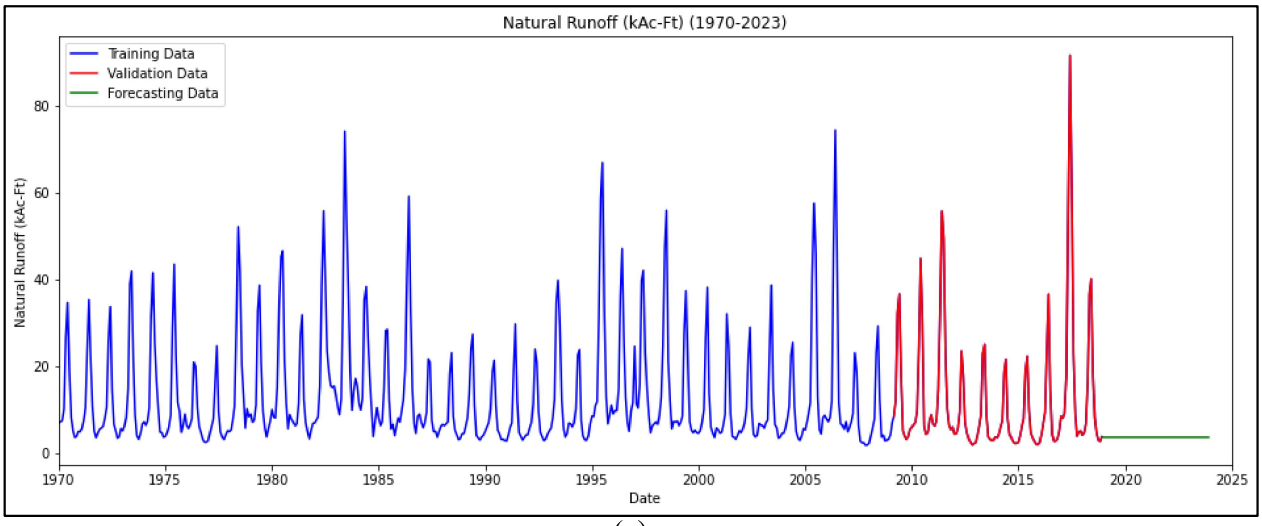
Natural Runoff (kAc-Ft) (1970-2023)
Training Data
Validation Data
Forecasting Data
Natural Runoff (kAc-Ft)
Date

(c)

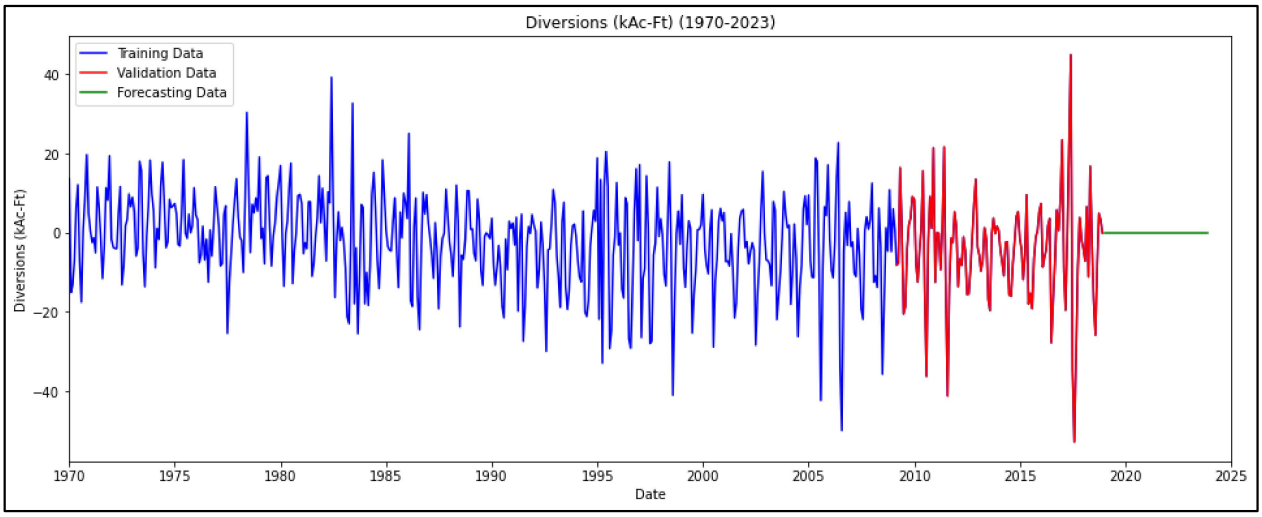
Diversions (kAc-Ft) (1970-2023)
Training Data
Validation Data
Forecasting Data
Diversions (kAc-Ft)
Date

(d)

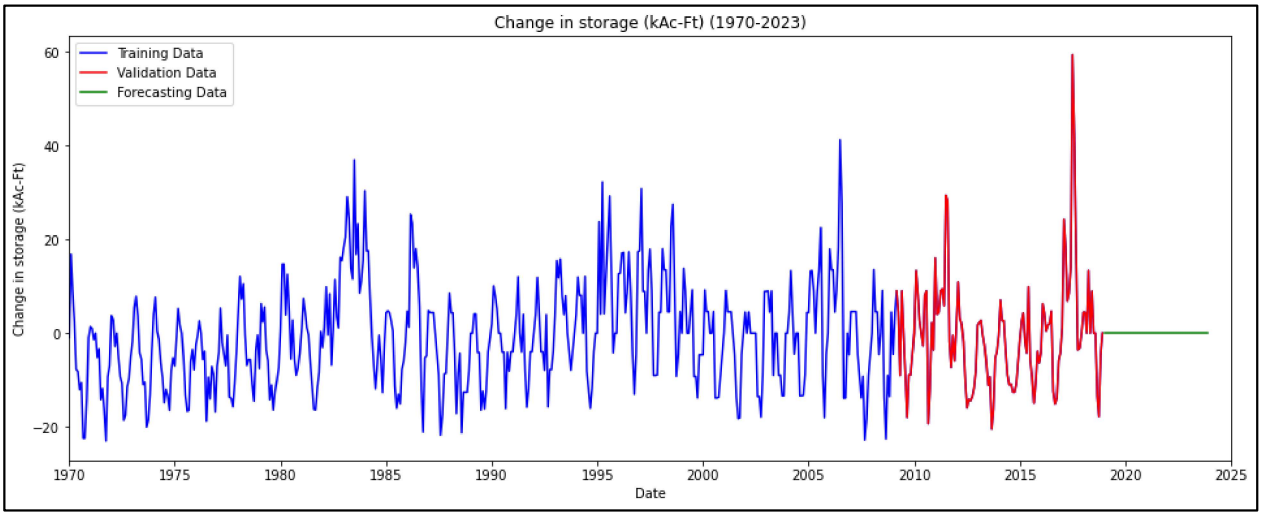
Change in storage (kAc-Ft) (1970-2023)
Training Data
Validation Data
Forecasting Data
Change in storage (kAc-Ft)
Date

(e)

Figure 13: The subfigures (a, b, c, d, e) represents the forecasting results of the fine-tuned RF model across the time scale of 2019 to 2023. The constant forecasting data across all the components underscore a challenge in our RF model's algorithm to regressive forecasting.

ii. Long Short-Term Memory (LSTM) model:

The Long Short-Term Memory (LSTM) model is applied to forecast water balance components, alongside calculating the change in storage using the water balance equation. The model results is evaluated through Root Mean Square Error (RMSE) and Mean Absolute Error (MAE) metrics, as detailed in Table 9. These metrics indicate the model's accuracy in predicting each of the water balance components.

Parameters (kAc-Ft)	**RMSE**	**MAE**
Precipitation	3.2522	2.2635
Evaporation	1.3649	1.0864
Natural Runoff	3.4543	2.6434
Diversions	6.7914	5.259
Change in storage	4.478	3.4367

Table 9: Shows the RMSE and MAE of the LSTM model across the validation dataset range for each of the components of the water balance equation.

Based on the output above it can be said that, despite a slightly poorer performance compared to previous models, which closely matched historical data due to overfitting, the LSTM model demonstrates a commendable ability to understand the input and follow the trajectory of historical

data. This is particularly evident in the model's visualization plots below which aligns with the historical trends. The detailed graphical representation of this analysis is represented below (Figure 14), which shows the LSTM model predictions in red alongside the historical data in blue, providing a visual comparison of the model performance against historical dataset (Figures 14a, c, e, g, i). A notable observation is the model's ability to forecast precipitation, which has high variability across the historical dataset. Conversely, the model tends to underestimate evaporation and overestimate natural runoff. Despite these discrepancies, the LSTM model's overall performance is exceptional, particularly in its ability to capture the seasonal patterns within each of the water balance components. The residual plots in figures below further illustrate the differences between predicted and historical data across the validation period for each water balance components.

These residual plots are particularly helpful as it reveals the model's performance and areas where further adjustments could enhance its forecasting accuracy (Figure 14b, d, f, h, j). It is also important to recall that the LSTM model is trained till 2/1/2009 and based on that learning it is able to predict the data for five years from 1/1/2019 to 12/1/2023. In summary, the LSTM base model shows a notable ability to capture and predict the dynamics of water balance components, showcasing its potential as a valuable tool for forecasting climate-related parameters.

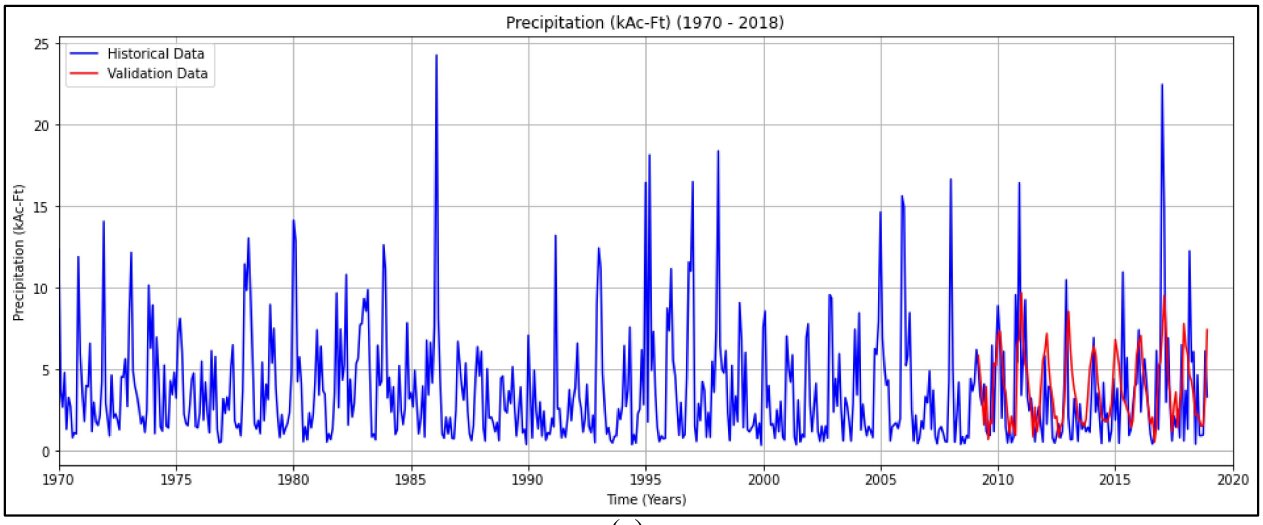
Precipitation (kAc-Ft) (1970 - 2018)
Historical Data
Validation Data
Precipitation (kAc-Ft)
Time (Years)

(a)

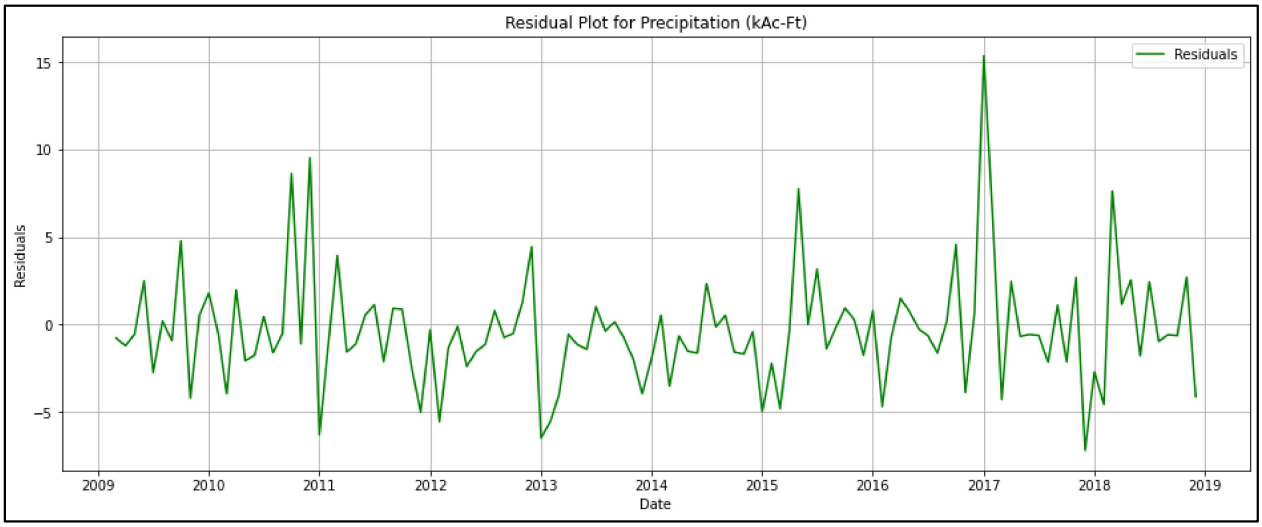
Residual Plot for Precipitation (kAc-Ft)
Residuals
Residuals
Date

(b)

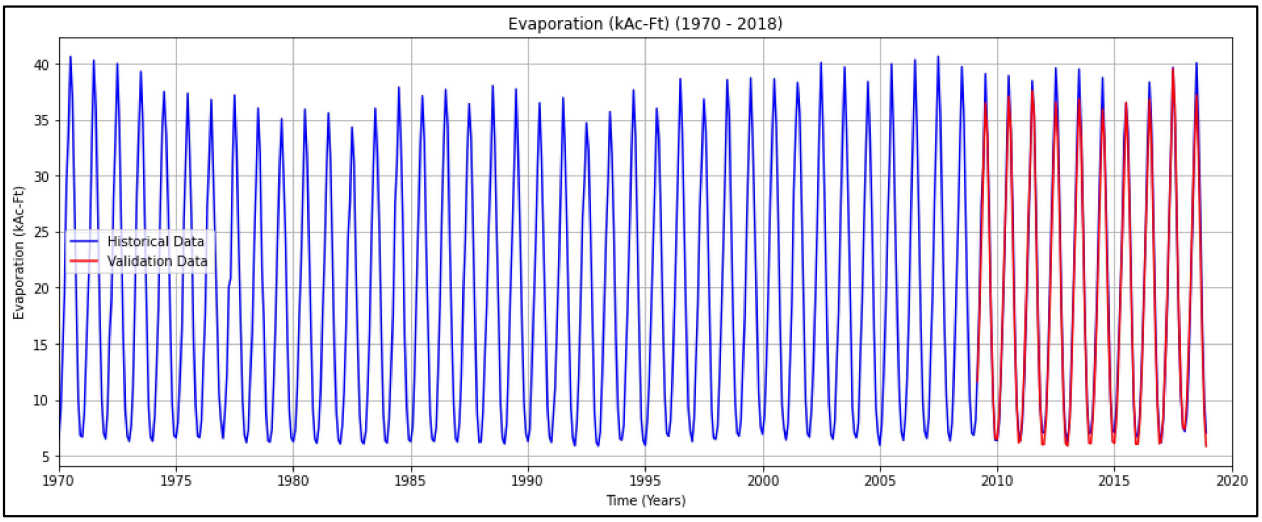
Evaporation (kAc-Ft) (1970 - 2018)
Historical Data
Validation Data
Evaporation (kAc-Ft)
Time (Years)

(c)

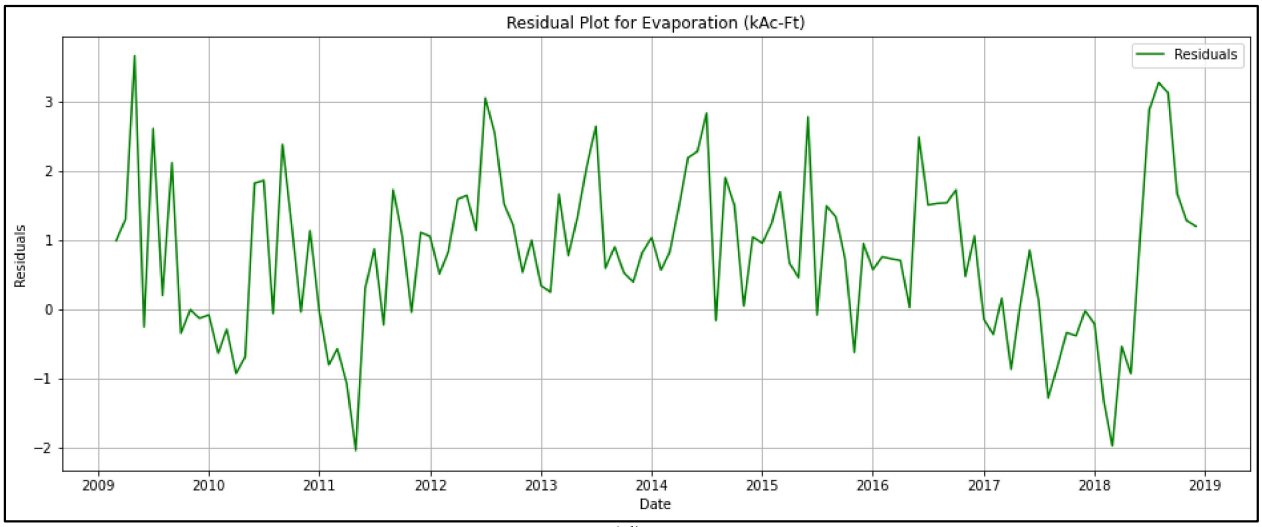
Residual Plot for Evaporation (kAc-Ft)
Residuals
Residuals
Date
3
2
1
0
−1
−2
2009
2010
2011
2012
2013
2014
2015
2016
2017
2018
2019

(d)

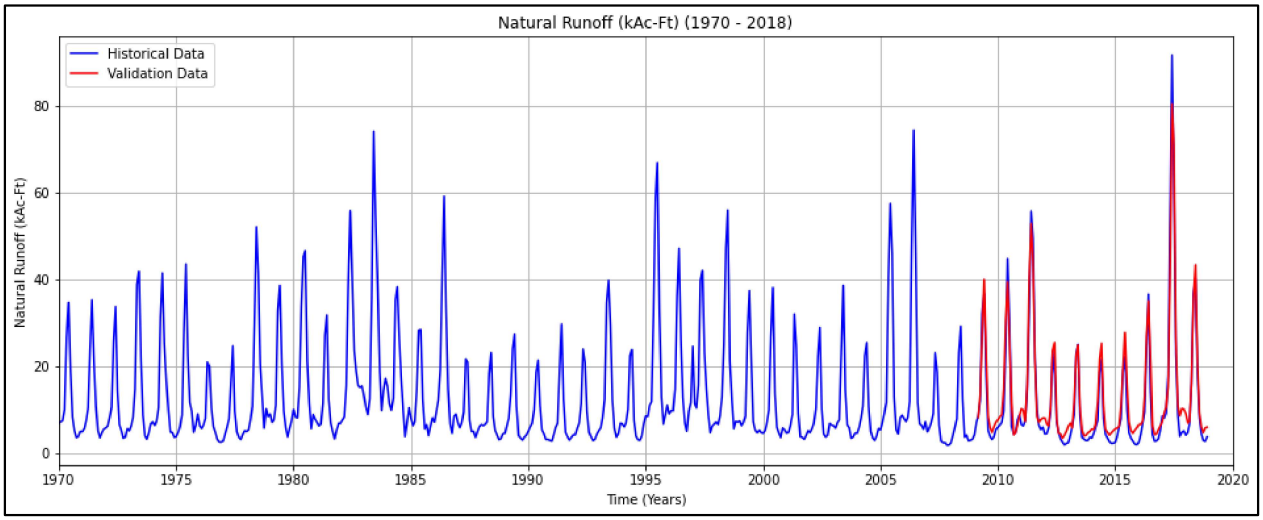
Natural Runoff (kAc-Ft) (1970 - 2018)
Historical Data
Validation Data
Natural Runoff (kAc-Ft)
Time (Years)
80
60
40
20
0
1970
1975
1980
1985
1990
1995
2000
2005
2010
2015
2020

(e)

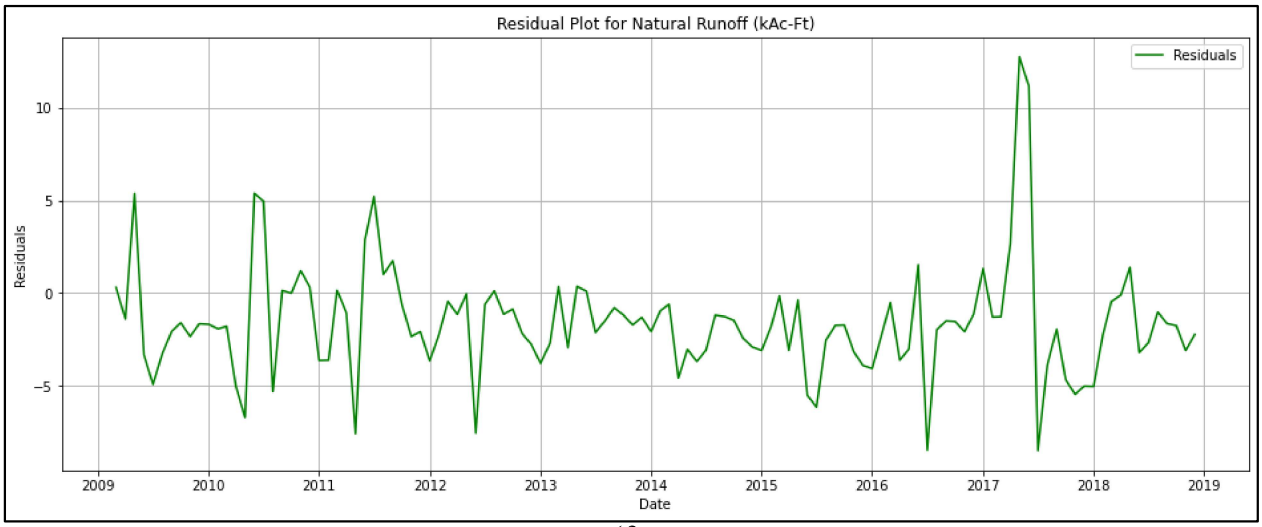
Residual Plot for Natural Runoff (kAc-Ft)
Residuals
Residuals
Date
10
5
0
−5
2009
2010
2011
2012
2013
2014
2015
2016
2017
2018
2019

(f)

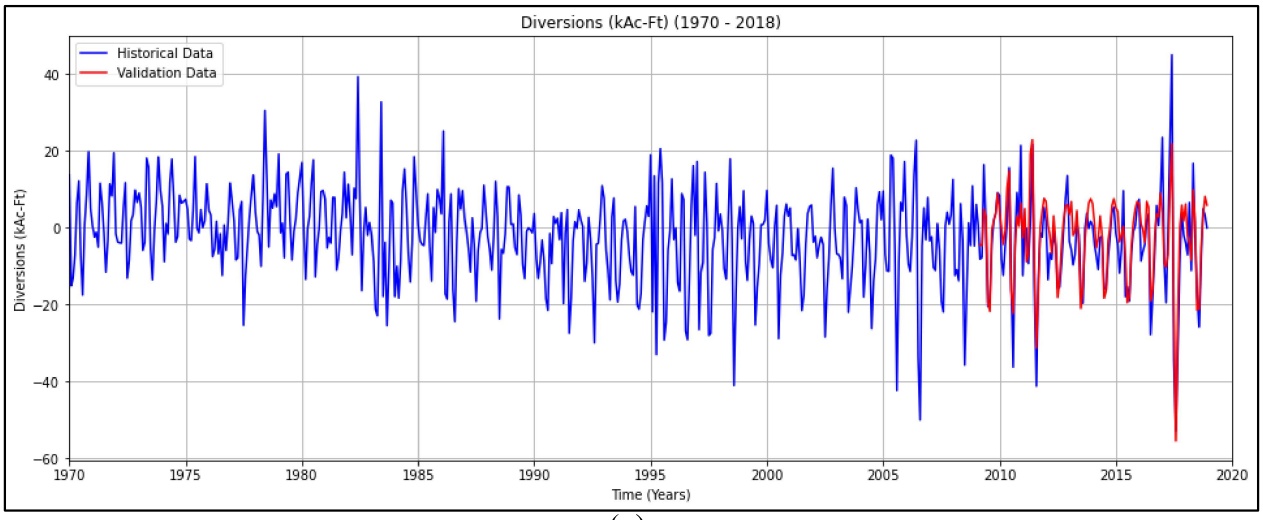
Diversions (kAc-Ft) (1970 - 2018)
Historical Data
Validation Data
Diversions (kAc-Ft)
Time (Years)

(g)

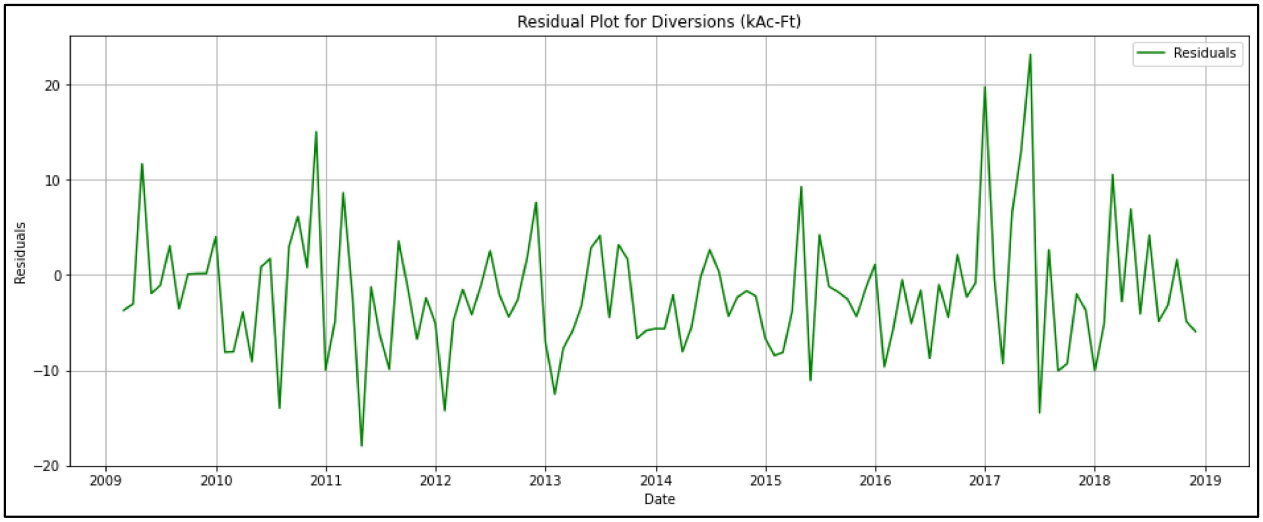
Residual Plot for Diversions (kAc-Ft)
Residuals
Residuals
Date

(h)

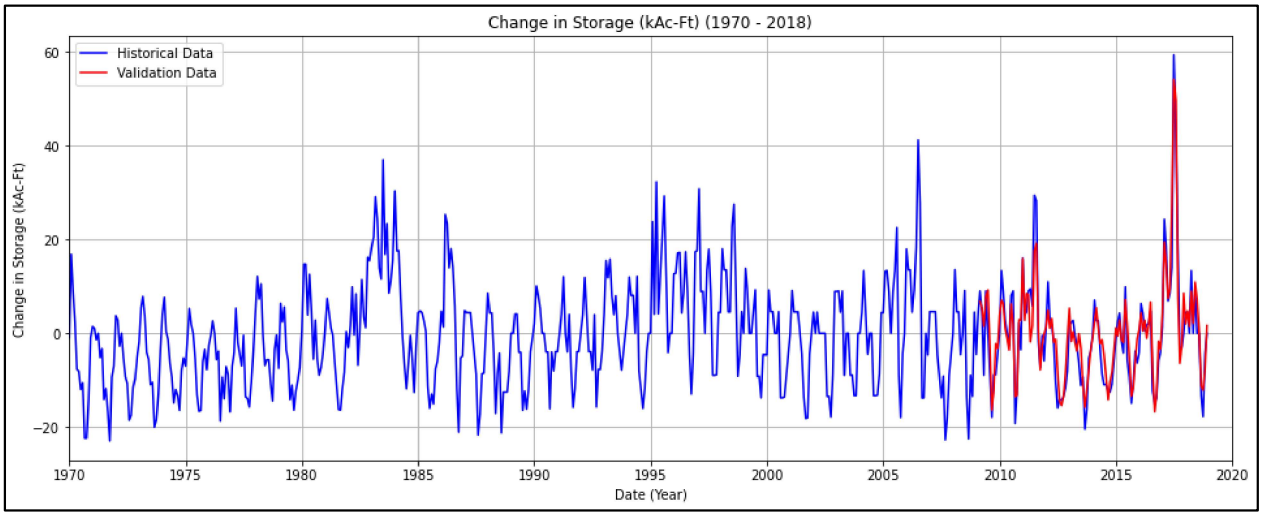
Change in Storage (kAc-Ft) (1970 - 2018)
Historical Data
Validation Data
Change in Storage (kAc-Ft)
Date (Year)

(i)

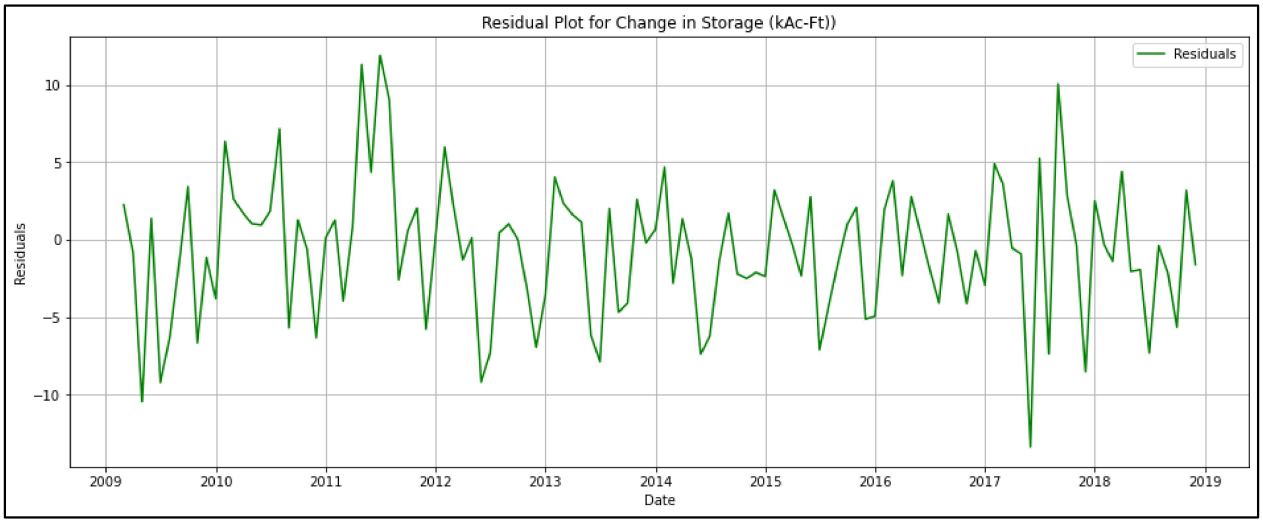

(j)

Figure 14: The figures (a, c, e, g, i) shows the LSTM model predicted data in red and the historical data in blue, offering a direct visual comparison across each component. The figures (b, d, f, h, j) represent residual plots, highlighting the difference between the model's predictions and the historical data.

The forecasting results depicted in the figure 15 shows the LSTM model's ability in identifying underlying patterns within the dataset, including the interdependencies among different components and successfully generating 5-year forecasts. The model successfully captures the seasonal highs and lows across all water balance components. Specifically in the forecasting values, the LSTM model reflects a pattern that is seen in precipitation, shows a slight increase in evaporation, and a significant increase in natural runoff. These results by LSTM model forecasting can be attributed to changing climate.

While the visual changes across these forecasting data may appear small at first glance, it's crucial to remember the magnitude of these shifts, which are measured in thousand-acre feet (kAc-Ft).

Furthermore, the model predicts a gradual decline in storage over the upcoming years, suggesting an insightful understanding of the climate change phenomenon and its incorporation into the forecasting. This ability to reflect climate trends within the predictions underscores the model's sophisticated learning mechanisms. An essential aspect of the LSTM model's operation is its reliance on its own previously predicted data for subsequent forecasting intervals. However, this iterative process while efficient also introduces the potential for an accumulation of errors, where inaccuracies at any given timestep would increase as LSTM model iteratively uses its own output for future predictions. This amplifies the margin of error as the model prediction continues over an extended forecast period. Despite this challenge, our research demonstrates that the LSTM model has a commendable level of reliability across its predictions for upcoming five-year from 1/1/2019 to 12/1/2023.

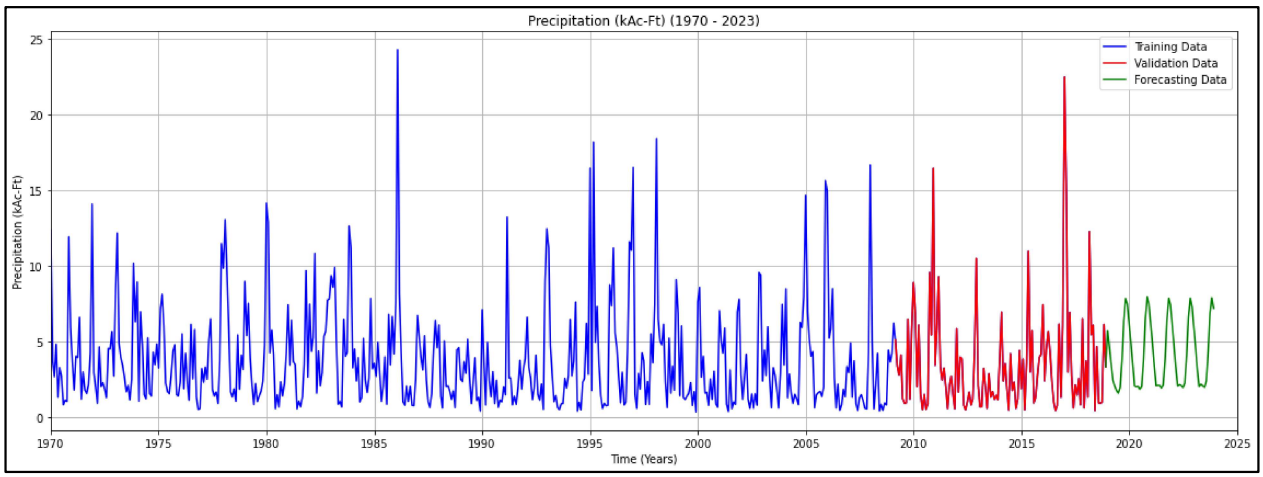

(a)

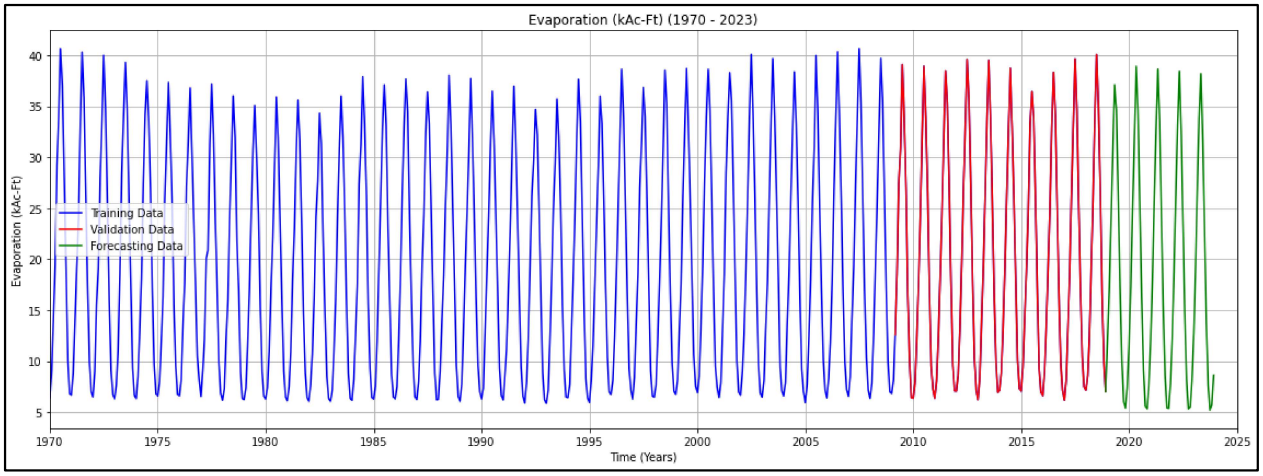
Evaporation (kAc-Ft) (1970 - 2023)
Training Data
Validation Data
Forecasting Data
Evaporation (kAc-Ft)
Time (Years)

(b)

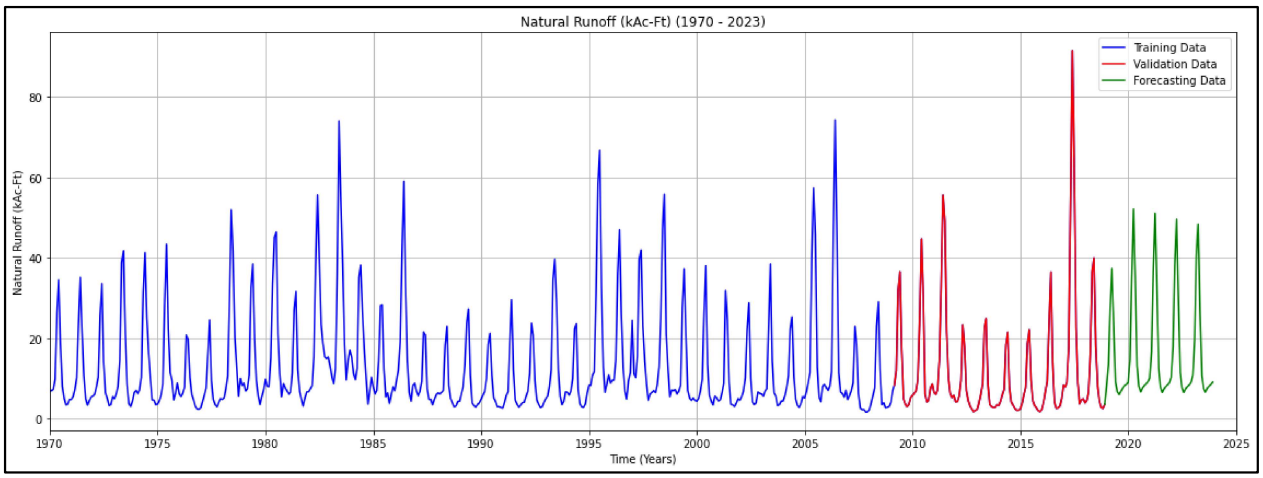
Natural Runoff (kAc-Ft) (1970 - 2023)
Training Data
Validation Data
Forecasting Data
Natural Runoff (kAc-Ft)
Time (Years)

(c)

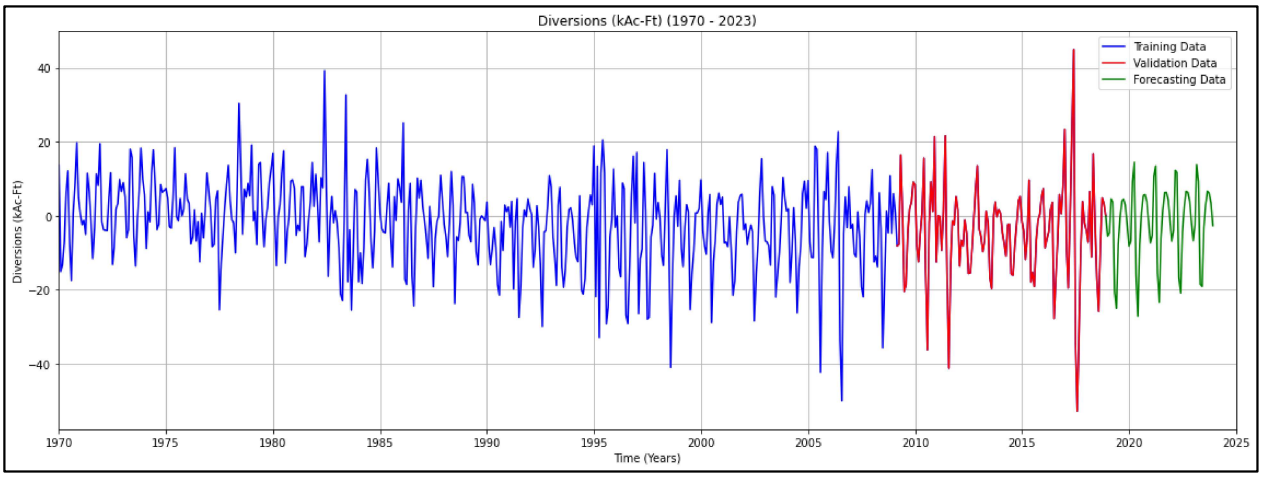
Diversions (kAc-Ft) (1970 - 2023)
Training Data
Validation Data
Forecasting Data
Diversions (kAc-Ft)
Time (Years)

(d)

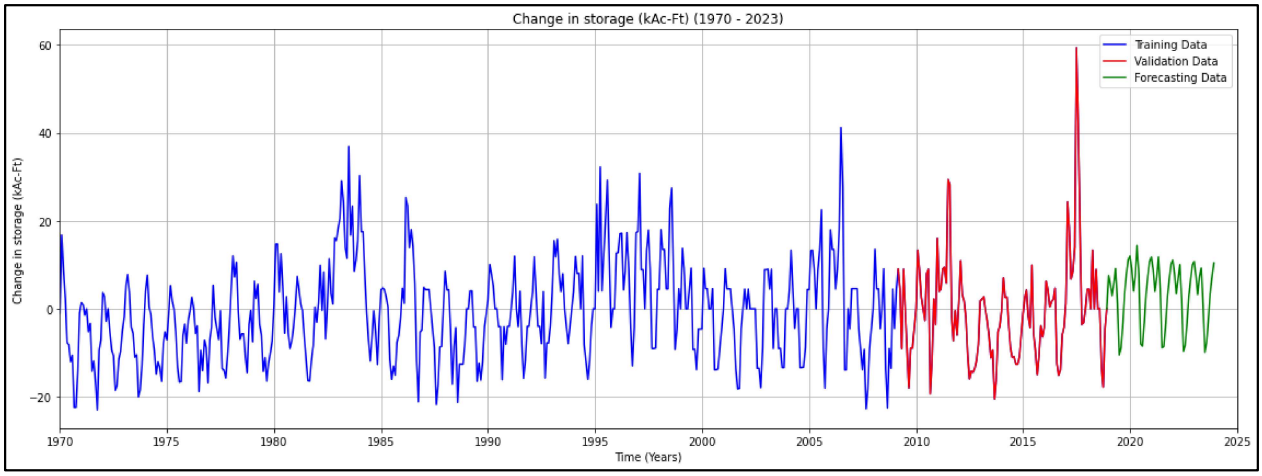

(e)

Figure 15: The figures (a,b,c,d,e) shows the visualization of model forecasting data in green for each of the water balance components.

In the last part of our analysis, the change in storage data (measured in kAc-Ft) derived from the LSTM model's predictions for the 5-year period from 1/1/2019 to 12/1/2023 are converted into water levels (feet) using the stage-volume curve method, as detailed in Section 2.2. These transformed LSTM prediction data for water levels are then compared against historical water level data, which is sourced from the Mono Lake website (Mono Lake Levels 1979-Present (Monthly)) to have direct comparison between predicted and historical water levels.

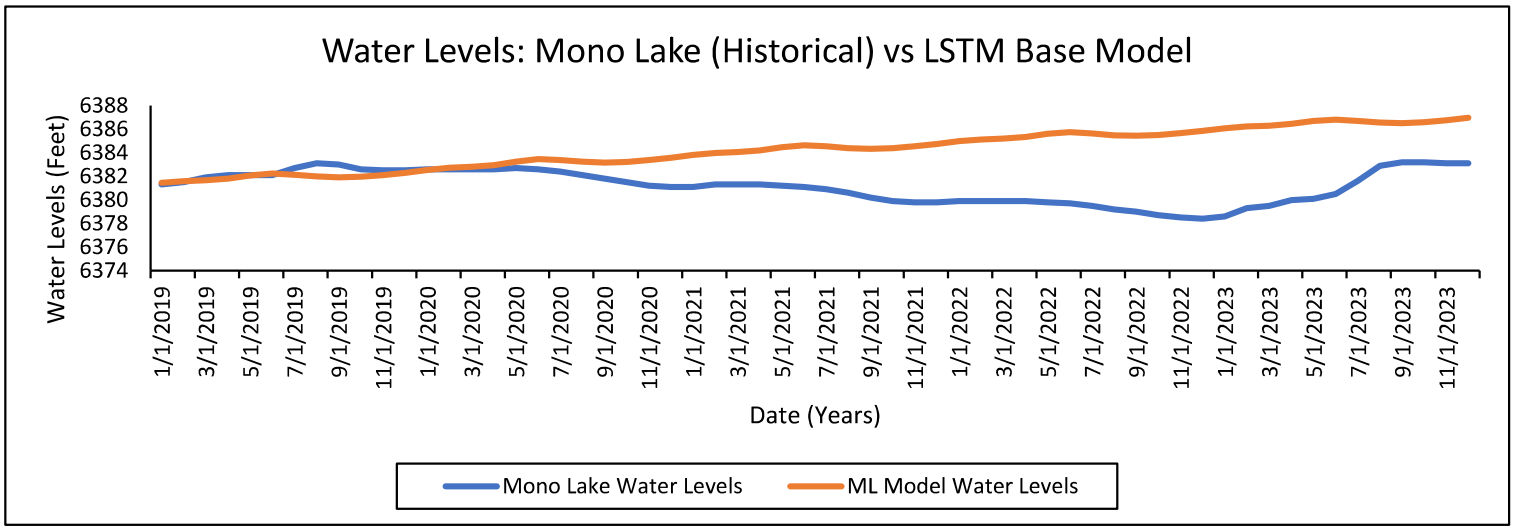

Figure 16: Shows the comparative analysis, illustrating the historical water levels of Mono Lake in blue and the LSTM model predictions in orange over the forecasting time period of 1/1/2019 to 12/1/2023.

From figure 16, it is observable that the model's predictions are slightly higher than the historical water levels of Mono Lake. However, it is still good, given that the model is only trained until the year 2009. Furthermore, this discrepancy could also be attributed to the accumulation of error, a phenomenon previously mentioned. Such error accumulation is easily visible, for example around the beginning of 2020, the model begins to establish a forecasting pattern of increasing water levels and then continues on that trend as the model relies on its own previous predictions for future forecasts. This can be observed as discrepancies between the model's forecasts and the historical levels become more obvious over an extended period of time.

To address this inherent limitation in the LSTM model, we explored a final combination approach aimed at refining the model's predictive accuracy. Specifically, by tuning the hyperparameters, we developed an ensemble model – 12 distinct member models – integrating their forecasting outputs together to create an LSTM Ensemble model. This approach is designed to enhance the precision and reliability of water level forecasts for Mono Lake using machine learning. The following section will delve directly into the outcomes of this ensemble results for the water levels, shedding light on its efficacy in improving the forecast accuracy compared to the one LSTM model.

3.2 Long Short-Term Memory (LSTM) Ensemble Model Analysis

The ensemble model was developed through meticulous adjustments in model architecture, training, lookback period, and dropout aiming to develop a spectrum of results for enhanced predictive accuracy. It is important to recall that the model complexity increases as the model ID increases from 1 to 12. Table 10 below outlines the comparative analysis of RMSE and MAE metrics, comparing the LSTM member model predictions with historical data for change in storage. Just like the previous model, this comparison spans across the validation dataset from 3/1/2009 to 12/1/2018 respectively.

Model ID	Layer & Units (Neurons)	No. of Epochs	Lookback Period (months)	Dropout	RMSE	MAE
Base	*1 Layer and 100 Units*	*50*	*48*	*0%*	*4.47802*	*3.43675*
Model 1	1 Layer and 100 Units	50	36	0%	5.780671	4.238276
Model 2	1 Layer and 100 Units	50	36	20%	4.328553	3.374905
Model 3	1 Layer and 100 Units	100	48	0%	5.259191	4.034933
Model 4	1 Layer and 100 Units	100	48	20%	4.481786	3.306287
Model 5	1 Layer and 100 Units	150	48	20%	5.116719	3.719537
Model 6	1 Layer and 100 Units	200	60	20%	5.179771	3.702729
Model 7	2 Layers and 400 Units	50	36	0%	5.609086	4.121331
Model 8	2 Layers and 400 Units	50	36	20%	4.804388	3.646154
Model 9	2 Layers and 400 Units	100	48	0%	5.871099	4.322593
Model 10	2 Layers and 400 Units	100	48	20%	5.169516	3.705442
Model 11	2 Layers and 400 Units	150	48	20%	5.458471	3.859242
Model 12	2 Layers and 400 Units	200	60	20%	5.144364	3.889063

Table 10: Represents the performance matrix of LSTM Ensemble model for the change in Storage by evaluating each of the member model's predictions against the historical data across the validation dataset from 3/1/2009 to 12/1/2018.

Based on observations from the table, it's evident that model performance remains almost similar as we transition from simpler models (Model 1) to more complex ones (Model 12). This progression sees both Root Mean Squared Error (RMSE) and Mean Absolute Error (MAE) metrics almost similar, indicating no correlation between model complexity and the predictive accuracy.

However, the LSTM Base model demonstrates acceptable accuracy, which is between model 4 and model 5 – the simpler and more complex model. A significant observation is the impact of increased dropout rates during model training, which notably increases model performance at almost all instances. This improvement can be attributed to the reduction of overfitting, as the model omits 20% of the units (neurons) in the training. Another critical factor influencing model performance is the lookback period. A longer lookback period and larger number of epochs enables the model to better recognize patterns within the data, consequently improving the model learning capability. However, it's essential to maintain a delicate balance when increasing model complexity, particularly concerning the lookback period and the number of epochs to avoid overfitting. Overall, the members of ensemble model produce diverse results across different scenarios, which is influenced by the changes in the LSTM model. This diversity in outcomes underscores the reliability of the ensemble approach, where combining predictions from multiple models yields better accuracy. The change in storage data, predicted by these member models were converted to water levels (in feet) using the stage-curve method. Detailed results of each of these water level predictions are presented in Appendix 2. Additionally, Appendix 3 contains figures illustrating the Change in Storage for each member model.

Figure shows the potential of the LSTM Ensemble models to accurately forecast the range of water levels from 2019 to 2023 by combining outputs from all 12 members. Notably, the LSTM Ensemble model demonstrates remarkable accuracy in near-term predictions, particularly for the two-year span from 2019 to 2021. This accuracy indicates the model's proficiency in capturing the seasonality and inherent patterns within water balance components, allowing for precise predictions in subsequent years. Upon detailed examination of the water levels forecasted by each member model in comparison to historical data from Mono Lake, it becomes apparent that the complexity of a model does not directly correlate with its accuracy. While some of the more complex models significantly overestimate or underestimate water levels in their forecasts, Model 4 strikes a good balance between simplicity and complexity, and aligns close with observed water levels of Mono Lake.

Moreover, the ensemble approach offers a distinct advantage by providing a comprehensive range that gives insights into future water level trends at Mono Lake. For instance, the ensemble model predicts that within the five-year window from 2019 to 2023, Mono Lake's water levels are expected to fluctuate between 6374 ft and 6393 ft. This prediction is especially noteworthy considering the dramatic climate change that has influenced Mono Lake water levels. The ensemble's predictions closely match the real-world observations of Mono Lake's water levels, falling within the LSTM Ensemble model range. Furthermore, an intriguing aspect of the model's performance is its projection of an increase in water levels towards the latter part of the forecast period, particularly from mid-2022 to 2023, which is noticable in figure 18 (c). This trend in the model's forecasts also correlates with the slight increase in the historical Mono Lake water levels, which is also observed during the same period.

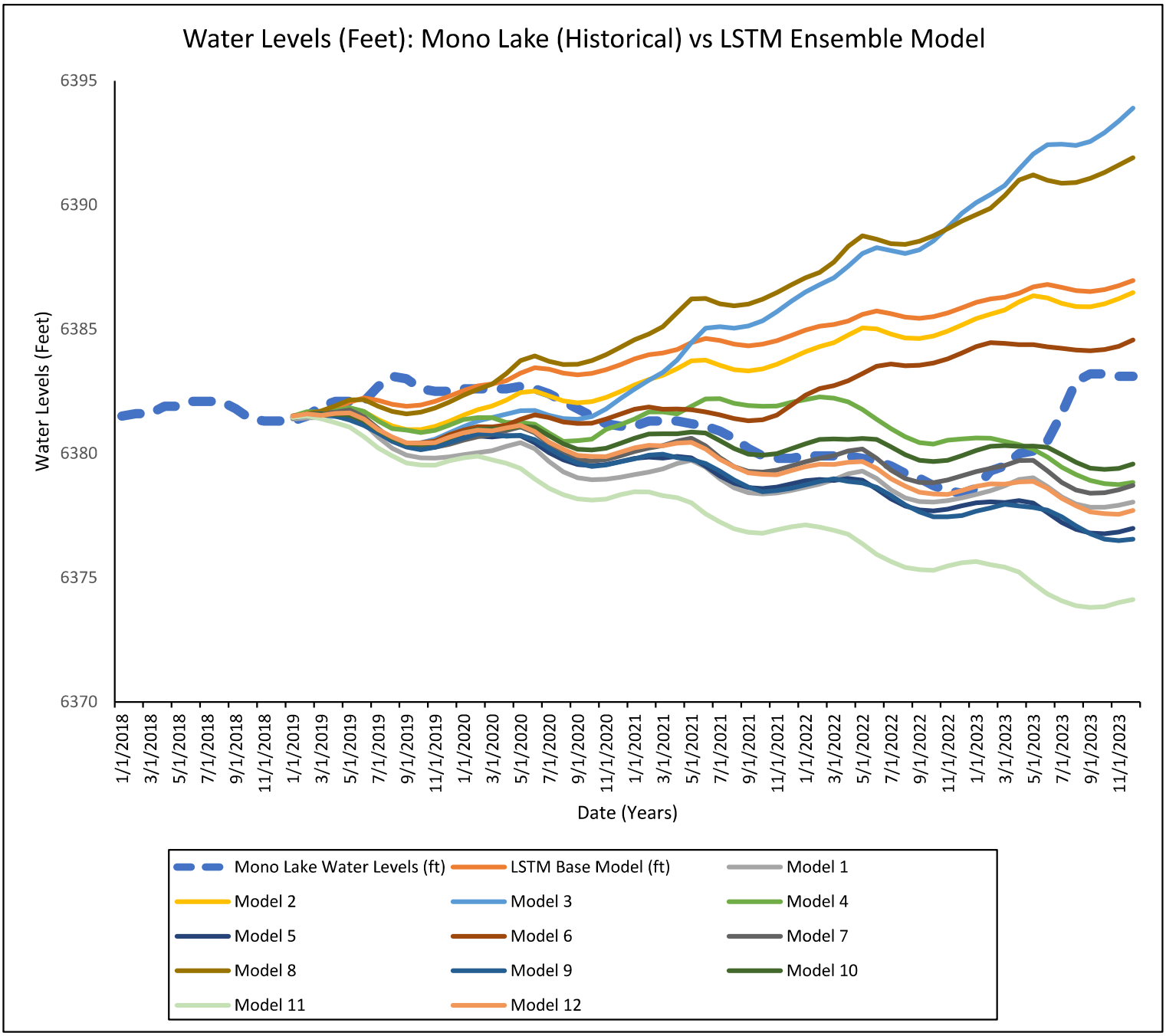
Water Levels (Feet): Mono Lake (Historical) vs LSTM Ensemble Model
Water Levels (Feet)
6395
6390
6385
6380
6375
6370
1/1/2018
3/1/2018
5/1/2018
7/1/2018
9/1/2018
11/1/2018
1/1/2019
3/1/2019
5/1/2019
7/1/2019
9/1/2019
11/1/2019
1/1/2020
3/1/2020
5/1/2020
7/1/2020
9/1/2020
11/1/2020
1/1/2021
3/1/2021
5/1/2021
7/1/2021
9/1/2021
11/1/2021
1/1/2022
3/1/2022
5/1/2022
7/1/2022
9/1/2022
11/1/2022
1/1/2023
3/1/2023
5/1/2023
7/1/2023
9/1/2023
11/1/2023
Date (Years)
Mono Lake Water Levels (ft)
LSTM Base Model (ft)
Model 1
Model 2
Model 3
Model 4
Model 5
Model 6
Model 7
Model 8
Model 9
Model 10
Model 11
Model 12

(a)

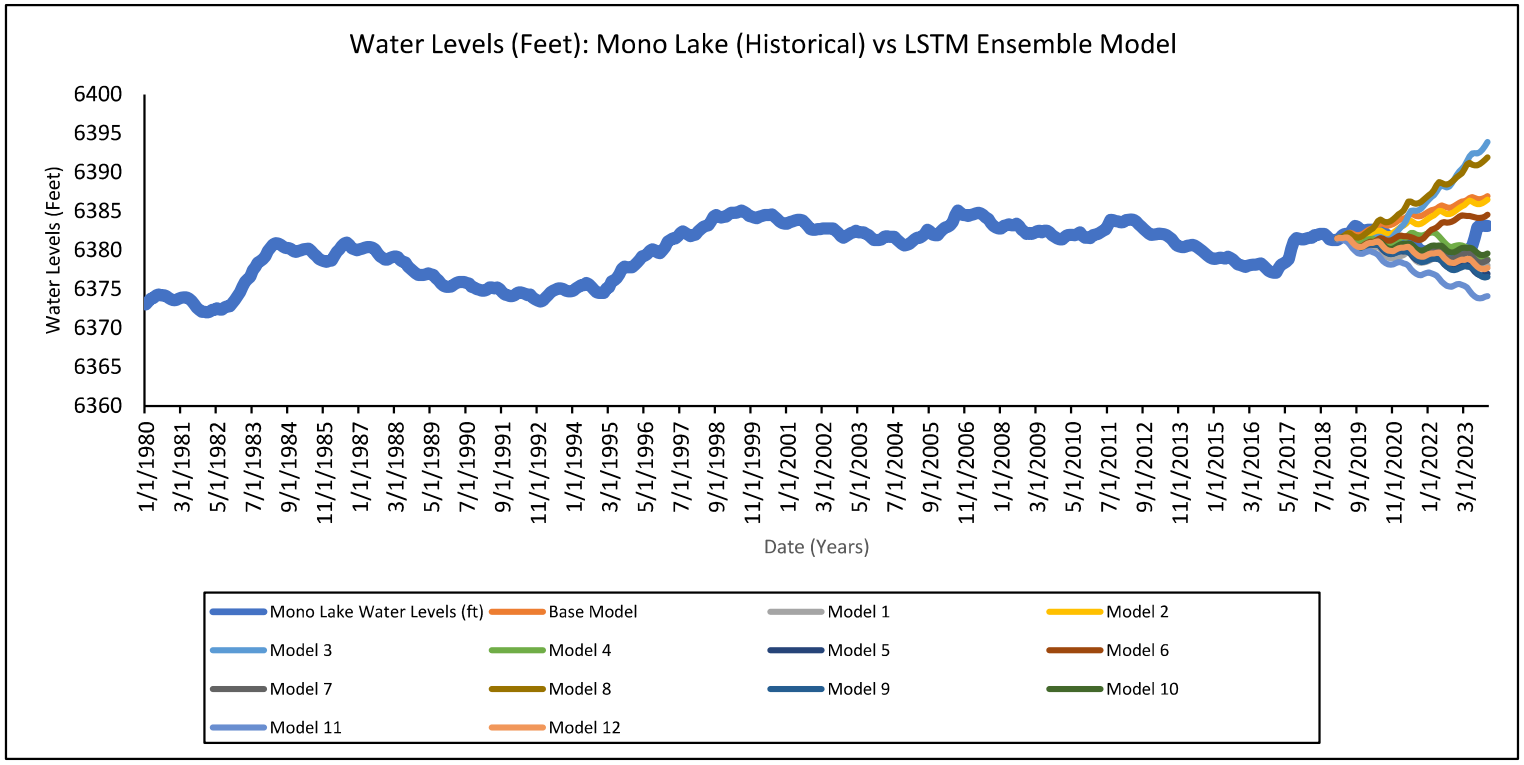
Water Levels (Feet): Mono Lake (Historical) vs LSTM Ensemble Model
Water Levels (Feet)
6400
6395
6390
6385
6380
6375
6370
6365
6360
1/1/1980
3/1/1981
5/1/1982
7/1/1983
9/1/1984
11/1/1985
1/1/1987
3/1/1988
5/1/1989
7/1/1990
9/1/1991
11/1/1992
1/1/1994
3/1/1995
5/1/1996
7/1/1997
9/1/1998
11/1/1999
1/1/2001
3/1/2002
5/1/2003
7/1/2004
9/1/2005
11/1/2006
1/1/2008
3/1/2009
5/1/2010
7/1/2011
9/1/2012
11/1/2013
1/1/2015
3/1/2016
5/1/2017
7/1/2018
9/1/2019
11/1/2020
1/1/2022
3/1/2023
Date (Years)
Mono Lake Water Levels (ft)
Base Model
Model 1
Model 2
Model 3
Model 4
Model 5
Model 6
Model 7
Model 8
Model 9
Model 10
Model 11
Model 12

(b)

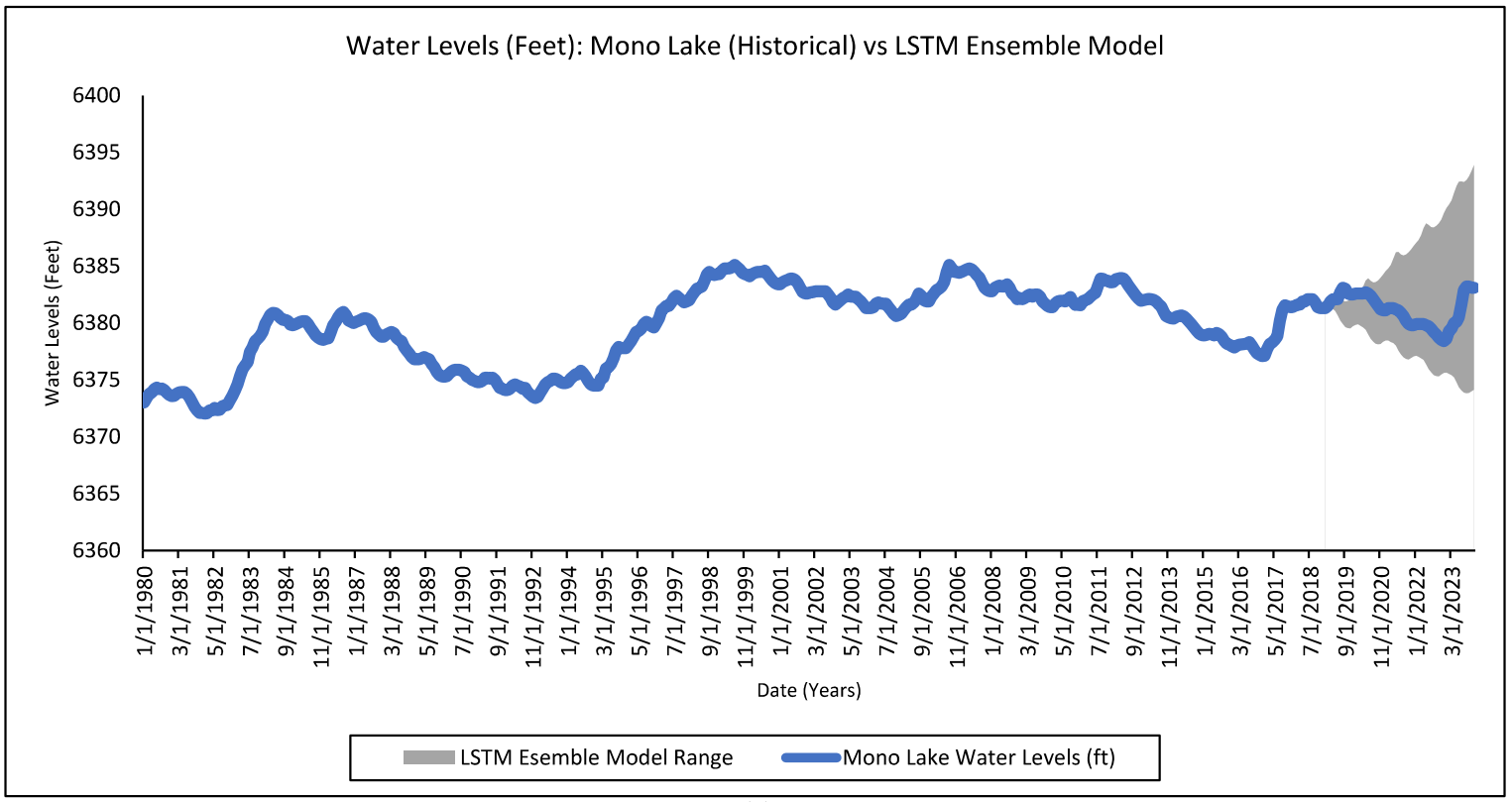
Water Levels (Feet): Mono Lake (Historical) vs LSTM Ensemble Model
Water Levels (Feet)
6400
6395
6390
6385
6380
6375
6370
6365
6360
1/1/1980
3/1/1981
5/1/1982
7/1/1983
9/1/1984
11/1/1985
1/1/1987
3/1/1988
5/1/1989
7/1/1990
9/1/1991
11/1/1992
1/1/1994
3/1/1995
5/1/1996
7/1/1997
9/1/1998
11/1/1999
1/1/2001
3/1/2002
5/1/2003
7/1/2004
9/1/2005
11/1/2006
1/1/2008
3/1/2009
5/1/2010
7/1/2011
9/1/2012
11/1/2013
1/1/2015
3/1/2016
5/1/2017
7/1/2018
9/1/2019
11/1/2020
1/1/2022
3/1/2023
Date (Years)
LSTM Esemble Model Range
Mono Lake Water Levels (ft)

(c)

Figure 17: (a) Visually represents the historical and Ensemble model data from 2018 to 2023. (b) Represent the historical Mono Lake water levels and the LSTM Ensemble model predictions over the time period of 1980 to 2023. (c) Shows the range of the LSTM Ensemble model over the forecasting period with the historical Mono Lake water levels from 1980 to 2023.

Lastly, the performance of the LSTM Ensemble model could potentially be further enhanced through hyperparameter optimization or by experimenting with other advanced deep learning models such as Gated Recurrent Units (GRU), Autoregressive Integrated Moving Average (ARIMA), and others. It is important to acknowledge that the LSTM models were trained only up to 2/1/2009, subsequently tested on validated dataset ranging from 3/1/2009 to 12/1/2018, and then used for forecasting from 1/1/2019 to 12/1/2023. This approach underscores an opportunity for model improvement by retraining the LSTM models on the entire dataset before forecasting, thereby refining their predictive accuracy and narrowing the forecasting range. However, the exploration of such alternative methods is beyond the scope of this research.

3.3 Implications for Mono Lake Water Resources Management

The application of machine learning for forecasting Mono Lake's water levels presents a significant advancement to enable better water resource management. The predictive accuracy of these LSTM Ensemble models, particularly in capturing the probable high and low of Mono Lake water levels, provides critical insight for managing Mono Lake's ecological balance, recreational value, and water supply for the Los Angeles Department of Water and Power (LADWP).

The LSTM Ensemble model's ability to forecast water levels within a reasonably accurate range is paramount for long-term water resource planning. Predicting water levels from 2019 to 2023 with reliable precision enables stakeholders to make informed decisions regarding water allocation, conservation efforts, and ecological preservation. For instance, the model's prediction that water levels would range between 6374 ft and 6393 ft allows for the anticipation of potential ecological stress conditions, guiding the implementation of conservation measures. Mono Lake's unique ecosystem, characterized by its saline nature and the presence of specialized flora and fauna, depends on stable water levels. This result underscores the importance of implementing adaptive management practices that can respond to predicted changes in water levels, ensuring the protection of Mono Lake's biodiversity. The ensemble model's predictions also have significant implications for water allocation and supply strategies. Given Mono Lake's role in supplying water to around 200,000 residents of Los Angeles, accurate forecasts of water levels will help balance the diversions to manage the urban demand for water supply while ensuring the needs of maintaining Mono Lake's health. Furthermore, the granular ability of LSTM Ensemble model to predict monthly water levels can aid in optimizing water diversion schedules, thereby minimizing the impact on Mono Lake's ecosystem while ensuring a reliable water supply for the city.

The predictive insights offered by the LSTM Ensemble model advocate for a cooperative and adaptive management approach to Mono Lake's water resources, incorporating model predictions, such that the stakeholders can develop strategies in response to the anticipated changes in future water levels. The findings from this research can also have direct policy implications, advocating for the development and implementation of water management policies that are informed by our modeling. By leveraging accurate water level forecasts, stakeholders can collaboratively develop

sustainable management practices that balance stable water levels with water supply needs in accordance with Decision 1631 (Decision 1631).

The authors believe that the application of LSTM Ensemble models for forecasting Mono Lake's water levels marks a pivotal advancement in the field of hydrology, environmental management, and machine learning, offering a blueprint for leveraging machine learning in the stewardship of natural resources. The model offers invaluable insights for sustaining ecological balance, optimizing water supply, and implementing cooperative management strategies to bring balance to Mono Lake water levels. As we move forward, the continuous refinement of machine learning models and the integration of their insights into management and policy frameworks will be essential for safeguarding lakes like Mono Lake to preserve our water resources.

Chapter 4 Conclusion

4.1 Summary

This thesis embarked on an application of advanced machine learning techniques to forecast Mono Lake water levels. Through rigorous machine learning modeling, this research has demonstrated the potential of machine learning – especially the LSTM Ensemble model – to accurately predict future water levels, offering invaluable insights for water resource management.

The research created and applied eight different models over three dataset types, specifically historical water levels, historical precipitation datasets, and historical Bayesian statistical (L2SWBM) datasets. The application of Support Vector Machine (SVM), Random Forests (RF), and Long Short-Term Memory (LSTM) models to Mono Lake's historical water levels highlighted the strengths and limitations of each method. The SVM model, despite extensive training, showed limited capability in capturing the variability of the lake's water levels. On the other hand, the RF model demonstrated improved performance, benefiting from its algorithm that captured complex patterns through multiple decision trees. However, the RF model performed poorly in the forecasting period. The LSTM model did show promising results on historical water levels, but when used on a historical precipitation dataset created from the Bayesian model, LSTM model showed exceptional results capturing the seasonality and variations. This observation led to the use of machine learning models on advanced Bayesian datasets, specifically from L2SWBM. Hence, the output of water balance components like precipitation, evaporation, natural runoff from the L2SWBM, and diversions led to the input for the machine learning model, including the RF, LSTM, and LSTM Ensemble model. While the RF model failed to generate promising results, the

LSTM model showed promising results in forecasting water balance components. This observation ultimately led to fine tuning of the LSTM model by changing model architecture, training, dropout, and lookback period, resulting in a family of 12 member models of the LSTM Ensemble model.

The key findings of this research underscore the LSTM Ensemble model's capability to capture the intricate patterns and seasonal fluctuations of precipitation, evaporation, runoff, and diversions. By integrating outputs from 12 diverse models, including the LSTM Base model, the ensemble approach provided a nuanced forecast that outperformed any individual model predictions. The forecasts indicated that Mono Lake's water levels would likely fluctuate within the range of 6374 ft to 6393 ft from 2019 to 2023, and notably, the historical water levels observed during this period fell within our model predicted range. These predictions are crucial for various stakeholders for sustaining ecological balance, optimizing water supply, and developing cooperative management strategies to bring stability to Mono Lake water levels. Furthermore, a comparative analysis of the LSTM Ensemble model revealed that model complexity and architecture did not correlate significantly with forecasting accuracy, but the research found that a balanced approach – not too simple or too complex model – created the most accurate and close predictions.

The practical implications of this research for Mono Lake's water resource management are profound. The LSTM Ensemble model's forecasts will enable policymakers and management to make informed decisions regarding water diversions, conservation efforts, and ecological preservation. By anticipating future water levels, stakeholders can proactively address potential challenges, ensuring that Mono Lake remains a viable habitat for its unique biodiversity while also meeting the water needs of the communities in Los Angeles. Moreover, this research contributes

to the broader field of hydrology, environmental modeling, and machine learning by demonstrating its capability and effectiveness in the stewardship of natural resources management.

4.2 Future Research:

While this research marks an advancement in hydrological forecasting, it is not without its challenges and limitations. The reliance on historical training datasets from 1970 to 2009 for LSTM models, with validation in subsequent period from 2009 to 2018, underscores a gap of model retraining over the entire dataset from 1970 to 2018 to improve its accuracy further. Looking ahead, several other avenues for future research emerge from this study. Continuous refinement of LSTM Ensemble models, including hyperparameter optimization and the exploration of alternative architectures, could further increase Mono Lake water levels forecasting accuracy. Integration of additional variables such as temperature, humidity, and others into the modeling process could provide a more holistic view of the factors influencing Mono Lake's water levels. Comparative analysis with other model algorithms, such as Gated Recurrent Units (GRU), Autoregressive Integrated Moving Average (ARIMA), and hybrid models, could also offer insights into the relative strengths and weaknesses of different approaches.

In conclusion, this thesis represents a meaningful contribution to the field of hydrology, climate forecasting, and water resource management. The successful application of LSTM Ensemble models to predict Mono Lake's water levels highlights the potential of machine learning to inform and guide environmental conservation and natural resource management efforts.

Bibliography

Abed, M., Imteaz, M. A., Ahmed, A. N., & Huang, Y. F. (2022). Modelling monthly pan evaporation utilising Random Forest and deep learning algorithms. *Scientific Reports 2022 12:1*, *12*(1), 1–29. https://doi.org/10.1038/s41598-022-17263-3

About Mono Lake. (n.d.). Retrieved December 30, 2023, from https://www.monolake.org/learn/aboutmonolake/

Aksoy, H., Unal, N. E., Eris, E., & Yuce, M. I. (2013). Stochastic modeling of Lake Van water level time series with jumps and multiple trends. *Hydrol. Earth Syst. Sci*, *17*, 2297–2303. https://doi.org/10.5194/hess-17-2297-2013

Al Sudani, Z. A., & Salem, G. S. A. (2022). Evaporation Rate Prediction Using Advanced Machine Learning Models: A Comparative Study. *Advances in Meteorology*, *2022*. https://doi.org/10.1155/2022/1433835

All Gridded Precipitation Datasets: NOAA Physical Sciences Laboratory. (n.d.). Retrieved February 14, 2024, from https://psl.noaa.gov/data/gridded/tables/precipitation.html

Altunkaynak, A. (2007). Forecasting surface water level fluctuations of lake van by artificial neural networks. *Water Resources Management*, *21*(2), 399–408. https://doi.org/10.1007/S11269-006-9022-6/METRICS

An Overview on Long Short Term Memory (LSTM) - Analytics Vidhya. (n.d.). Retrieved January 2, 2024, from https://www.analyticsvidhya.com/blog/2022/03/an-overview-on-long-short-term-memory-lstm/

Badillo, S., Banfai, B., Birzele, F., Davydov, I. I., Hutchinson, L., Kam-Thong, T., Siebourg-Polster, J., Steiert, B., & Zhang, J. D. (2020). An Introduction to Machine Learning.

Clinical Pharmacology & Therapeutics, *107*(4), 871–885. https://doi.org/10.1002/CPT.1796

Barrera-Animas, A. Y., Oyedele, L. O., Bilal, M., Akinosho, T. D., Delgado, J. M. D., & Akanbi, L. A. (2022). Rainfall prediction: A comparative analysis of modern machine learning algorithms for time-series forecasting. *Machine Learning with Applications*, *7*, 100204. https://doi.org/10.1016/J.MLWA.2021.100204

Bonakdari, H., Ebtehaj, I., Samui, P., & Gharabaghi, B. (2019). Lake Water-Level fluctuations forecasting using Minimax Probability Machine Regression, Relevance Vector Machine, Gaussian Process Regression, and Extreme Learning Machine. *Water Resources Management*, *33*(11), 3965–3984. https://doi.org/10.1007/S11269-019-02346-0/FIGURES/5

Borovkova, S., & Tsiamas, I. (2019). An ensemble of LSTM neural networks for high-frequency stock market classification. *Journal of Forecasting*, *38*(6), 600–619. https://doi.org/10.1002/FOR.2585

Bouktif, S., Fiaz, A., Ouni, A., & Serhani, M. A. (2020). Multi-Sequence LSTM-RNN Deep Learning and Metaheuristics for Electric Load Forecasting. *Energies 2020, Vol. 13, Page 391*, *13*(2), 391. https://doi.org/10.3390/EN13020391

Breiman, L. (2001). Random forests. *Machine Learning*, *45*(1), 5–32. https://doi.org/10.1023/A:1010933404324/METRICS

Buyukyildiz, M., Tezel, G., & Yilmaz, V. (2014). Estimation of the Change in Lake Water Level by Artificial Intelligence Methods. *Water Resources Management*, *28*(13), 4747–4763. https://doi.org/10.1007/S11269-014-0773-1/FIGURES/4

Castanedo, F. (2013). A review of data fusion techniques. *The Scientific World Journal*, *2013*. https://doi.org/10.1155/2013/704504

Choi, J. Y., & Lee, B. (2018). Combining LSTM Network Ensemble via Adaptive Weighting for Improved Time Series Forecasting. *Mathematical Problems in Engineering*, *2018*. https://doi.org/10.1155/2018/2470171

Collins, A., & Liu, P. (2023). *Los Angeles Department of Water & Power Item 3: Mono Lake Current Conditions 2*.

Decision 1631. (n.d.). Retrieved December 30, 2023, from https://www.monolake.org/learn/aboutmonolake/savingmonolake/d1631/

Demir, V. (2021). *Enhancing Monthly Lake Levels Forecasting Using Heuristic Regression Techniques with Periodicity Data Component: Application of Lake Michigan*. https://doi.org/10.21203/rs.3.rs-726003/v1

Deng, B., Liu, P., Chin, R. J., Kumar, P., Jiang, C., Xiang, Y., Liu, Y., Lai, S. H., & Luo, H. (2022). Hybrid metaheuristic machine learning approach for water level prediction: A case study in Dongting Lake. *Frontiers in Earth Science*, *10*, 1545. https://doi.org/10.3389/FEART.2022.928052/BIBTEX

Ferdinandy, B., Gerencsér, L., Corrieri, L., Perez, P., Újváry, D., Csizmadia, G., & Miklósi, Á. (2020). Challenges of machine learning model validation using correlated behaviour data: Evaluation of cross-validation strategies and accuracy measures. *PLoS ONE*, *15*(7). https://doi.org/10.1371/JOURNAL.PONE.0236092

Ficklin, D. L., Stewart, I. T., & Maurer, E. P. (2013). Effects of projected climate change on the hydrology in the Mono Lake Basin, California. *Climatic Change*, *116*(1), 111–131. https://doi.org/10.1007/S10584-012-0566-6/FIGURES/9

Fry, L. M., Apps, D., & Gronewold, A. D. (2020). Operational Seasonal Water Supply and Water Level Forecasting for the Laurentian Great Lakes. *Journal of Water Resources Planning and Management*, *146*(9), 04020072. https://doi.org/10.1061/(ASCE)WR.1943-5452.0001214

Geographic Names Information System. (n.d.-a). Retrieved March 8, 2024, from https://edits.nationalmap.gov/apps/gaz-domestic/public/search/names/263070

Geographic Names Information System. (n.d.-b). Retrieved December 30, 2023, from https://edits.nationalmap.gov/apps/gaz-domestic/public/search/names/263070

Gini, G., Galey, L., Fuentes, O., & Gonzalez, R. V. (2024). Transfemoral Amputee Stumble Detection through Machine-Learning Classification: Initial Exploration with Three Subjects. *Prosthesis 2024, Vol. 6, Pages 235-250*, *6*(2), 235–250. https://doi.org/10.3390/PROSTHESIS6020018

Gossard, A., VanDeWeghe, A., Venumuddula, M. R., Wegener, C., & Gronewold, A. (2023). *Closing the Water Balance of Mono Lake in North America's Great Basin*. AGU. https://agu.confex.com/agu/fm23/meetingapp.cgi/Paper/1241939

Greff, K., Srivastava, R. K., Koutník, J., Steunebrink, B. R., & Schmidhuber, J. (2015). LSTM: A Search Space Odyssey. *IEEE Transactions on Neural Networks and Learning Systems*, *28*(10), 2222–2232. https://doi.org/10.1109/TNNLS.2016.2582924

Gronewold, A. D., Clites, A. H., Hunter, T. S., & Stow, C. A. (2011). An appraisal of the Great Lakes advanced hydrologic prediction system. *Journal of Great Lakes Research*, *37*(3), 577–583. https://doi.org/10.1016/J.JGLR.2011.06.010

Gronewold, A. D., Smith, J. P., Read, L. K., & Crooks, J. L. (2020). Reconciling the water balance of large lake systems. *Advances in Water Resources*, *137*, 103505. https://doi.org/10.1016/J.ADVWATRES.2020.103505

Gronewold, A. D., & Stow, C. A. (2014). Unprecedented Seasonal Water Level Dynamics on One of the Earth's Largest Lakes. *Bulletin of the American Meteorological Society*, *95*(1), 15–17. https://doi.org/10.1175/BAMS-D-12-00194.1

Güldal, V., & Tongal, H. (2010). Comparison of recurrent neural network, adaptive neuro-fuzzy inference system and stochastic models in eğirdir lake level forecasting. *Water Resources Management*, *24*(1), 105–128. https://doi.org/10.1007/S11269-009-9439-9/METRICS

Gunn, S. R. (1998). *Support Vector Machines for Classification and Regression*.

Håkanson, L., Parparov, A., & Hambright, K. D. (2000). Modelling the impact of water level fluctuations on water quality (suspended particulate matter) in Lake Kinneret, Israel. *Ecological Modelling*, *128*(2–3), 101–125. https://doi.org/10.1016/S0304-3800(00)00200-3

Hersbach, H., Bell, B., Berrisford, P., Horányi, A., Sabater, J. M., Nicolas, J., Poli, P., Radu, R., Schepers, D., Simmons, A., Soci, C., Laloyaux, P., Owono, A. O., Ribas, R., & Suttie, M. (n.d.). *Climate Change Characteristics of ERA5 and innovations for ERA6*.

Hochreiter, S., & Urgen Schmidhuber, J. ¨. (1991). *Long Short-Term Memory*.

Huang, A., Rao, Y. R., Lu, Y., & Zhao, J. (2010). Hydrodynamic modeling of Lake Ontario: An intercomparison of three models. *Journal of Geophysical Research: Oceans*, *115*(12). https://doi.org/10.1029/2010JC006269

Hussein, E. A., Ghaziasgar, M., Thron, C., Vaccari, M., & Bagula, A. (2021). Basic Statistical Estimation Outperforms Machine Learning in Monthly Prediction of Seasonal Climatic

Parameters. *Atmosphere 2021, Vol. 12, Page 539*, *12*(5), 539. https://doi.org/10.3390/ATMOS12050539

Karimi, S., Shiri, J., Kisi, O., & Makarynskyy, O. (2012). Forecasting Water Level Fluctuations of Urmieh Lake Using Gene Expression Programming and Adaptive Neuro-Fuzzy Inference System. *Http://Dx.Doi.Org/10.1260/1759-3131.3.2.109*, *3*(2), 109–125. https://doi.org/10.1260/1759-3131.3.2.109

Khatibi, R., Ghorbani, M. A., Naghipour, L., Jothiprakash, V., Fathima, T. A., & Fazelifard, M. H. (2014). *Inter-comparison of time series models of lake levels predicted by several modeling strategies*. https://doi.org/10.1016/j.jhydrol.2014.01.009

Kisi, O., Shiri, J., & Nikoofar, B. (2012). Forecasting daily lake levels using artificial intelligence approaches. *Computers & Geosciences*, *41*, 169–180. https://doi.org/10.1016/J.CAGEO.2011.08.027

L.A.'s new water war: Keeping its supply from Mono Lake - Los Angeles Times. (n.d.). Retrieved December 30, 2023, from https://www.latimes.com/environment/story/2023-02-19/los-angeles-dwp-fights-to-keep-spigot-open-at-mono-lake

Lavers, D. A., Simmons, A., Vamborg, F., & Rodwell, M. J. (2022). An evaluation of ERA5 precipitation for climate monitoring. *Quarterly Journal of the Royal Meteorological Society*, *148*(748), 3152–3165. https://doi.org/10.1002/QJ.4351

Li, M., & Wang, Z. (2021). An LSTM-Based ensemble learning approach for time-dependent reliability analysis. *Journal of Mechanical Design*, *143*(3). https://doi.org/10.1115/1.4048625/1087577

Liu, G., Tang, Z., Qin, H., Liu, S., Shen, Q., Qu, Y., & Zhou, J. (2022). Short-term runoff prediction using deep learning multi-dimensional ensemble method. *Journal of Hydrology*, *609*, 127762. https://doi.org/10.1016/J.JHYDROL.2022.127762

Makridakis, S., Spiliotis, E., & Assimakopoulos, V. (2018). Statistical and Machine Learning forecasting methods: Concerns and ways forward. *PLOS ONE*, *13*(3), e0194889. https://doi.org/10.1371/JOURNAL.PONE.0194889

Mccreedy, C., & Heath, S. K. (n.d.). *ATYPICAL WILLOW FLYCATCHER NESTING SITES IN A RECOVERING RIPARIAN CORRIDOR AT MONO LAKE, CALIFORNIA*.

MERRA. (n.d.). Retrieved February 14, 2024, from https://gmao.gsfc.nasa.gov/reanalysis/MERRA/reanalysis_precipitation_climatology.php

Microsoft Cognitive Toolkit. (2017). https://www2.inceptasolutions.com/2017/04/17/microsoft-cognitive-toolkit-updated-deep-learning-toolkit/

Molinos, J. G., Viana, M., Brennan, M., & Donohue, I. (2015). Importance of Long-Term Cycles for Predicting Water Level Dynamics in Natural Lakes. *PLoS ONE*, *10*(3). https://doi.org/10.1371/JOURNAL.PONE.0119253

Mono Lake - Google Maps. (n.d.). Retrieved March 8, 2024, from https://www.google.com/maps/place/Mono+Lake/@37.9880455,-119.0500868,61139m/data=!3m1!1e3!4m6!3m5!1s0x809648435f30b0bd:0x121a56f42738210c!8m2!3d38.0128316!4d-118.9761519!16zL20vMGNtbGM?entry=ttu

Mono Lake Levels 1979-Present (Monthly). (n.d.). Retrieved January 22, 2024, from https://www.monobasinresearch.org/data/levelmonthly.php

Mono Lake Volcanic Field | U.S. Geological Survey. (n.d.). Retrieved December 30, 2023, from https://www.usgs.gov/volcanoes/mono-lake-volcanic-field

Mosaffa, H., Sadeghi, M., Mallakpour, I., Naghdyzadegan Jahromi, M., & Pourghasemi, H. R. (2022). Application of machine learning algorithms in hydrology. *Computers in Earth and Environmental Sciences*, 585–591. https://doi.org/10.1016/B978-0-323-89861-4.00027-0

Myakisheva, N. V., Gaidukova, E. V., Shanochkin, S. V., & Batmazova, A. A. (2021). Seasonal and Annual Probabilistic Forecasting of Water Levels in Large Lakes (Case Study of the Ladoga Lake). *International Letters of Natural Sciences*, *82*, 13–19. https://doi.org/10.18052/www.scipress.com/ilns.82.13

Nakisa, B., Rastgoo, M. N., Rakotonirainy, A., Maire, F., & Chandran, V. (2018). Long short term memory hyperparameter optimization for a neural network based emotion recognition framework. *IEEE Access*, *6*, 49325–49338. https://doi.org/10.1109/ACCESS.2018.2868361

Natural History. (n.d.). Retrieved December 30, 2023, from https://www.monolake.org/learn/aboutmonolake/naturalhistory/

Obringer, R., & Nateghi, R. (2018). Predicting Urban Reservoir Levels Using Statistical Learning Techniques. *Scientific Reports 2018 8:1*, *8*(1), 1–9. https://doi.org/10.1038/s41598-018-23509-w

OpenStreetMap. (n.d.). Retrieved December 30, 2023, from https://www.openstreetmap.org/#map=6/39.705/-118.268

Oxburgh, R., Broecker, W. S., & Wanninkhof, R. H. (1991). The carbon budget of Mono Lake. *Global Biogeochemical Cycles*, *5*(4), 359–372. https://doi.org/10.1029/91GB02475

Peter Vorster. (1985). A Water Balance Forecast Model for Mono Lake, California. *US Forest Service, Berkeley, California Box 245, Berkeley, CA 94201.*

Probst, P., & Boulesteix, A.-L. (2018). To Tune or Not to Tune the Number of Trees in Random Forest. *Journal of Machine Learning Research*, *18*(181), 1–18. http://jmlr.org/papers/v18/17-269.html

Raschka, S. (2018). *Model Evaluation, Model Selection, and Algorithm Selection in Machine Learning*. https://arxiv.org/abs/1811.12808v3

Sengoz, C., Ramanna, S., Kehler, S., Goomer, R., & Pries, P. (2023). Machine Learning Approaches to Improve North American Precipitation Forecasts. *IEEE Access*, *11*, 97664–97681. https://doi.org/10.1109/ACCESS.2023.3309054

Siami-Namini, S., Tavakoli, N., & Namin, A. S. (2019). The Performance of LSTM and BiLSTM in Forecasting Time Series. *Proceedings - 2019 IEEE International Conference on Big Data, Big Data 2019*, 3285–3292. https://doi.org/10.1109/BIGDATA47090.2019.9005997

Slater, L. J., Arnal, L., Boucher, M. A., Chang, A. Y. Y., Moulds, S., Murphy, C., Nearing, G., Shalev, G., Shen, C., Speight, L., Villarini, G., Wilby, R. L., Wood, A., & Zappa, M. (2023). Hybrid forecasting: blending climate predictions with AI models. *Hydrology and Earth System Sciences*, *27*(9), 1865–1889. https://doi.org/10.5194/HESS-27-1865-2023

Song, X., Liu, Y., Xue, L., Wang, J., Zhang, J., Wang, J., Jiang, L., & Cheng, Z. (2020). Time-series well performance prediction based on Long Short-Term Memory (LSTM) neural network model. *Journal of Petroleum Science and Engineering*, *186*, 106682. https://doi.org/10.1016/J.PETROL.2019.106682

State of the Lake. (n.d.-a). Retrieved April 21, 2023, from https://www.monolake.org/learn/stateofthelake/

State of the Lake. (n.d.-b). Retrieved December 30, 2023, from https://www.monolake.org/learn/stateofthelake/

Stine Scott. (1993). *Historic and Modern Distribution of Shore-Fringing Wetlands, Mono Lake, California*. https://www.monobasinresearch.org/images/mbeir/auxreports/21-springs.pdf

Supervised vs. Unsupervised Learning: What's the Difference? - IBM Blog. (n.d.). Retrieved January 1, 2024, from https://www.ibm.com/blog/supervised-vs-unsupervised-learning/

SWRCB Mono Lake Decision 1631. (1994). https://www.waterboards.ca.gov/waterrights/board_decisions/adopted_orders/decisions/d1600_d1649/wrd1631.pdf

Szymańska, E. (2018). Modern data science for analytical chemical data – A comprehensive review. *Analytica Chimica Acta*, *1028*, 1–10. https://doi.org/10.1016/J.ACA.2018.05.038

Table A-1. Bathymetry of Mono Lake . (n.d.).

Tezel, G., & Buyukyildiz, M. (2016). Monthly evaporation forecasting using artificial neural networks and support vector machines. *Theoretical and Applied Climatology*, *124*(1–2), 69–80. https://doi.org/10.1007/S00704-015-1392-3/FIGURES/4

The Mono Basin Project. (n.d.). Retrieved March 8, 2024, from https://web.archive.org/web/20140310092544/http://wsoweb.ladwp.com/Aqueduct/historyoflaa/monobasin.htm

Tsagris, M., Lagani, V., & Tsamardinos, I. (2018). Feature selection for high-dimensional temporal data. *BMC Bioinformatics*, *19*(1), 1–14. https://doi.org/10.1186/S12859-018-2023-7/TABLES/3

Tyralis, H., & Papacharalampous, G. (2017). Variable Selection in Time Series Forecasting Using Random Forests. *Algorithms 2017, Vol. 10, Page 114*, *10*(4), 114. https://doi.org/10.3390/A10040114

van de Schoot, R., Depaoli, S., King, R., Kramer, B., Märtens, K., Tadesse, M. G., Vannucci, M., Gelman, A., Veen, D., Willemsen, J., & Yau, C. (2021). Bayesian statistics and modelling. *Nature Reviews Methods Primers 2021 1:1*, *1*(1), 1–26. https://doi.org/10.1038/s43586-020-00001-2

van Ravenzwaaij, D., Cassey, P., & Brown, S. D. (2018). A simple introduction to Markov Chain Monte–Carlo sampling. *Psychonomic Bulletin & Review*, *25*(1), 143. https://doi.org/10.3758/S13423-016-1015-8

VanDeWeghe, A., Lin, V., Jayaram, J., & Gronewold, A. D. (2022). Changes in Large Lake Water Level Dynamics in Response to Climate Change. *Frontiers in Water*, *4*, 805143. https://doi.org/10.3389/FRWA.2022.805143/BIBTEX

Wang, Q., & Wang, S. (2020). Machine Learning-Based Water Level Prediction in Lake Erie. *Water 2020, Vol. 12, Page 2654*, *12*(10), 2654. https://doi.org/10.3390/W12102654

Wee, W. J., Zaini, N. B., Ahmed, A. N., & El-Shafie, A. (2021). A review of models for water level forecasting based on machine learning. *Earth Science Informatics*, *14*(4), 1707–1728. https://doi.org/10.1007/S12145-021-00664-9/TABLES/6

What is Supervised Learning? | *Google Cloud*. (n.d.). Retrieved January 1, 2024, from https://cloud.google.com/discover/what-is-supervised-learning

White, M. S., Xenopoulos, M. A., Hogsden, K., Metcalfe, R. A., & Dillon, P. J. (2008). Natural lake level fluctuation and associated concordance with water quality and aquatic

communities within small lakes of the Laurentian Great Lakes region. *Hydrobiologia*, *613*(1), 21–31. https://doi.org/10.1007/S10750-008-9469-Y/FIGURES/6

Woolway, R. I., Sharma, S., & Smol, J. P. (2022). Lakes in Hot Water: The Impacts of a Changing Climate on Aquatic Ecosystems. *BioScience*, *72*(11), 1050–1061. https://doi.org/10.1093/BIOSCI/BIAC052

Xiao, L., Zhong, M., & Zha, D. (2021). Runoff Forecasting Using Machine-Learning Methods: Case Study in the Middle Reaches of Xijiang River. *Frontiers in Big Data*, *4*, 752406. https://doi.org/10.3389/FDATA.2021.752406

Yarar, A., Onucyildiz, M., & Copty, N. K. (2009). Modelling level change in lakes using neuro-fuzzy and artificial neural networks. *Journal of Hydrology*, *365*(3–4), 329–334. https://doi.org/10.1016/J.JHYDROL.2008.12.006

Yu, P. S., Chen, S. T., & Chang, I. F. (2006). Support vector regression for real-time flood stage forecasting. *Journal of Hydrology*, *328*(3–4), 704–716. https://doi.org/10.1016/J.JHYDROL.2006.01.021

Yu, Y., Si, X., Hu, C., & Zhang, J. (2019). A Review of Recurrent Neural Networks: LSTM Cells and Network Architectures. *Neural Computation*, *31*(7), 1235–1270. https://doi.org/10.1162/NECO_A_01199

Zhu, S., Hrnjica, B., Ptak, M., Choiński, A., & Sivakumar, B. (2020). Forecasting of water level in multiple temperate lakes using machine learning models. *Journal of Hydrology*, *585*, 124819. https://doi.org/10.1016/J.JHYDROL.2020.124819

Appendices – I

Table from Bathymetry of Mono Lake (Smoothed Pelagos)
https://www.monobasinresearch.org/images/mbeir/dappendix/tablea-1.pdf

Stage (ft)	Area (ac)	Volume (ac-ft)	Salinity (g/l)
6300	14776	302324	693
6301	15162	317293	661
6302	15536	332642	630
6303	15903	348362	602
6304	16259	364443	575
6305	16609	380877	550
6306	16952	397657	527
6307	17289	414777	505
6308	17623	432233	485
6309	17949	450019	466
6310	18264	468126	448
6311	18574	486544	431
6312	18882	505272	415
6313	19189	524308	400
6314	19498	543651	386
6315	19808	563304	372
6316	20117	583267	359

6317	20424	603537	347
6318	20727	624113	336
6319	21025	644989	325
6320	21319	666161	315
6321	21609	687625	305
6322	21895	709378	295
6323	22179	731415	287
6324	22455	753732	278
6325	22723	776321	270
6326	22986	799175	262
6327	23246	822291	255
6328	23505	845667	248
6329	23766	869302	241
6330	24029	893199	235
6331	24292	917360	228
6332	24557	941785	223
6333	24826	966476	217
6334	25094	991436	211
6335	25366	1016666	206
6336	25643	1042171	201
6337	25926	1067955	196
6338	26215	1094026	192
6339	26509	1120388	187

6340	26805	1147045	183
6341	27101	1173998	179
6342	27398	1201247	174
6343	27695	1228794	171
6344	27987	1256635	167
6345	28277	1284767	163
6346	28565	1313188	160
6347	28848	1341895	156
6348	29124	1370881	153
6349	29391	1400138	150
6350	29650	1429659	147
6351	29904	1459436	144
6352	30158	1489467	141
6353	30409	1519750	138
6354	30662	1550286	135
6355	30920	1581077	133
6356	31182	1612128	130
6357	31449	1643443	128
6358	31720	1675028	125
6359	31998	1706886	123
6360	32283	1739027	121
6361	32575	1771456	118
6362	32873	1804180	116

6363	33182	1837207	114
6364	33517	1870557	112
6365	33869	1904250	110
6366	34224	1938297	108
6367	34593	1972705	106
6368	35070	2007537	104
6369	35619	2042882	103
6370	36266	2078825	101
6371	36970	2115443	99
6372	37688	2152772	97
6373	38409	2190820	96
6374	39127	2229588	94
6375	39915	2269109	92
6376	40724	2309428	91
6377	41531	2350556	89
6378	42325	2392484	88
6379	43012	2435153	86
6380	43670	2478494	85
6381	44256	2522457	83
6382	44783	2566976	82
6383	45295	2612015	80
6384	45799	2657562	79
6385	46310	2703617	78

6386	46734	2750139	76
6387	47112	2797062	75
6388	47492	2844364	74
6389	47865	2892042	72
6390	48245	2940097	71
6391	48584	2988512	70
6392	48893	3037250	69
6393	49194	3086294	68
6394	49491	3135637	67
6395	49796	3185280	66
6396	50093	3235225	65
6397	50375	3285459	64
6398	50660	3335976	63
6399	50930	3386771	62
6400	51204	3437838	61
6401	51469	3489175	60
6402	51720	3540769	59
6403	51967	3592613	58
6404	52208	3644700	58
6405	52451	3697030	57
6406	52685	3749598	56
6407	52904	3802392	55
6408	53117	3855403	54

6409	53326	3908624	54
6410	53534	3962054	53
6411	53741	4015692	52
6412	53939	4069532	52
6413	54134	4123568	51
6414	54327	4177799	50
6415	54527	4232226	50
6416	54730	4286854	49
6417	54924	4341681	48
6418	55120	4396703	48
6419	55318	4451922	47
6420	55534	4507348	46
6421	55756	4562993	46
6422	55976	4618859	45
6423	56205	4674950	45
6424	56450	4731278	44
6425	56760	4787883	44
6426	57066	4843440	43
6427	57365	4900496	43
6428	57668	4957793	42
6429	57972	5015397	42
6430	58276	5073424	41
6431	58569	5132187	41

6432	58853	5191152	40
6433	59136	5250319	40
6434	59412	5309688	39
6435	59675	5369259	39
6436	59920	5429032	39
6437	60150	5489007	38
6438	60365	5549184	38
6439	60565	5609563	37
6440	60750	5670144	37

Appendices – II

LSTM Ensemble Model Results in Water Levels (Feet)

Dates (Monthly)	Mono Lake Water Levels (ft)	LSTM Base Model (ft)	Model 1	Model 2	Model 3	Model 4	Model 5	Model 6	Model 7	Model 8	Model 9	Model 10	Model 11	Model 12
1/1/2019	6381.3	6381.5	6381.4	6381.4	6381.4	6381.5	6381.5	6381.5	6381.4	6381.4	6381.5	6381.5	6381.4	6381.5
2/1/2019	6381.5	6381.6	6381.4	6381.6	6381.5	6381.7	6381.5	6381.6	6381.5	6381.6	6381.6	6381.6	6381.5	6381.6
3/1/2019	6381.9	6381.7	6381.4	6381.6	6381.5	6381.7	6381.5	6381.5	6381.6	6381.7	6381.6	6381.6	6381.4	6381.5
4/1/2019	6382.1	6381.8	6381.5	6381.7	6381.5	6381.7	6381.6	6381.6	6381.7	6381.9	6381.5	6381.6	6381.2	6381.6
5/1/2019	6382.1	6382.1	6381.5	6381.8	6381.4	6381.8	6381.5	6381.5	6381.8	6382.2	6381.3	6381.6	6381.1	6381.6
6/1/2019	6382.1	6382.2	6381.2	6381.7	6381.1	6381.7	6381.2	6381.2	6381.5	6382.2	6381.1	6381.3	6380.7	6381.4
7/1/2019	6382.7	6382.1	6380.7	6381.4	6380.8	6381.3	6380.9	6380.8	6381.0	6381.9	6380.8	6380.9	6380.2	6381.0
8/1/2019	6383.1	6382.0	6380.2	6381.1	6380.6	6381.0	6380.6	6380.5	6380.6	6381.7	6380.5	6380.6	6379.9	6380.7
9/1/2019	6383.0	6381.9	6379.9	6381.0	6380.4	6380.9	6380.4	6380.4	6380.3	6381.6	6380.3	6380.4	6379.6	6380.4
10/1/2019	6382.6	6381.9	6379.8	6381.0	6380.4	6380.8	6380.3	6380.4	6380.2	6381.7	6380.2	6380.4	6379.5	6380.4
11/1/2019	6382.5	6382.1	6379.8	6381.1	6380.6	6380.9	6380.4	6380.5	6380.2	6381.8	6380.2	6380.4	6379.5	6380.4
12/1/2019	6382.5	6382.3	6379.9	6381.3	6380.8	6381.1	6380.5	6380.8	6380.4	6382.1	6380.4	6380.6	6379.7	6380.6
1/1/2020	6382.6	6382.5	6379.9	6381.5	6381.1	6381.4	6380.6	6380.9	6380.5	6382.3	6380.6	6380.8	6379.8	6380.8
2/1/2020	6382.6	6382.7	6380.0	6381.8	6381.3	6381.4	6380.7	6381.1	6380.7	6382.6	6380.8	6381.0	6379.9	6380.9
3/1/2020	6382.6	6382.8	6380.1	6381.9	6381.4	6381.4	6380.7	6381.1	6380.8	6382.8	6380.8	6381.0	6379.7	6380.9
4/1/2020	6382.6	6382.9	6380.3	6382.1	6381.6	6381.2	6380.7	6381.1	6380.9	6383.2	6380.7	6381.0	6379.6	6381.0
5/1/2020	6382.7	6383.2	6380.4	6382.5	6381.7	6381.2	6380.7	6381.4	6381.1	6383.7	6380.7	6381.1	6379.4	6381.1
6/1/2020	6382.6	6383.4	6380.2	6382.5	6381.7	6381.2	6380.4	6381.6	6380.8	6383.9	6380.6	6381.0	6379.0	6380.9
7/1/2020	6382.4	6383.4	6379.7	6382.3	6381.5	6380.8	6380.0	6381.4	6380.4	6383.7	6380.2	6380.7	6378.6	6380.5
8/1/2020	6382.1	6383.2	6379.3	6382.1	6381.4	6380.5	6379.7	6381.3	6380.0	6383.6	6379.9	6380.4	6378.3	6380.2
9/1/2020	6381.8	6383.2	6379.0	6382.0	6381.4	6380.5	6379.6	6381.2	6379.7	6383.6	6379.6	6380.2	6378.2	6379.9
10/1/2020	6381.5	6383.2	6378.9	6382.1	6381.5	6380.6	6379.5	6381.2	6379.7	6383.7	6379.5	6380.1	6378.1	6379.9
11/1/2020	6381.2	6383.4	6379.0	6382.3	6381.8	6381.0	6379.6	6381.4	6379.8	6384.0	6379.5	6380.2	6378.2	6379.9
12/1/2020	6381.1	6383.6	6379.0	6382.5	6382.2	6381.2	6379.7	6381.6	6379.9	6384.3	6379.7	6380.4	6378.3	6380.1
1/1/2021	6381.1	6383.8	6379.1	6382.8	6382.6	6381.4	6379.8	6381.8	6380.1	6384.6	6379.8	6380.6	6378.5	6380.2
2/1/2021	6381.3	6384.0	6379.3	6383.0	6382.9	6381.7	6379.9	6381.9	6380.2	6384.8	6379.9	6380.8	6378.4	6380.3
3/1/2021	6381.3	6384.0	6379.4	6383.1	6383.3	6381.7	6379.8	6381.8	6380.3	6385.1	6380.0	6380.8	6378.3	6380.3
4/1/2021	6381.3	6384.2	6379.6	6383.4	6383.8	6381.6	6379.9	6381.8	6380.5	6385.7	6379.8	6380.8	6378.2	6380.4
5/1/2021	6381.2	6384.5	6379.7	6383.7	6384.5	6381.9	6379.8	6381.8	6380.6	6386.2	6379.8	6380.9	6378.0	6380.4
6/1/2021	6381.1	6384.6	6379.5	6383.8	6385.0	6382.2	6379.5	6381.7	6380.3	6386.2	6379.6	6380.8	6377.6	6380.2
7/1/2021	6380.9	6384.5	6379.0	6383.5	6385.1	6382.2	6379.1	6381.6	6379.8	6386.0	6379.3	6380.5	6377.2	6379.8
8/1/2021	6380.6	6384.4	6378.6	6383.4	6385.0	6382.0	6378.8	6381.4	6379.5	6385.9	6378.9	6380.2	6377.0	6379.5
9/1/2021	6380.2	6384.3	6378.4	6383.3	6385.1	6381.9	6378.6	6381.3	6379.3	6386.0	6378.6	6380.0	6376.8	6379.2

10/1/2021	6379.9	6384.4	6378.4	6383.4	6385.3	6381.9	6378.6	6381.4	6379.2	6386.2	6378.5	6379.9	6376.8	6379.2
11/1/2021	6379.8	6384.5	6378.4	6383.6	6385.7	6381.9	6378.6	6381.5	6379.3	6386.5	6378.5	6380.0	6376.9	6379.1
12/1/2021	6379.8	6384.7	6378.5	6383.8	6386.1	6382.1	6378.8	6381.9	6379.5	6386.8	6378.6	6380.2	6377.0	6379.3
1/1/2022	6379.9	6385.0	6378.6	6384.1	6386.5	6382.2	6378.9	6382.3	6379.7	6387.1	6378.7	6380.4	6377.1	6379.5
2/1/2022	6379.9	6385.1	6378.8	6384.3	6386.8	6382.3	6378.9	6382.6	6379.8	6387.3	6378.9	6380.6	6377.0	6379.6
3/1/2022	6379.9	6385.2	6378.9	6384.5	6387.1	6382.2	6378.9	6382.7	6379.9	6387.7	6379.0	6380.6	6376.9	6379.6
4/1/2022	6379.9	6385.3	6379.2	6384.8	6387.5	6382.1	6379.0	6382.9	6380.1	6388.3	6378.9	6380.6	6376.7	6379.6
5/1/2022	6379.8	6385.6	6379.3	6385.0	6388.1	6381.8	6378.9	6383.2	6380.2	6388.8	6378.8	6380.6	6376.4	6379.7
6/1/2022	6379.7	6385.7	6379.0	6385.0	6388.3	6381.4	6378.6	6383.5	6379.8	6388.6	6378.6	6380.6	6375.9	6379.4
7/1/2022	6379.5	6385.6	6378.5	6384.8	6388.2	6381.0	6378.2	6383.6	6379.3	6388.4	6378.3	6380.3	6375.7	6379.0
8/1/2022	6379.2	6385.5	6378.2	6384.6	6388.0	6380.7	6377.9	6383.5	6379.0	6388.4	6377.9	6380.0	6375.4	6378.7
9/1/2022	6379.0	6385.4	6378.1	6384.6	6388.2	6380.4	6377.7	6383.5	6378.8	6388.5	6377.7	6379.7	6375.3	6378.4
10/1/2022	6378.7	6385.5	6378.0	6384.7	6388.5	6380.4	6377.7	6383.6	6378.8	6388.8	6377.5	6379.7	6375.3	6378.4
11/1/2022	6378.5	6385.7	6378.1	6384.9	6389.1	6380.5	6377.8	6383.8	6378.9	6389.0	6377.4	6379.7	6375.5	6378.3
12/1/2022	6378.4	6385.9	6378.2	6385.2	6389.7	6380.6	6377.9	6384.0	6379.1	6389.4	6377.5	6379.9	6375.6	6378.5
1/1/2023	6378.6	6386.1	6378.4	6385.4	6390.1	6380.6	6378.0	6384.3	6379.3	6389.6	6377.7	6380.1	6375.6	6378.7
2/1/2023	6379.3	6386.2	6378.5	6385.6	6390.4	6380.6	6378.1	6384.5	6379.4	6389.9	6377.8	6380.3	6375.5	6378.8
3/1/2023	6379.5	6386.3	6378.7	6385.8	6390.8	6380.5	6378.0	6384.4	6379.5	6390.4	6378.0	6380.3	6375.4	6378.8
4/1/2023	6380.0	6386.4	6379.0	6386.1	6391.4	6380.4	6378.1	6384.4	6379.7	6391.0	6377.9	6380.3	6375.2	6378.9
5/1/2023	6380.1	6386.7	6379.0	6386.3	6392.0	6380.2	6378.0	6384.4	6379.7	6391.2	6377.8	6380.3	6374.8	6378.9
6/1/2023	6380.5	6386.8	6378.7	6386.3	6392.4	6379.8	6377.6	6384.3	6379.3	6391.0	6377.7	6380.2	6374.3	6378.6
7/1/2023	6381.6	6386.7	6378.2	6386.0	6392.4	6379.4	6377.2	6384.2	6378.8	6390.9	6377.5	6380.0	6374.1	6378.2
8/1/2023	6382.9	6386.5	6378.0	6385.9	6392.4	6379.1	6377.0	6384.2	6378.5	6390.9	6377.1	6379.6	6373.9	6377.9
9/1/2023	6383.2	6386.5	6377.8	6385.9	6392.6	6378.9	6376.8	6384.1	6378.4	6391.1	6376.8	6379.4	6373.8	6377.6
10/1/2023	6383.2	6386.6	6377.8	6386.0	6392.9	6378.8	6376.8	6384.2	6378.4	6391.3	6376.6	6379.4	6373.8	6377.6
11/1/2023	6383.1	6386.7	6377.9	6386.2	6393.4	6378.7	6376.8	6384.3	6378.5	6391.6	6376.5	6379.4	6374.0	6377.6
12/1/2023	6383.1	6387.0	6378.0	6386.5	6393.9	6378.8	6377.0	6384.6	6378.7	6391.9	6376.5	6379.6	6374.1	6377.7

Appendices – III

Forecasting dataset of Change in storage for each of the LSTM Ensemble member models

Model 1:

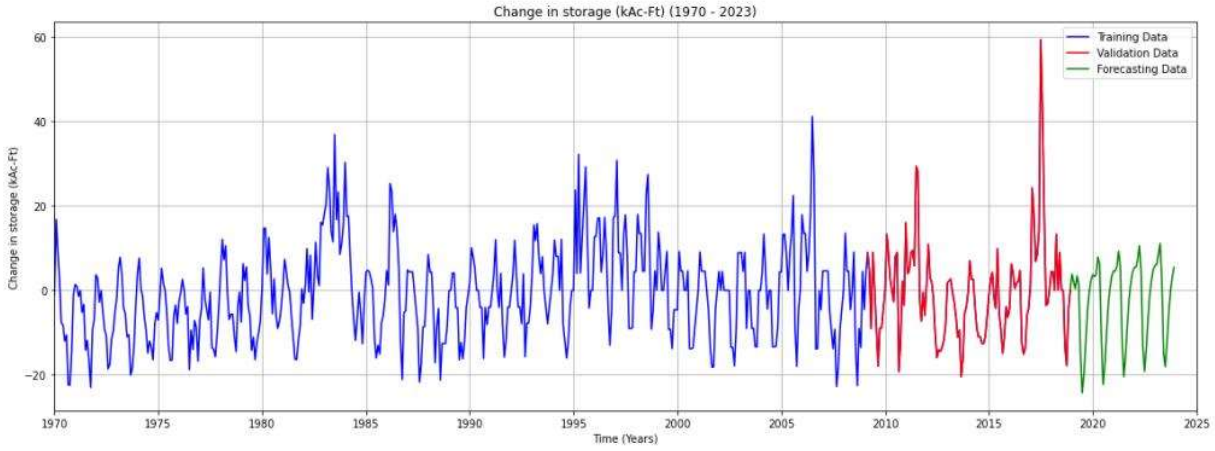

Model 2:

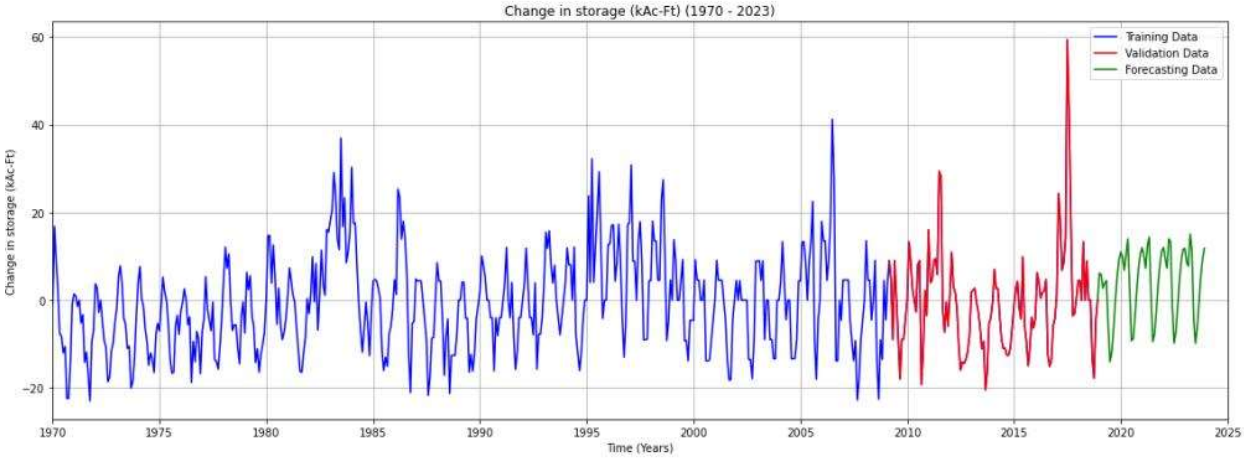

Model 3:

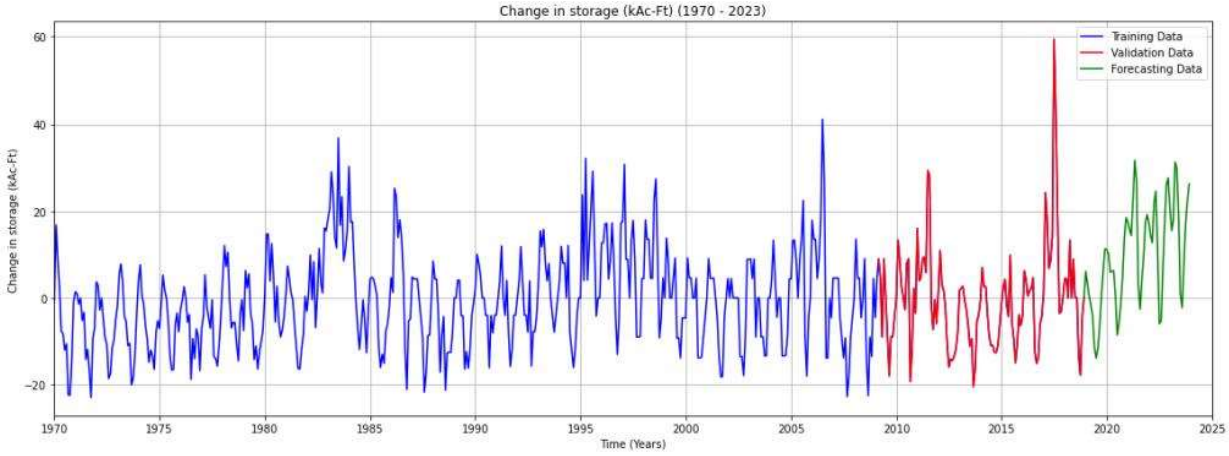

Model 4:

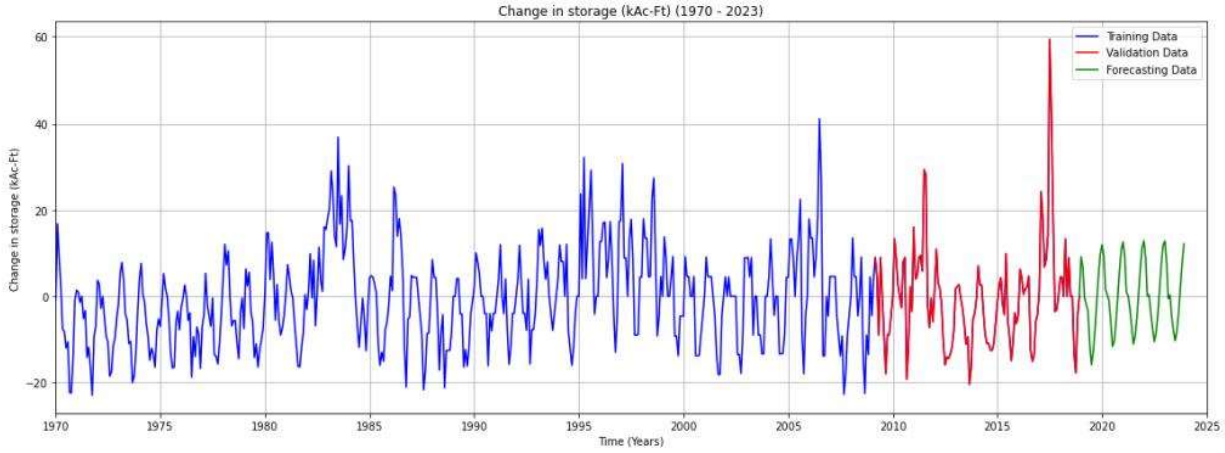

Model 5:

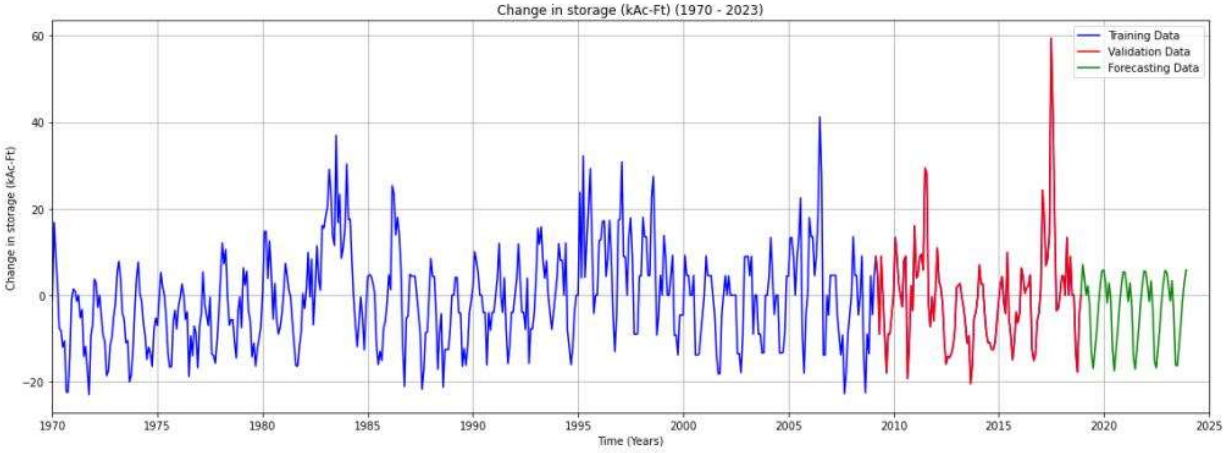

Model 6:

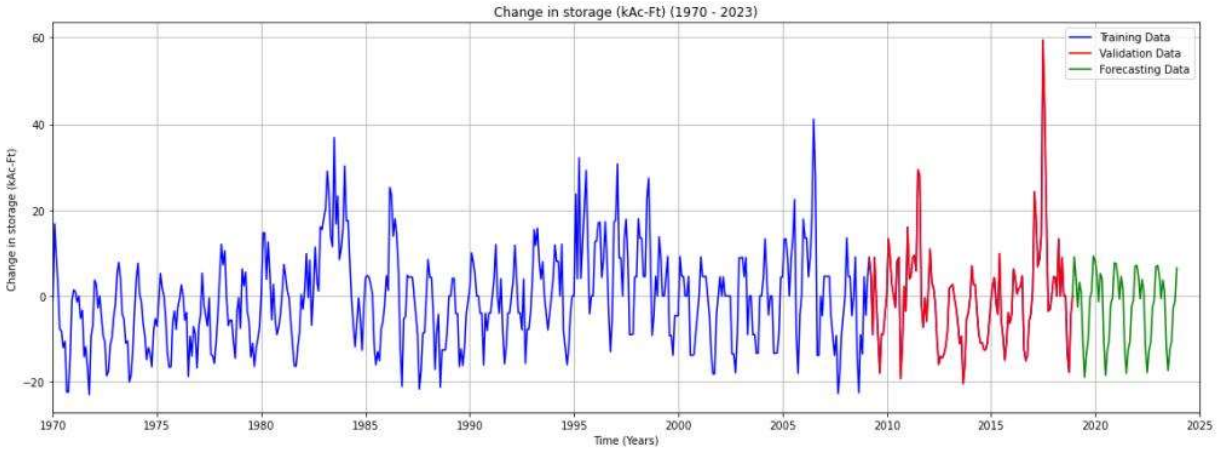

Model 7:

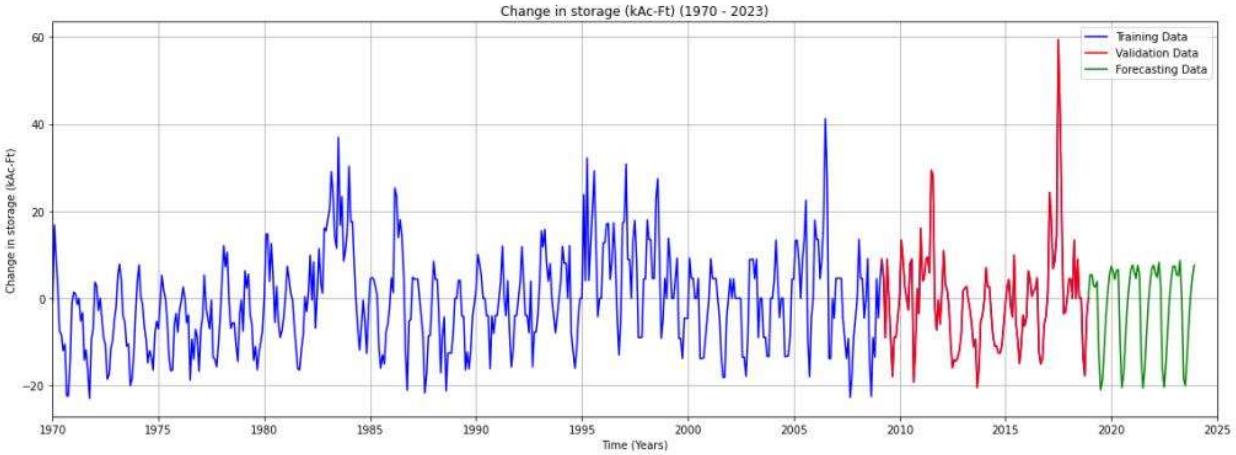

Model 8:

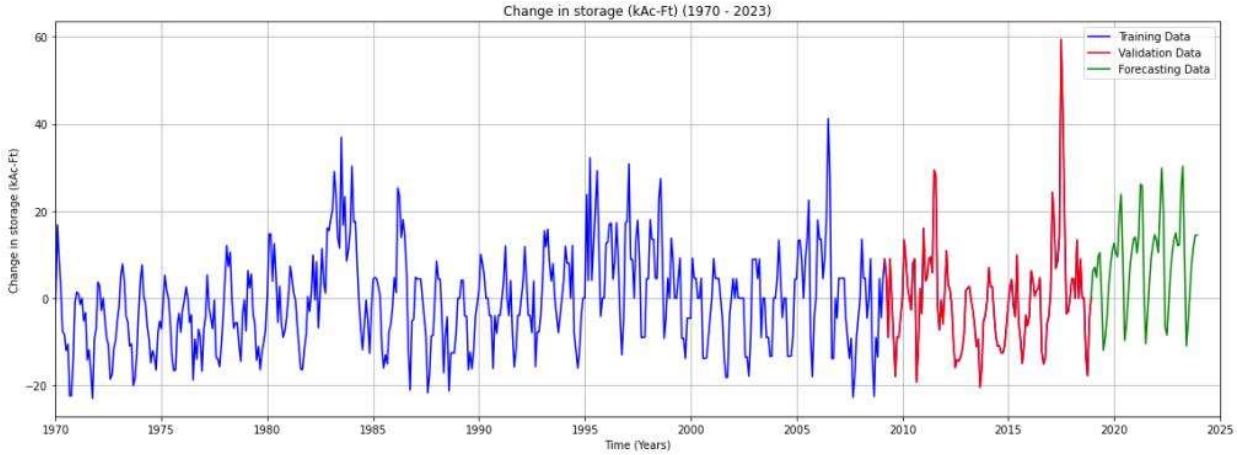

Model 9:

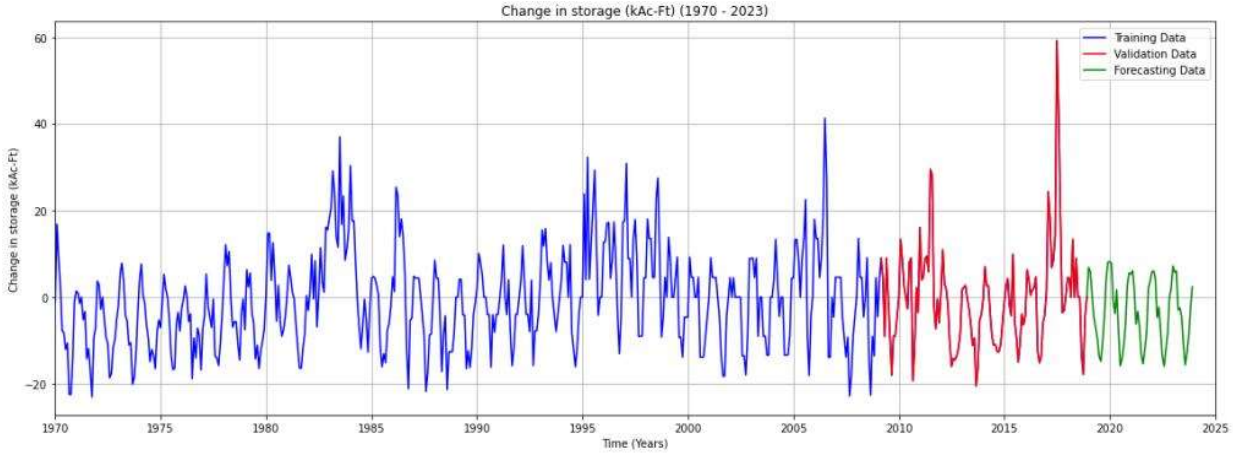

Model 10:

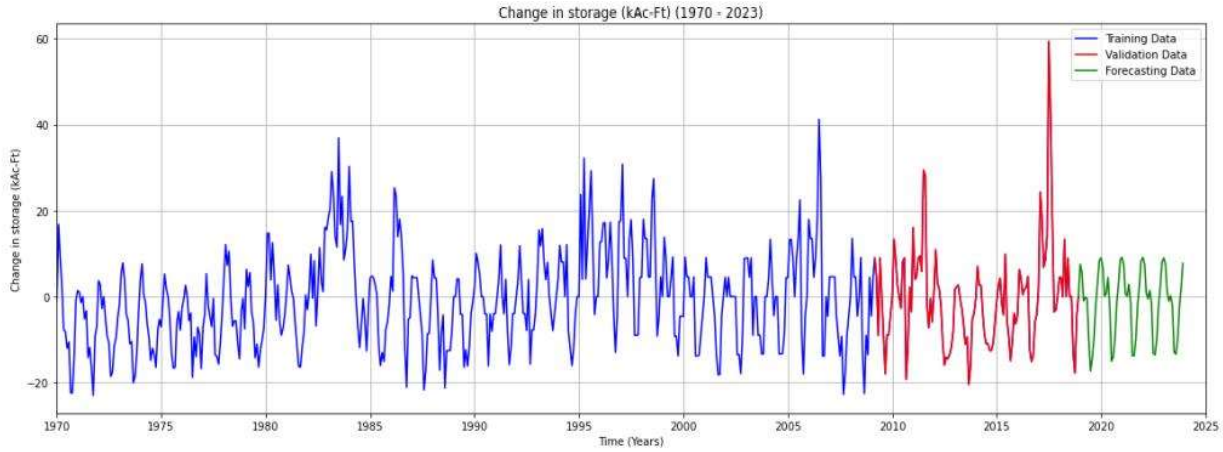

Model 11:

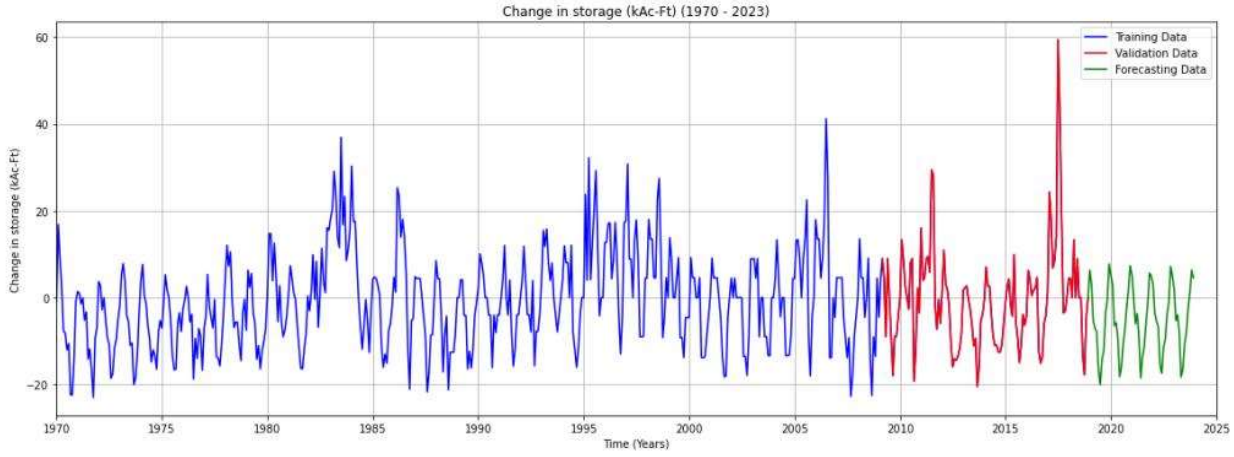

Model 12:

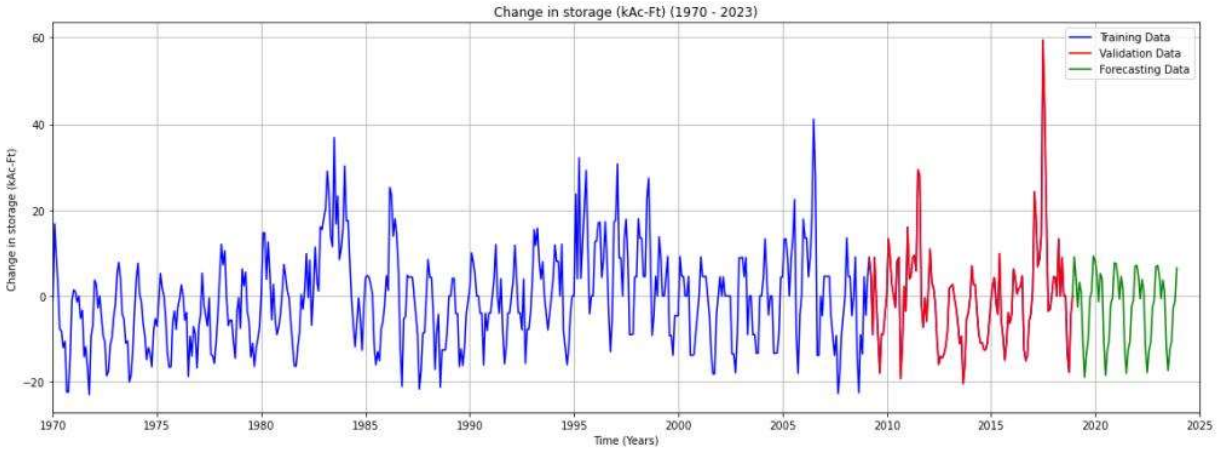
Change in storage (kAc-Ft) (1970 - 2023)
Training Data
Validation Data
Forecasting Data
Change in storage (kAc-Ft)
Time (Years)
60
40
20
0
−20
1970
1975
1980
1985
1990
1995
2000
2005
2010
2015
2020
2025